INVESTIGATION OF OSCILLATORY MECHANISMS AND THALAMO-CORTICAL CIRCUITRY OF THE VISUAL SYSTEM BY SIMULTANEOUS EEG-fMRI

by

ALİ BAYRAM

BS, Electronics & Communication Engineering, Yıldız Technical University, 2001

MSc, Biomedical Engineering, Boğaziçi University, 2005

Submitted to the Institute of Biomedical Engineering

in partial fulfillment of the requirements

for the degree of

Doctor

of

Philosophy

Boğaziçi University

2015

ACKNOWLEDGMENTS

I would like to express my deepest gratitude to my advisor, Professor Dr. Ahmet Ademoğlu, for his invaluable guidance, inspiration, and patience that he has provided throughout the course of my research. I would also like to express my special appreciation and thanks to Professor Dr. Tamer Demiralp for encouraging my research, for his invaluable support, suggestions, criticisms, and for taking the time to patiently review manuscripts. They have not only provided an excellent atmosphere for doing research, they have also given me priceless advices on my career.

I would like to thank Professor Dr. Cengizhan Öztürk. I am indebted for his inspiration, guidance and the tremendous support including providing me with opportunities to access jobs. I would especially like to thank Professor Dr. K. Nevzat Tarhan for his endless support and demonstrated confidence in me. Thanks to his support, NPIstanbul Neuropsychiatry Hospital had been my research laboratory for 6 years. I would like to express my special thanks to Professor Dr. Başar Bilgiç for his valuable support, inspiration, and cooperation. I will always remember his solution-oriented and kind personality. I am also thankful to Dr. Esin Öztürk Işık for taking the time to review this dissertation and serving on the committee.

I would like to thank Esin Karahan Şenvardar, Dr. Adil Deniz Duru, Müge Özker, Dr. Mehmet Ergen, Dr. Yasemin Ergen, Dr. Zübeyir Bayraktaroğlu, Basri Erdoğan, Bora Cebeci, Itır Kaşıkçı, Elif Kurt, Ezgi Tuna Erdoğan, Tuba Songür, Sedat Aydın, Ali Bilgin Arslan for their friendship and assistance. All of you supported me, shared your expertise, and contributed to all phases of my Ph.D. thesis.

Last, but not the least, I thank my family for their endless love. Their prayer for me was what sustained me thus far. Without their support, this work would not have been possible.

ABSTRACT

INVESTIGATION OF OSCILLATORY MECHANISMS AND THALAMO-CORTICAL CIRCUITRY OF THE VISUAL SYSTEM BY SIMULTANEOUS EEG-fMRI

Neural oscillation is an indispensable phenomena in the functioning of the cortical networks. Evoked neural oscillations triggered by external rhythmic stimulation mimic spontaneous ongoing oscillations, thus could shed light on the intrinsic specialization and tuning of the cortical networks. In this thesis, flickering light stimulation is used to constitute steady state for a wide range of temporal frequencies (6-46 Hz) during simultaneous electroencephalography (EEG) and blood oxygenation level dependent (BOLD) functional magnetic resonance imaging (fMRI) scans of 40 healthy volunteers. Firstly, thalamo–cortical loop of the visual system is the subject of interest. Our findings prove that high correlation between the frequency response characteristics of the lateral geniculate nucleus (LGN) and the primary visual cortex (V1) supports the oscillatory tuning property of the thalamo–cortical interactions. Secondly, contribution of oscillations in the modeling of hemodynamic response is discussed based on the sensitivity of BOLD components (phasic and tonic) to temporal frequency. Our results show that, tonic BOLD component is decreasing more sharply than phasic component with increasing frequencies pointing higher dependency of tonic BOLD response to the stimulation frequency. Finally, EEG informed fMRI analysis is conducted for the sake of testing resonance phenomena. The correlation maps between the BOLD responses and the steady state visually evoked potential (SSVEP) amplitudes show significant correlation for the beta and gamma bands but not for alpha band. This result supports the view that the global amplitude maximum of the SSVEP in the alpha band is due to the synchronization without synaptic activity (BOLD) increase.

Keywords: Electroencephalography, Functional magnetic resonance imaging, Oscillator networks, Steady state visually evoked potentials, BOLD transients, Resonance phenomena, EEG informed fMRI analysis.

ÖZET

GÖRSEL SİSTEMDEKİ OSİLATÖR MEKANİZMALARIN VE TALAMO-KORTİKAL DEVRENİN EŞZAMANLI EEG-fMRG İLE ARAŞTIRILMASI

Kortikal ağların işlevselliğinde, nöron salınımları vazgeçilmez bir olgudur. Harici ritmik bir uyaran ile tetiklenen uyarılmış salınımlar, süregiden spontan salınımları taklit ederler ve bu sayede kortikal ağların içsel özellikleri ve uyumuna ışık tutabilirler. Bu tezde, titreyen ışık uyaranı, 40 sağlıklı gönüllüde, eş zamanlı elektroensefalografi (EEG) ve kanın oksijenlenme seviyesine bağımlı (KOSB) fonksiyonel manyetik rezonans görüntüleme (fMRG) kayıtlamaları sırasında, geniş bir zamansal frekans yelpazesinde (6-46 Hz) durağan hal oluşturmak için kullanılmaktadır. Görsel sistemdeki talamo–kortikal döngü, öncelikli ilgilenilen konudur. Lateral genikulat çekirdeğin (LGN) ve primer görme korteksinin (V1) frekans yanıtları arasındaki yüksek korelasyonla ilgili bulgumuz, talamo–kortikal etkileşimlerin salınım bazlı uyumunu desteklemektedir. İkinci olarak, hemodinamik yanıtın modellenmesinde salınımların katkısı, KOSB (fazik ve tonik) bileşenlerinin zamansal frekansa hassasiyeti baz alınarak tartışılmaktadır. Bulgularımız, tonik KOSB bileşeninin artan frekans ile fazik yanıttan daha keskin düştüğünü, dolayısıyla uyarım frekansına tonik KOSB yanıtının daha duyarlı olduğunu işaret etmektedir. Son olarak, rezonans olgusunun test edilmesi adına EEG bilgisiyle fMRG analizi gerçekleştirilmektedir. KOSB yanıtlarının ve DHUP genliklerinin arasındaki korelasyon haritaları, beta ve gama bantlarında belirgin korelasyon göstermekte fakat alfa bandında göstermemektedir. Bu sonuç, alfa bandındaki DHUP genliğinin global maksimumu sinaptik aktivite (KOSB) artışı olmadan senkronizasyon sonucunda ortaya çıktığı görüşünü destekler.

Anahtar Sözcükler: Elektroensefalografi, Fonksiyonel manyetik rezonans görüntüleme, Osilatör ağlar, Durağan hal görsel uyarım potansiyelleri, geçici KOSB yanıtları, Rezonans olayı, EEG bilgisiyle fMRG analizi.

TABLE OF CONTENTS

LIST OF FIGURES

LIST OF TABLES

LIST OF SYMBOLS

Y	Measured Time Series Data of fMRI
X	Design Matrix
β	Regression Parameter
e	Noise Term
c	Contrast Matrix
α_{FWE}	Familywise Error Corrected Threshold

LIST OF ABBREVIATIONS

fMRI	Functional Magnetic Resonance Imaging
EEG	Electroencephalography
SSVEP	Steady State Visually Evoked Potential
BOLD	Blood Oxygenation Level Dependent
LFPs	Local Field Potentials
LGN	Lateral Geniculate Nucleus
V1	Primary Visual Cortex
MEG	Magnetoencephalogram
SQUIDs	Superconducting Quantum Interference Devices
PET	Positron Emission Tomography
18F–FDG	Fluorodeoxyglucose
HbR	Deoxy–hemoglobin
HbO2	Oxy–hemoglobin
CBF	Cerebral Blood Flow
CBV	Cerebral Blood Volume
CMRO2	Cerebral Metabolic Rate of Oxygen
ISI	Inter Stimulus Interval
LED	Light Emitting Diode
MPRAGE	Magnetization Prepared Gradient Echo
GE	Gradient Echo
TR	Time of Repetition
TE	Time of Echo
EPI	Echo Planar Imaging
ECG	Electrocardiogram
AAS	Average Artifact Subtraction
BCG	Ballistocardiographic
PSU	Post Stimulus Undershoot
HRF	Hemodynamic Response Function

SNR	Signal to Noise Ratio
FWHM	Full Width at Half Maximum
SPM	Statistical Parametric Mapping
GLM	General Linear Model
3D	Three Dimensional
FWE	Familywise Error
RFT	Random Field Theory
RESEL	Resolution Element
ROI	Region of Interest
MNI	The Montreal Neurological Institute
ANOVA	Analysis of Variance
SE	Standard Error
FSL	FMRIB's Software Library
PSO	Post–Stimulus Overshoot
pBOLD	Positive BOLD
NREM	Non–Rapid Eye Movement
EROs	Event Related Oscillations
MUA	Multi–Unit Spiking Activity
EIN	Excitation–Inhibition Networks
ANC	Adaptive Noise Canceling
PCA	Principal Component Analysis
ICA	Independent Component Analysis
FFT	Fast Fourier Transforms
PEs	Parameter estimates

1. INTRODUCTION

Neuroimaging studies conducted to examine activities of the human brain suggest that synchronization is a fundamental property of cortical networks and serves cognitive functions. Likewise, the loss of neural synchrony might be the representative of the cognitive dysfunction associated with pathological brain stages [1]. Thus, detecting and recording the synchronized activities are of utmost importance in functional neuroimaging. Emergence of oscillatory activities of a neuronal network is the outcome of the cortical synchronization, and they can be measured in the macroscopic domain by the electroencephalography (EEG) technique over the scalp. In this regard, EEG represents spatial sum of the synchronous electrical activity of neurons belonging to multiple large neuronal groups with high temporal resolution. However, low spatial resolution, which is the main drawback of this technique, is one of the concerns that the current scientific efforts are focused on. At this point, due to its high spatial resolution, functional magnetic resonance imaging (fMRI) could open a new window and provide complementary knowledge about the localizations of the oscillatory brain dynamics. However, oscillatory activities that could be detected easily by EEG do not always represent a clear counterpart as a significant fMRI blood oxygenation level dependent (BOLD) signal. This is due to the implicit assumption and expectation of the most studies that EEG and fMRI measures pick up more or less similar neuronal activity or fMRI depends on existence of a linear relationship between the neuronal activity and the oxygenation of the brain tissue.

In this sense, studies dealing with fMRI BOLD contrast and investigating effects of oscillatory activities of cortical circuitry could shed light on many aspects of neurovascular coupling between neuronal activities and consequential vascular response. Moreover, oscillatory based fMRI research could serve localization and functional connectivity efforts.

1.1 Motivation and Objective

The scope of this work covers the examination of the oscillatory activities in the human visual system, the BOLD contrast mechanism, and the EEG informed fMRI analysis via steady state visual evoked oscillations. First of all, while discussing the roles of lateral geniculate nucleus (LGN) and primary visual cortex (V1) which are effective anatomical structures in early visual system, their interaction and response selectivity at various temporal frequencies are regarded as critical cornerstones for oscillations. This point of view allows to reveal contributions of the anatomical structures in oscillatory activities of thalamo–cortical loop by fMRI.

There are important contributions in the literature about the possibility that the transient and sustained components of the BOLD response represent different underlying neuronal processes. Therefore, examining the relationship between the temporal frequency parameter of the visual stimulation and BOLD transients is another scope of this thesis. The way that the frequency of an oscillation effects transients of the BOLD response is an important issue that has to be considered based on the neurovascular coupling perspective.

As a final theme of this study, EEG informed fMRI analysis of the resonance phenomenon is the focus of attention. Although, local field potential (LFP) power as an index of postsynaptic membrane oscillations has been shown to be temporally well correlated with the BOLD response to sensory stimuli [2]. The amplitudes of the EEG do not reflect simply the total neuronal activity or LFPs, but only synchronized neuronal activities. Moreover neural structures such as the thalamus and basal ganglia, which have a radial or noncolumnar organization, are less likely to make any significant contributions to the scalp EEG, even when large LFPs can be recorded from them [3]. Findings concerning thalamic activity associated with alpha power increases, for instance, have not revealed coherent cortical correlates of scalp EEG alpha oscillations; instead by identifying inverse relationships, they identified brain regions that increase their activity in the absence of marked alpha activity [4]. Finally, in the light of driven synchronous patterns, estimating the properties of the transfer function from EEG

power to BOLD signal change is another purpose of this dissertation for different frequency bands using simultaneous EEG–fMRI recordings in order to derive implications for the resonance phenomena.

1.2 Outline of the Thesis

This dissertation is organized in the following manner:

Chapter 2 focuses on the anatomical and physiological properties of human visual system and describes the signal processing capabilities and the synaptic organization of structures starting from the retina to the cerebral cortex.

Chapter 3 presents an overview about the non-invasive functional neuroimaging modalities with superiorities and disadvantages of each imaging method in order to gain insight about them and to make projection for possible multimodal neuroimaging approaches. Besides, this chapter is covering the basic principles of study and paradigm design strategies, and stimulus presentation techniques in fMRI. Methodology of the data collection section includes technical details of the experimental setup, subject recruitment, visual stimulation, and the data acquisition procedures of simultaneous EEG and fMRI recordings that were planned and carried on.

Chapter 4 covers the investigation of BOLD–fMRI signal changes due to the visually driven thalamo–cortical oscillations. First of all, physiological background of transient and sustained BOLD responses, task–related model based BOLD fMRI analysis, and statistical inference are presented in general. After that, participation of LGN and V1 to the thalamo-cortical oscillations is criticized based on their BOLD responses to the temporal frequency parameter of the visual stimuli via model based fMRI analysis. Besides, specifically BOLD response of the primary visual cortex is analyzed without using any model based approach by focusing on transient and sustained BOLD components. Temporal frequency dependent characteristics of BOLD components are described. The results are presented and the discussion is made while

considering the oscillations and neurovascular coupling.

Chapter 5 includes the speculations of resonance phenomena according to the results derived from EEG informed fMRI analysis. Source of EEG signal, EEG measurement, analysis, simultaneous EEG & fMRI measurement technique and fusion methods are presented at the beginning. Results are discussed in accordance with the resonance phenomena in steady state visually evoked responses.

Chapter 6 summarizes the dissertation research. It provides summary of the specific achievements of this work.

2. ANATOMY AND PHYSIOLOGY OF THE HUMAN VISUAL SYSTEM

Human visual system is the part of central nervous system which interprets information from visible light to build a perception. Transmission of the visual information from the eye to the cortex is enabled by the primary visual projection pathway (Figure 2.1). In this pathway, the external visual stimulus, visible light is initially converted into an internal neuronal signal by the retina.

The neuronal signal is carried from the retina through the optic nerves, dividing and partially crossing over into the optic chiasm. Majority of the axons in the optic nerve terminate in the lateral geniculate nuclei (LGN) of the thalamus. Finally, LGN sends outputs via optic radiation that terminate in the visual cortex where further visual processing takes place [5].

2.1 The Retina

The retina, which is the innermost layer of the eye, is the light sensitive neural portion of it. The first steps in the processing of visible light within the retina comprise transduction of light energy into electrical signals, refinement of these signals by synaptic interactions, and transmitting them to central targets. Neurons of the retina that perform these processes can be classified into five basic classes: photoreceptors, bipolar cells, ganglion cells, horizontal cells, and amacrine cells.

The retina includes two types of photoreceptors: rods and cones. Both types have an outer and an inner segment. Outer segment of photoreceptors is composed of membranous disks containing light–sensitive photopigment besides the inner segment contains the cell nucleus and gives rise to synaptic terminals that contact bipolar or horizontal cells. Horizontal cells and amacrine cells mediate lateral interactions in the outer and inner plexiform layers, respectively. A tree–neuron chain – photoreceptor cell

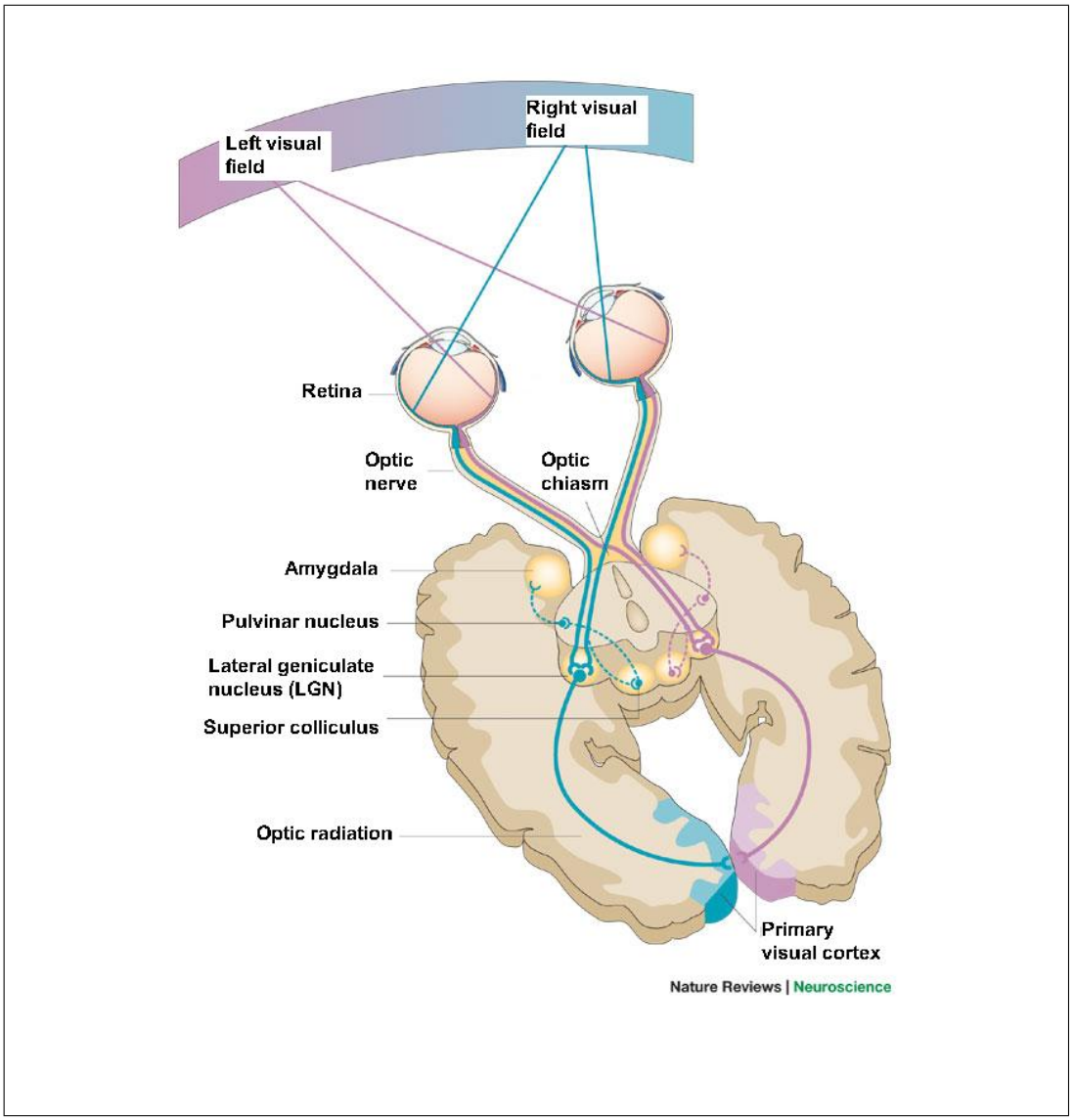

Figure 2.1 The primary projection pathways of the visual system. Adapted from Ref. [6].

to bipolar cell to ganglion cell – is the most direct pathway of the visual information that transmitted from photoreceptors to the optic nerve. The principle difference between the ganglion cells and most other cells in the retina is in the characteristics of their electrical response. The neuronal inner circuitry of the retina covers the graded electrical activity rather than action potentials. Because action potentials are not required to transmit information over the relatively short distances involved. The much larger axons of the ganglion cells, which have action potentials, form the optic nerve and carry information about retinal stimulation to the rest of the central nervous system.

2.1.1 Functional Specification of the Rod and Cone Systems

The two types of photoreceptors, rods and cones are specialized for different aspects of vision. Type of photopigment they contain, pattern of synaptic connections, and distribution across the retina are distinguishable properties of them.

The rod system is highly sensitive to light but has very low spatial resolution. Conversely, the cone system has very high spatial resolution but is relatively insensitive to light. Convergence nature of the neural circuitry makes rod system a better detector of light but reduces the spatial resolution of it. Each bipolar cell is connected by a number of rods, and many rod bipolar cells contact a given amacrine cell. In contrast, the cone system is much less convergent. Each retinal ganglion cell that dominate central vision receives input from only one cone bipolar cell, which, in turn, is connected with a single cone in the fovea.

Another difference is that, unlike rods, which contain a single photo pigment, cones are differentiated to detect short (blue), medium (green), and long (red) wavelengths of light which also allow us to see color. There are also individual cones, like rodes, which are entirely color blind.

Illumination level of the environment is also an effective determinant in photoreceptor responses. As illumination level increases, cones become more and more dominant in deciding what is seen, especially in the case of normal indoor lighting or sunlight.

Under conditions of high levels of steady illumination, the response of a rod system saturates, but the cone does not. The adaptation mechanisms of the cones are more efficient than rodes. Adaptation difference between rods and cones under gradually changing light flash stimulation is illustrated in figure 2.2. The response of cones recover more than four times faster (about 200 milliseconds), even in the maximum current response case.

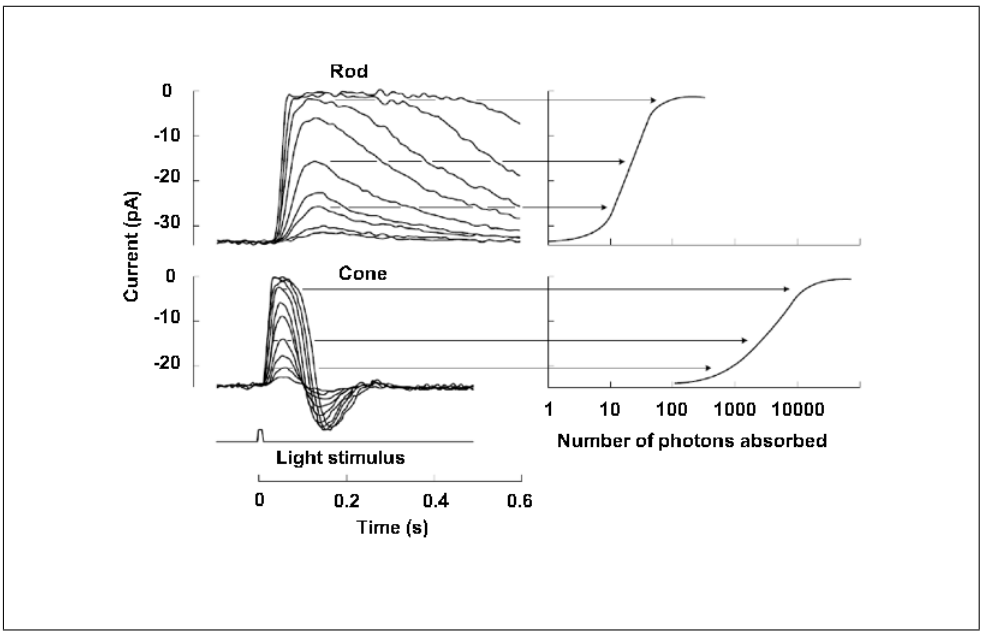

Figure 2.2 Adaptation difference between rods and cones under gradually increasing light intensity of flash stimuli [7].

The distribution of rods and cones across the surface of the retina also has important effects on vision. Despite the cone dominated vision in daytime light levels, the total number of rods in the human retina (about 90 million) far exceeds the number of cones (roughly 4.5 million). However, this correlation changes impressively in the fovea. In the fovea, cone density increases rapidly and in the center of the fovea there is no rod any more. Thats why, acuity is reduced by 75 percent at the line of just 6 "degree" eccentric to the line of sight. Besides, the presence of rodes in high density away from the fovea, explains why the threshold for detection a light stimulus is lower outside the region of central vision.

2.1.2 Receptive field: Detecting luminance change

Receptive field of a neuron is an area where the presence of an appropriate stimulus causes neuronal activity change. Photoreceptors have receptive fields which are limited to their precise location on the retina. Besides, each bipolar cell has a receptive field which covers a small circular patch of the retina. Typically their receptive fields did not extend beyond 1 mm in diameter and have overlapping distributions. Center of

the receptive field receives direct connections from a small number of photoreceptors, while the ring shaped surround field receives inputs from a larger set of photoreceptors which are connected via the horizontal cells. The response to the stimulation of the "center" of the receptive field is always inhibited by the stimulation of the "surround". In this sense, response of a bipolar cell to the stimulation of its receptive field is based on the luminance contrast between center and surround rather than level of illumination.

In fact, bipolar cells are separated into two classes based on their responses to the stimulation of their receptive field, "on"–center and "off"–center. When a spot of light turns on in the receptive field center, on–center bipolar cell depolarizes thus on–center ganglion cell produces a burst of action potentials. While off–center bipolar cell hyperpolarizes which in turn off–center ganglion cell decreases rate of discharge of action potential. When the spot falls on the surround field, the response of the on–center ganglion cell decreases below its resting level. Off–center cells show similar surround antagonism. Because of this property, cells are much more active while responding to small spots of light than to uniform illumination of the visual field.

Selective response to the light intensity increments and decrements of two cell types can be described by their physiological properties and relations. In the absence of light, photoreceptors are depolarized and depolarization leads to transmitter release (Glutamate) at their synapses. As mentioned before, photoreceptors and bipolar cells have graded potentials rather than action potentials. Graded depolarization leads to an increase in the amount of glutamate release in a graded manner. Besides, on–center and off–center bipolar cells have different types of glutamate receptors. On–center bipolar cells have metabotropic receptors (mGluR6) that cause the cells to hyperpolarize in response to glutamate release. On the other hand, off–center bipolar cells express ionotropic receptors (AMPA and kainate) that cause depolarization. Due to the receptor difference, glutamate has opposite effects on two bipolar cell types. Graded depolarization of both on– and off–bipolar cells results in increment of glutamate release and consequent depolarization of ganglion cells which have ionotropic receptors (AMPA, kainite, and NMDA receptors).

Similar to the on– and off–center response mechanism, antagonistic surround property is thought to emerge thanks to lateral interactions by horizontal cells. Horizontal cells receive inputs from photoreceptors and connected with many other horizontal cells. Horizontal cell population represent wide range of the retinal surface. They have GABA transmitter which has a hyperpolarization effect on photoreceptor terminals and reduces the light–evoked response.

Adaptation mechanism also important in luminance change detection of ganglion cells. Background level of illumination directly influences the relation between the intensity of spot illumination and evoked discharge rate. Operating light intensity limits of a ganglion cell adaptively shift in the case of increment in background illumination which in turn necessitates to increase stimulation intensity in order to get same discharge rate. In this sense, stimulation light intensity is not directly correlated with the firing rate but rather luminance contrast.

As can be seen, the signal carried by ganglion cells pass through the optic nerve, the optic chiasm, and the optic tractus to the visual centers is already highly processed by the retina [7, 5].

2.2 Central Visual Pathways

As defined in the previous section, larger axons of the ganglion cells form the optic nerve carry information about retinal stimulation to the rest of the central nervous system. The optic nerves of two eyes meet and decussate at the optic chiasm. About 60% of axons cross and switch their sides, whereas remaining 40% run on the same side. Since the crossing axons are from the nasal side of the retina (hemiretina), each optic tract carries information from the contralateral side of the visual field.

2.3 The Lateral Geniculate Nucleus

Lateral geniculate nucleus (LGN) is the major target for each optic tract. About 90% of the retinal ganglion cells send inputs to LGNs. There are two lateral geniculate bodies located in the dorsal part of the thalamus on the left and right hemisphere of the brain. In the cross–section figure of LGN (Figure 2.3), arrangement of the six definite layers of the cell bodies can be seen. These layers folded around the optic tract like a bent knee (genu is Latin for "knee") [7].

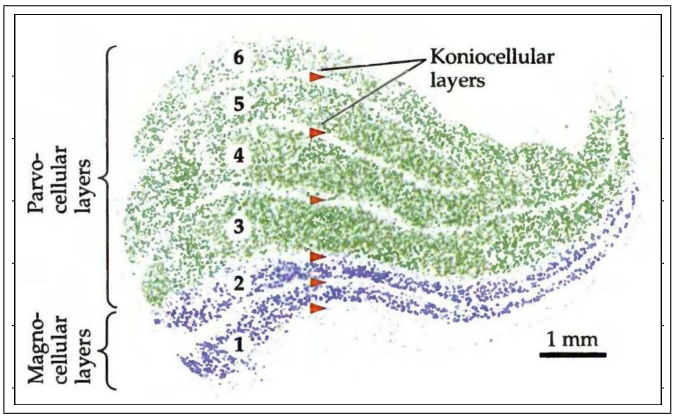

Figure 2.3 Cross–section figure of the human lateral geniculate nucleus showing the magnocellular, parvocellular, and koniocellular layers [7].

LGN layers are distinguished primarily on the bases of cell type that they contain. First two inner layers (ventral layers 1 and 2) are called the magnocellular layers, besides the outer four (dorsal layers 3, 4, 5, and 6) are called the parvocellular layers. Magnocellular layers contain M–cells larger in cell body, dendritic tree and receptive field as compared to P–cells of the parvocellular layers.

Functional properties of M and P ganglion cells give idea about the contribution of their pathway to visual perception and the reason of their separated representation as a consequence of parallel processing. In addition to larger receptive field, M ganglion cells have faster propagation velocity of action potential than P ganglion cells. Responses of M ganglion cells are transient while those of P ganglion cells are more sustained (tonic). Besides, spectral or color information is transmitted by only P ganglion cells thanks to the different classes of cones that drive their receptive field. Moreover,

P ganglion cells are very sensitive to spatial frequency allowing spatial resolution in detection of shape and size. On the other hand, M ganglion cells respond more vigorously to tiny luminance changes and very sensitive to temporal frequency allowing detection of rapid movements, and speed. The separate pathways for different types of information that is initiated by the retina seems to be maintained by the LGN.

There is also a third distinct type of pathway named the koniocellular or K–cell pathway. Koniocellular layers exist in the interlaminar zones that separate each magno– and parvocellular layers. Konio cells are different from the other ganglion cells in terms of their function and neurochemistry. Fine–caliper retinal axons give input to konio cells which, in turn, project to superficial layers of primary visual cortex not uniformly. Koniocellular pathway carries specific spectral information derived from short wavelength (blue) sensitive cones. Contribution of the K–cell pathway to the visual perception is not clear, but the earlier evolutionary origin of this pathway might be the reason of separated processing of short wavelength signals.

Individual ganglion cells of lateral geniculate nucleus are originated from either left or right eye means purely monocular. Furthermore, LGN receives contralateral or ipsilateral inputs at the separate layers. Thus, information carried by the retinal cells continues to be segregated at the level of LGN. Magnocellular layer 1 and parvocellular layers 4 and 6 get input from the contralateral eye (nasal retina), whereas magnocellular layer 2 and parvocellular layers 3 and 5 get input from the ipsilateral eye (temporal retina).

The lateral geniculate nucleus receives inputs directly from the retina, and most of the cells send axons on to the cerebral cortex. In this sense, LGNs contain only one synaptic stage which implies simplicity. Thus, this observation may lead to the idea that the LGNs passively relay information from the retina to the cortex. However, LGNs receive fibers also back from the primary visual cortex (layer 6 of primary visual cortex), and from the brainstem reticular formation, which takes part in attention network. Moreover, some geniculate cells make local synapses via their short axons within the nucleus. In this circuitry, direct monosynaptic feedbacks connections form

the excitatory inputs while interneurons in the LGN and the reticular nucleus make inhibitory connections.

The response of the LGN neurons to light is much the same as the response of the retinal ganglion cells. Similarities are that both of them have center–surround receptive field organization, selectivity for luminance increases or decreases, and similar responses to color. Based on their response characteristics, excitatory and inhibitory connections seem to modulate the response of the LGN neurons but do not cause any profound transformation. It is most probably that the major role of feedback is to maintain top–down attention.

2.4 The Primary Visual Cortex

Neurons of lateral geniculate nucleus send their axons through the optic radiations which is a portion of internal capsule and these axons terminate in the primary visual cortex (area V1), or striate cortex (Brodmann's area 17; BA17) in the occipital lobe of the brain. Primary visual cortex, like all neocortex, is divided into six cellular layers which have different properties concerning cell density, cellular morphology, and connections. In primates, due to the laminar complexity, extra letters (Latin and Greek) are used to designate subdivisions of the layer 4 (4A, 4B, and 4C). Concerning cell density, layer 4C and 6 are the highest density layers, while layers 1, 4B, and 5 are the layers with lowest density. Layers 2–3, and 4A have moderate density. There are two major classes of cortical cells; pyramidal cells and stellate cells. All layers except 4C composed of mostly pyramidal cells. Spiny stellate neurons are located in all layers and dominant in layer 4C.

Brief description of input and output connections of visual cortex might shed light on its complexity, although the functional organization of the circuitry is not fully understood. Initially, layer 4C and 4A are the main target of LGN axons. Sublayer 4Cα (upper half of 4C) receives axons from the ganglion cells of magnocellular layers, while sublayer 4Cβ (lower half of 4C) receives inputs from parvocellular layers. Fibers

from the parvocellular layers also terminate in sublayer 4A to a lesser extent. Side branches (collaterals) of the LGN axons that project to layer 4C also terminate in layer 6. Konio cells project to layer 1 and layer 2–3 of primary visual cortex as defined in the previous section.

Subdivisions of Layer 4C (4Cα and 4Cβ) have different projections which implies that separation of geniculate (magnocellular and parvocellular) layers is the starting point of two different pathways and systems. Layer 4Cα send axons to layer 4B, while 4Cβ outputs synapse with the deepest part of layer 3. Neurons in layer 2–3 give rise to axons that terminate heavily in layer 5. Many of the projections of layers 2–3, 4B, 5, 6 have collaterals that make local connections. Layers 1, 4A, and 4C do not send axons out of the cortex. Pyramidal neurons in the layers 2–3, and 4B of visual cortex are the source of projections to other cortical regions. Neurons in the deeper cortical layers send their axons to subcortical targets, including superior colliculus in the midbrain (target of layer 5) and lateral geniculate body (target of layer 6).

Not only the lateral geniculate but also V2, V3, V4, V5 (or MT), MST, FEF, LIB, and inferotemporal cortex send inputs to V1.

2.4.1 Receptive Fields

When a spot of light turns on in the visual field, by using microelectrodes one can record the cells in the retina and LGN responding normally to the light stimulation. However, it is very difficult to find any cells responding the same stimulation in the primary visual cortex. Ineffectiveness of the stimulation is due to the fact that neurons of primary visual cortex respond in a different way. Based on their receptive field type, neurons in the visual cortex can be classified into two main groups: simple cells and complex cells.

Receptive fields of simple cells are arranged in distinct bars (rectangles) with particular range of orientations and on and off antagonistic subregions. Characteristic

receptive field allow simple cells to respond specific orientation and spatial frequency of visual stimulation. When the stimulus is presented in the off region or with an orientation which is different than it tuned, the response of the neuron is reduced. In this sense, the neuron's preferred orientation is the orientation that the most prominent response is recorded.

First model for simple cell receptive field is proposed by David Hubel and Torsten Wiesel, who conducted pioneering studies on this field and also first discovered receptive fields of simple and complex cells. According to their model, several adjacent receptive fields arranged along a straight line and of the same sign (either on–center or off–center) are thought to be converged in the receptive field of simple cell (Figure 2.4). Recent findings continues to support this model.

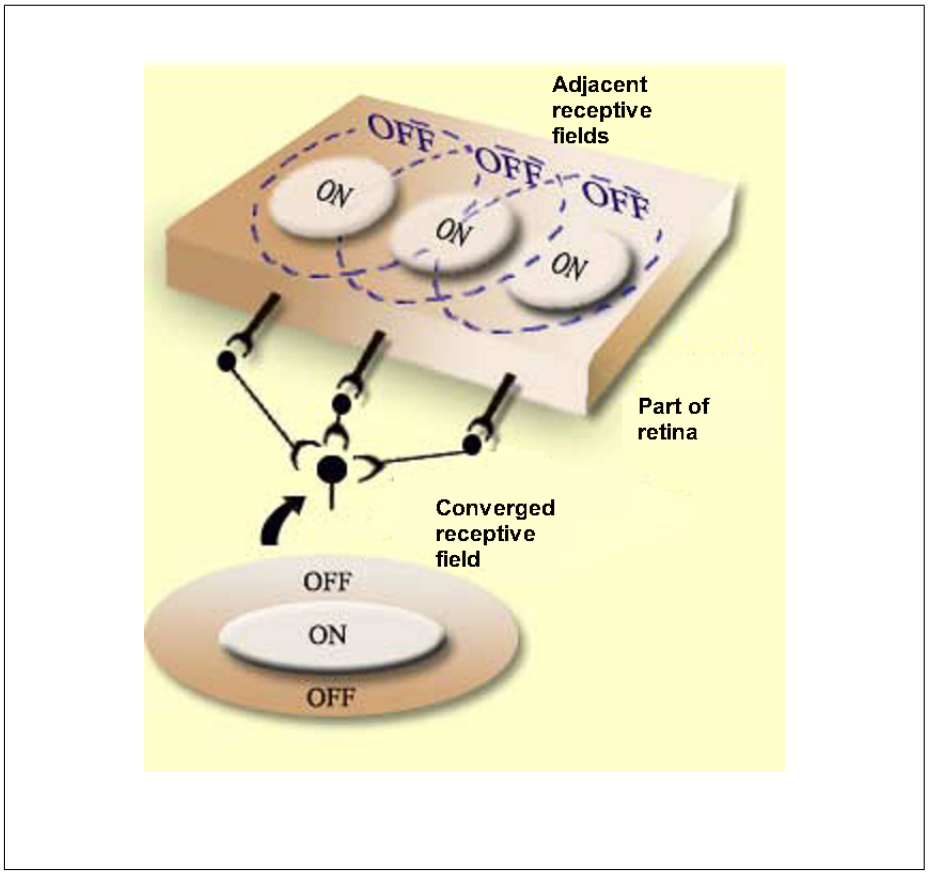

Figure 2.4 The convergence of adjacent receptive fields.

Complex cells have receptive fields with particular orientation and spatial frequency like simple cells but their receptive fields do not have antagonistic surround

subregions. Moreover, receptive fields of complex cells are not sensitive to the location of the stimulus, in other words they are insensitive to spatial phase of the stimulus. Besides, they are insensitive to contrast polarity, which means they response both: increments and decrements of the visual stimulation intensity. Regardless of position and the contrast polarity, complex cells respond the rectangle shaped stimulus with a preferred orientation and width. In the case of more than one preferred stimulation, the response of the complex cell does not increase linearly, thats why, prediction of the stimulus is not possible from the output of the complex neuron.

2.4.2 Columnar Organization

Neurons that play similar roles, functions and have similar properties make spatial groups which constitute cortical organization. Visual cortex is organized in not only layers that is parallel to the surface but also columns which is perpendicular to the surface. Cortical columns have similar functions and properties, which cover preferred orientation of the stimulation, ocular dominance and receptive field location in the visual field. In this sense columnar organization can be separated into two: Ocular dominance columns and orientation columns.

Axons of Lateral geniculate that terminate in visual cortex are individually monocular but from both eyes. Despite the fact that ocular dominance columns receive inputs from both eyes, all the cortical neurons settled in a column have the same eye preference. Figure 2.5 shows the occular dominance map of a cortical patch of V1. Like the eye preference, there are narrow cortical columns in which, cells have similar preferred orientation. This concept is shown by using vertical electrode penetration of the V1 (Figure 2.5). Moreover, in the oblique electrode penetration, it is shown that the preferred orientation changes gradually.

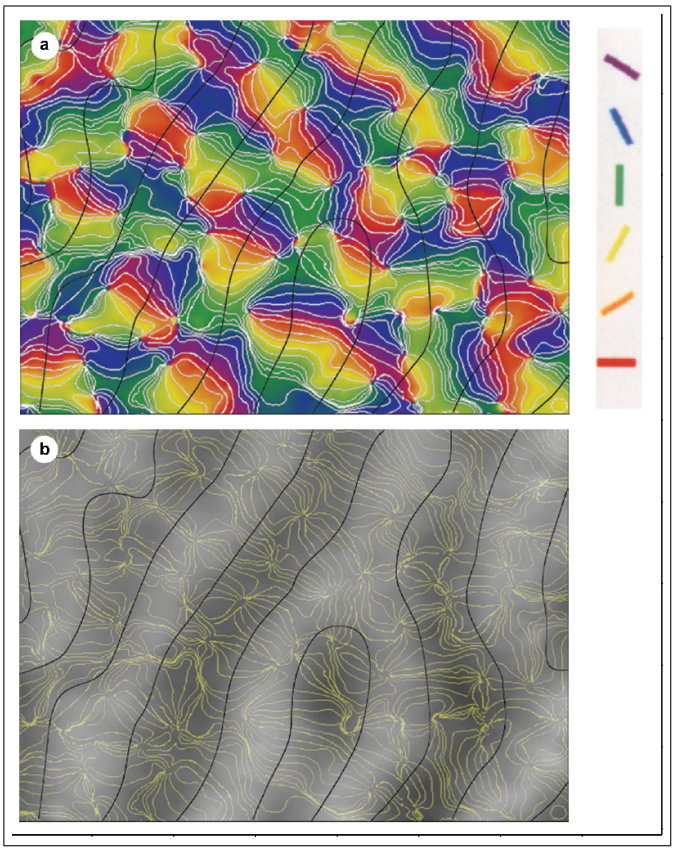

Figure 2.5 (a) Optical imaging map of orientation preference in macaque striate cortex. The layout of columns with different orientation selectivities is denoted by the colour code. The black lines represent the borders of ocular dominance columns. (b) Iso-orientation contours from (a) superimposed on an optical imaging map of the ocular dominance columns [8].

3. NON–INVASIVE MEDHODS FOR IMAGING THE BRAIN FUNCTION

Non–invasive imaging of the brain functions or functional neuroimaging is the utilization of neuroimaging modalities to measure complicated functional activities of our brain. The measurement capability of a modality depends primarily on measured signal which is sensitive to neuronal events, and presence of predefined relation (transfer function) between the changes in the measured signal and the functional activity. In this sense, initially we will discuss basic modalities, in order to define pros and cons of them, source of their signal, analysis approaches, and possible and effective fusion methods. After giving information about study design strategies and stimulus presentation techniques in fMRI recordings, methodology of the data collection covering technical details of the experimental setup, subject recruitment, visual stimulation, and the data acquisition procedures will be presented in this chapter.

3.1 Basic Modalities

Neuroimaging modalities differentiate from each other according to what they display or the source of their signal. Methods that are sensitive to neuronal electrical processes and recording the electrical voltages or magnetic fields of electrical currents are the most direct ways of measuring the neuronal activity, namely Electroencephalogram (EEG) and Magnetoencephalogram (MEG). On the other hand, functional Magnetic Resonance Imaging (fMRI), and Positron Emission Tomography (PET) are important indirect ways of imaging, since they measure chemical activities, hemodynamic, and metabolic responses (e.g. cerebral blood flow) as the results of a functional neuronal activity.

EEG is the measurement of the electrical activity along the surface of the scalp via electrodes that are placed at standard locations known as the 10–20 system. Summed excitatory and inhibitory post synaptic potentials of pyramidal neurons

constitute EEG signals. Besides, measuring potentials on the scalp is only possible with the quasi–synchronous firing of large number of neurons in organized layers due to the low signal intensity [9, 10]. Synchronization of a neuronal network is actually the key concept of EEG rather than summation of neuronal activations [11]. Moreover their orientation must be perpendicular to the scalp surface in order to achieve maximum signal intensity, since the voltage difference between the basal and apical dendrites forms a measurable signal (dipole) and have a direction. MEG is the measurement technique of the magnetic fields that is generated by electrical currents occurring due to the neuronal activities. Array of SQUIDs (superconducting quantum interference devices) is very sensitive and most common magnetometer system that can measure magnetic fields of the brain in the orders of 10–103 femtotesla (1 fT=10–15 T). Despite the sensitivity of the detectors, magnetic field, which is in the detectable range, is produced by approximately 50,000 activated neurons with same orientation (such as pyramidal neurons). In a modern MEG device, more than 300 SQUIDs placed in a helmet shaped vessel and allowing measurements over the head. Since ionic currents produce an orthogonally oriented magnetic field, detectable signal is produced mainly by the pyramidal neurons that are oriented tangential to the cortical surface.

There are important differences between EEG and MEG in spite of the similarity of the source of their measured signal. Electrical fields are distorted by scull and scalp more than the magnetic fields, that's why MEG signals represent more precise data about activations than EEG. However, intensity decay of magnetic field with increasing distance is more than that of electrical field, thus EEG covers more brain areas than MEG. Direction of the signal source is more important for MEG recordings, that is, activations with tangential direction are detectable with EEG to some extent but radial components of an active area are not detectable with MEG. Unlike MEG, EEG recording needs a reference point for measurements. Besides, MEG recording requires a specific shielded room and stable subjects, on the other hand EEG is portable and more flexible than MEG.

EEG and MEG are the most direct ways of measuring neuronal activities, thus excellent for tracking time–course of activities with high temporal resolution (on the

order of milliseconds). This property alone makes them indispensible for functional neuroimaging studies. However both have limitations. First of all, localization of activated areas (sources) within the brain by using the measurements on the scalp namely inverse problem is complicated and does not have a unique solution. Even feasible solutions can be obtained for cortex, it is difficult to provide sufficient and reliable inverse problem solutions especially for subcortical regions. In a nutshell, poor spatial resolution is the primary limitation of EEG and MEG. Secondly, source of the EEG and MEG signals are in the vector form, thus covers addition and subtraction of activations at different locations which may cause misleading in data interpretations. In other words, existence of the neurons with variable orientation and loss of synchrony means invisible brain regions for both: EEG and MEG. Thirdly, EEG and MEG give information about the activations but not about the structure and anatomy of the brain. That's why data is presented as combined images in terms of activation overlaid anatomical/template images. In order to overcome limitations of EEG and MEG, one has to take into account information that the other neuroimaging modalities hold.

Functional MRI monitors neuronal activities by measuring signal intensity changes in the brain images with relatively high resolution (millimeters). The most widely used fMRI technique is Echo Planar Imaging (EPI) which is based on the monitoring of blood oxygenation level–dependent (BOLD) effect [12, 13, 14]. BOLD effect is the change in image intensity coupled mainly with deoxy–hemoglobin (HbR; hemoglobin without bound oxygen molecules) content of the blood. Since, BOLD–fMRI technique is sensitive to the changes in magnetic susceptibility, increase and decrease of paramagnetic deoxy–hemoglobin content in the diamagnetic plasma of the blood induce signal intensity changes. Besides, blood oxygenation level is highly correlated with neuronal activity in terms of neuro–vascular coupling which is a mechanism for adjusting hemodynamic responses according to local metabolic needs. Thus, BOLD signal changes in time–domain occur due to the combined effects of cerebral blood flow (CBF), cerebral blood volume (CBV), and cerebral metabolic rate of oxygen (CMRO2) which are the hemodynamic, vascular and metabolic responses triggered by neuronal activities.

Relatively high spatial resolution of fMRI allows us to localize activated areas

more precisely. However, hemodynamic response period of the BOLD signal initiated by a neuronal activity lasts over several seconds, because of the slow vascular response. Thus, it takes much more time to get a significant change in BOLD signal when compared with the underlying neuronal process. In this sense, main disadvantage of fMRI is its slow response time, which makes the analysis of fast neuronal dynamics difficult and results in overlapping of BOLD signal changes generated by different individual events.

PET is a nuclear imaging technique which depends on measurement of positron emissions from radioactively labeled chemicals that are metabolically active and injected into the blood stream. Radioactively labeled compounds (radiotracers) can be detected from the outside of the body by PET scanner and specialized three–dimensional image reconstruction techniques with the spatial resolution which typically falls somewhere between that of fMRI and EEG/MEG. Various organic molecules which accumulate or participate and perform functional metabolic activity in the brain, can be labeled with PET isotopes and used as radiotracers. For instance, one can use Fluorodeoxyglucose (18F–FDG), as a glucose analog, to monitor the distribution of glucose uptake and coupling synaptic activity. In addition, regional CBV or CBF can also be measured with different radiotracers. However, PET has a very low temporal resolution (tens of seconds to minutes) due to the hemodynamic or metabolic utilization process in the body. Besides, number of measurements made on a subject is limited due to the radiation exposure.

Among these modalities, EEG and fMRI are promising candidates that can give hand to achieve localization of activities with both high temporal and spatial resolution by the possibility of simultaneous acquisition. Before that, experimental designing is the critical issue of fMRI. Since fMRI is an indirect way of functional imaging, and fMRI signal represents combined effects, comparison strategies are necessary in most cases and will be mentioned in the fallowing sections briefly.

3.2 Task–Related FMRI Experiment; Design and Strategies

At the beginning of an fMRI research, main hypothesis is formulated, and suitable stimulus and paradigm are selected and adapted into this formula. Paradigm can be defined as a temporal pattern of an experimental structure that models predictions of the functional and cognitive outcomes during the fMRI experiment. Many possible sensory stimuli are applicable to evaluate, modulate or interfere with brain dynamics, and different types of periods with or without stimulation in the temporal pattern is called condition. Besides, desired cognitive or functional effects are mostly the products of comparison of conditions, and comparison strategy is the core of a task–related paradigm design.

Among the fMRI studies, subtraction is the most popular comparison strategy of the task–related paradigms. Main effect is achieved by subtracting effects of two (or more) conditions, namely 'active' and 'control' conditions. In essence, this technique is based on the assumption of that, desired effect (effect of stimulation) is added onto the activities of control condition (e.g. intrinsic activities) without any interaction among them during the active condition. It is actually difficult to separate activities and assume pure insertion while considering highly integrated functional networks of the brain. Nevertheless, unimodal association areas such as primary visual area might be more suitable for this type of strategy due to their single sensory information processing property. Moreover, this technique is easy to implement and suitable for canceling background noise, and intrinsic activities which lasts during whole fMRI scan and not easy to model.

Interaction between components is highly complicated if there is not enough complementary data and sufficiently detailed definition of cognitive components. In order to characterize or investigate interactions, factorial comparison strategy, which implements conditions including different subsets of cognitive components, can be used as an alternative of subtraction analysis. Subsets of components are empty subset (condition without any cognitive component), multiple subsets (condition with more than one cognitive component), and single subsets (condition with one cognitive compo-

nent). BOLD response resulting from a single cognitive component can be achieved by subtraction of two conditions including single and empty subsets. Alternatively, effect of same cognitive component can be achieved by subtraction of two conditions including double and single subsets if there is no interaction. Differentiation of these two subtraction process in the factorial design allow us to investigate interactions.

Conjunction analysis is another way of dealing with interactions. In this approach instead of subtraction, intersections of conditions are used. Conditions including more than one cognitive component and sharing same desired particular component are presented and areas that show common BOLD response pattern are detected. In a similar way, subject differences in a group can be eliminated without changing conditions by finding activated areas that are common among subjects. Separating cognitive components in a condition is not easy to implement because in many of the cases multimodal stimulations or responses are needed, and highly correlated functions accompany main processes. In this sense, conjunction analysis could be helpful to purify basic processes involved during particular cognitive component.

In addition to the interaction effects among cognitive components, analyzing the particular component and the effect of its difficulty level on the BOLD response is possible with parametric design. Parametric design is based on the increment of cognitive demand of a component without changing its way of processing in the brain and presenting different difficulty levels in different conditions beside control condition. Changing difficulty level is important in the case of multiple active regions are found significantly correlated with a single cognitive component. Factorial design might help us to find specific anatomical regions which have a BOLD response changing with difficulty levels of the task and differentiate basis of the main process. However, if task is difficult more than a certain level, neuronal networks mostly share the weight, and increasing the cognitive demand often results in participation of other networks which makes parametric approach not easy to implement.

There are also other alternative comparison strategies which are mostly modified or combined versions of subtraction, parametric, factorial, and conjunction analysis in

the literature. Main concern in paradigm design and strategy should be consistency with the hypothesis of the study.

3.3 FMRI Protocols for Stimulus Presentation

Functional MRI experiments have two main types of protocols; stimulus driven, and resting–state. Stimulus driven protocols use any sensory stimuli to generate activity of the desired function in the brain and constitute conditions to evaluate the outputs as described in the previous section. Besides, without any experimental manipulation or stimulation, neuronal networks produce intrinsic activations, and these spontaneous brain activities are in the scope of resting–state scans.

Stimulus presentation strategies are mostly determined by considering properties of stimulation processing phases of the brain, and response properties of the measured BOLD signal. Various presentation strategies including blocked, event–related, and combined designs are applicable for stimulus driven fMRI experiments.

In the block design, conditions, which are presented with certain duration, covers repetitively or sequentially presented stimuli in order to maintain a certain cognitive task. Duration of a condition (block length) is mostly determined while considering the BOLD signal increase that is aimed to achieve for significant results. High BOLD signal change relative to the event related design makes experiments statistically more powerful. However, the most important drawback of the block design comes from the cognitive aspects. Presenting same kind of stimulus may cause adaptation, low expectancy for change, and low attention level. On the other hand, event related design reduces prediction and increases attention of the subject since each successive stimulation does not necessarily similar. Besides, event–related design allows us to analyze and detect transient variations of BOLD signal due to the unexpected or short term events. Unexpected events may emerge due to the internal processes such as epileptic seizure or hallucinations. However, event related experiments are time consuming because in order to prevent overlapping, inter stimulus interval (ISI) of different conditions must

be long enough. ISI is mostly chosen to cover dispersion of the BOLD response (spreading out of the response about 12–20 s) which is generated by the previous stimuli. As an alternative way to deal with long lasting event related fMRI experiments, ISI can be shorten by utilizing varied ISI namely rapid–presentation (jittered) event related design with a minimum of 4s, since the time to peak during stimulation is commonly observed about 4–8 s. Short ISI increases statistical power and efficiency due to the increased number of stimuli, while decreasing efficiency with overlap. Arranging and optimizing order of the conditions in a controlled manner (pseudo–random) is also another important way of increasing statistical power.

3.4 Methodology of the Data Collection

Forty healthy volunteers (20 female, 20 male; mean age 25.8 ± 3.7 years) without any sensory system related pathology and neuro–pschiatric history took part in the study. All subjects had normal or corrected-to-normal vision acuity. Ethical approval was obtained from the local ethics committee of Istanbul University, Istanbul Faculty of Medicine prior to commencing the study. Every participant was informed about the procedure and signed informed consent before the application of the experiment. The subjects were instructed to sleep at their habitual bedtime to prevent feeling sleepy during the experiment.

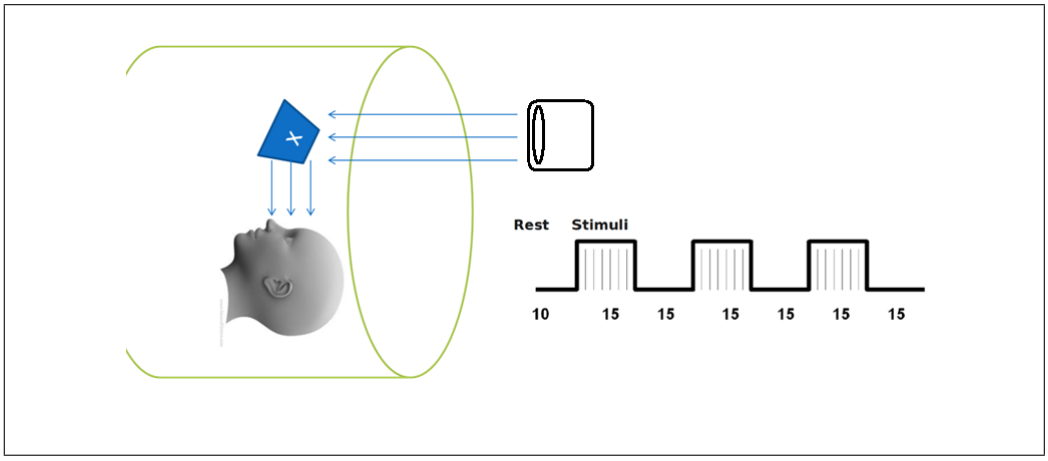

Figure 3.1 Demonstrative figure of experimental setup.

The visual stimuli were reflected on a white surface by a flashing light at temporal frequencies of 6, 8, 10, 12, 14, 18, 22, 26, 30, 34, 38, 42, and 46 Hz. Light was "on" during the half time of a period, thus the energy was constant across all frequencies. Light source was an electro–magnetically isolated set of light emitting diodes (LED) driven by a digital I/O card (NI DAQCard–6062E) and located one meter away from the rear side of the magnet. Screen was a rear facing 45° inclined diffuser surface (field of view 54.8°) attached to the top of the head coil of the MRI system and used for diffuse reflection of the exposed light (Figure 3.1). Subjects' task was to maintain focus on and to view passively the fixation cross drawn on the center of the reflection surface.

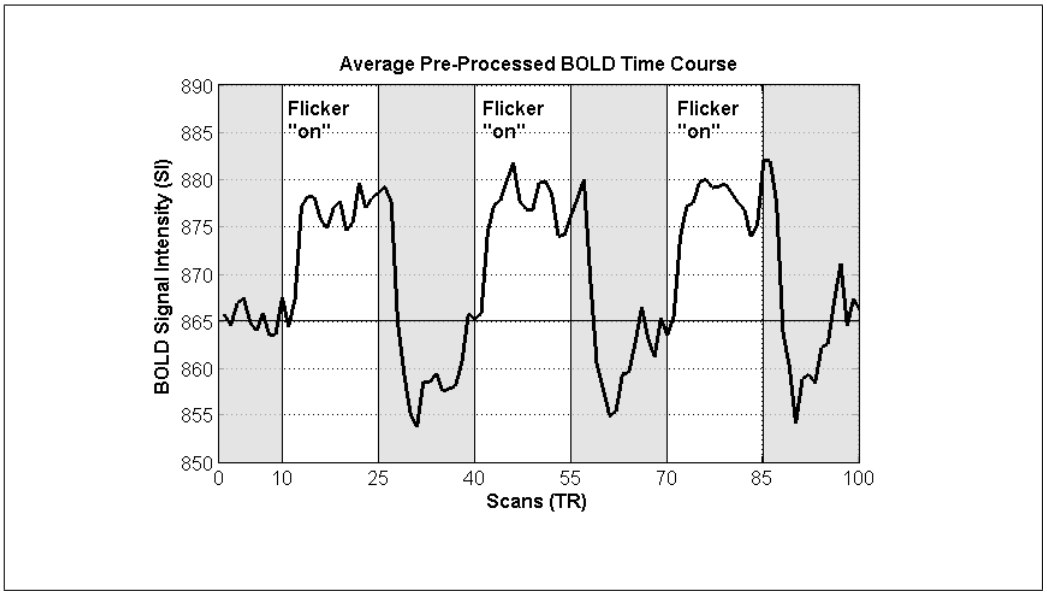

Figure 3.2 Experimental protocol and average pre–processed BOLD response of the subject ABA.

Stimulus (flickering light stimulation), and rest (stimulus–free) conditions were used in the experiment. Time periods of conditions were defined based on the duration of a dynamic scan (2.981 s) by utilizing "external device synchronization output" of the MR scanner detected via digital I/O card. Signal output of digital I/O card and synchronization output of MRI scanner were connected with EEG amplifier to simultaneously register event markers on the EEG trace. Stimuli were delivered during 15 dynamic scans (44.7 s), followed by rest periods with same length. In each functional scan, sequence was initiated with a rest period lasting 10 dynamics and three consecutive stimulus and rest periods were presented (totally 100 dynamics)(Figure 3.2).

There were thirteen separate scans for each flickering frequency. Order of scans was randomized to avoid any bias on BOLD responses.

3.4.1 MRI Data Acquisition

Magnetic resonance imaging was performed using a 1.5T Philips Achieva MRI system equipped with SENSE–Head–8 coil at NPISTANBUL Neuropsychiatry Hospital, Istanbul. At the beginning of each experiment, routine cranial MRI examination was performed to detect possible abnormalities in healthy subjects. Additionally, whole–brain high resolution structural scans were acquired using a T1–weighted MPRAGE sequence with voxel size of 1.25x1.25x1.2 mm (130 sagital slices, TR/TE = 8.6/4.0 ms, acquisition matrix 192x192, scan duration 369.8 s). Thirteen functional scans were acquired using T2*–weighted gradient echo (GE), echo planar imaging (EPI) with identical scan parameters (100 dynamic scans, 32 axial slices, slice thickness = 4 mm (without gap), in–plane resolution = 3.59x3.59 mm, FOV = 230 x 230 mm^2, TE = 50 ms, TR = 2981 ms). Two dynamics were acquired prior to each fMRI scan in order to obtain tissue magnetization. Subjects were allowed to rest among fMRI scans to relax their eyes without changing scan positions.

3.4.2 EEG Data Acquisition

EEG was recorded simultaneously by using an MR compatible EEG amplifier (BrainAmp MR+, Brain Products, Germany) with 30 channels EEG (extended 10/20 system) and 1 channel ECG. The EEG signal filtered between 0.01 and 250 Hz was digitized with a sampling rate of 5 kHz. The clocks of the MR scanner and the EEG digitizer were synchronized using a hardware (SynchBox, Brain Products, Germany) to obtain MR gradient artifacts as a constant waveform in the EEG recordings. Gradient artifacts were removed according to the Average Artifact Subtraction (AAS) method described by Allen and coworkers [15] implemented in the Brain Analyzer software (Brain Products, Germany). After this procedure, the ballistocardiographic (BCG)

artifacts were removed with a similar technique based on an average template of the BCG artifact using the timing of the R wave in the ECG trace [16].

4. BOLD–FMRI SIGNAL CHANGES IN RESPONSE TO TEMPORAL FREQUENCY OF THE VISUAL STIMULATION

4.1 BOLD Response and Model-Based FMRI Analysis

4.1.1 Raw BOLD Response and Transients

Intrinsic BOLD contrast mechanism of functional MR imaging was described shortly in the chapter 3. Here, we will discuss BOLD effect and time course of the response to a brief transient stimulus. Many BOLD fMRI study uses model of the activity induced BOLD response while conducting model based analysis. However, it is important to note that the main concern is the signal change that corresponds to stimulus mediated activities, not the spontaneous BOLD fluctuations which can be found with a detailed description elsewhere [17].

BOLD signal is altered by magnetic susceptibility change which is closely related with the magnetic properties of deoxy-hemoglobin (HbR-paramagnetic) and oxy-hemoglobin (HbO2-diamagnetic) concentration. Ogawa et al. [14] presented in their pioneer work that decrease of HbO2:HbR ratio decreases the BOLD signal. As a result HbR concentration is the basic physical parameter to which MR signal is sensitive. It has to be highlighted that fMRI BOLD signal is not direct representative of the neuronal activity, instead combined changes in CBF, CBV, and CMRO2. As a result of a short transient stimulus, combined effects of CBF, CBV, and CMRO2 result in a time course presented in figure 4.1. BOLD response curve which is comprised of transient compartments with positive response is termed hemodynamic response signal.

First transient effect is initial dip which is defined as the early negative BOLD response. This response is not always observable due to the small intensity change for a short time period. Initial dip is a potentially important fast signal but source of it is

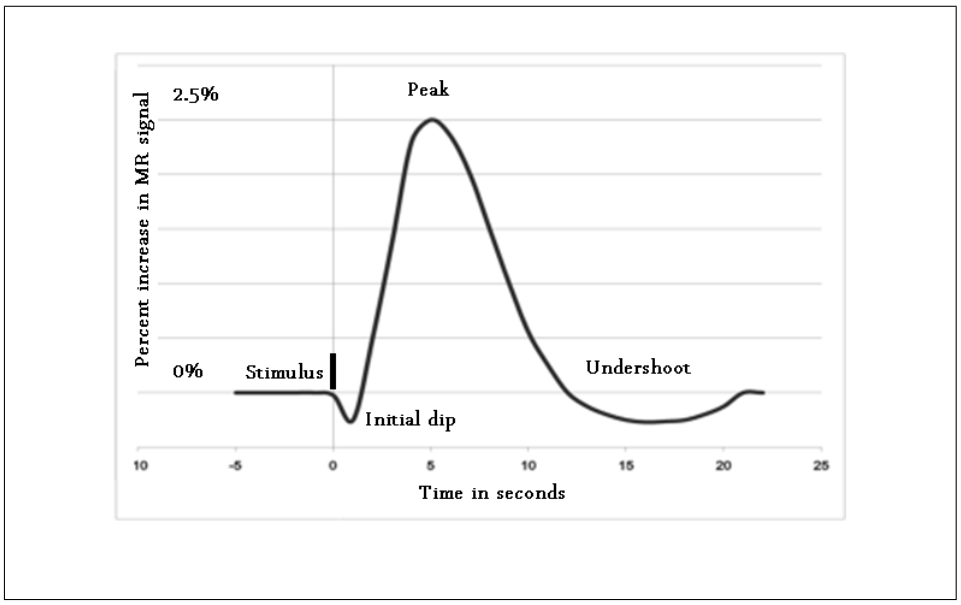

Figure 4.1 Demonstration of hemodynamic response signal to a brief stimulation.

a controversial issue. It is proposed that the reason of the initial dip is rapid increase of CMRO2 before CBF start to increase [18]. According to this hypothesis, initial dip has a potential to localize activation with superior sensitivity because of the close relation between neuronal activity and O2 metabolism. In essence, potential benefits will probably attract further investigations.

BOLD signal starts to increase 1–2 seconds after stimulus onset and reaches a peak in 4–6 seconds. Most significant signal change is positive BOLD response. Positive response is described by the higher increase of CBF response triggered by activity than the increase of CMRO2. Actually, expectation about the BOLD signal might be the decrease due to the HbR concentration increase caused by neuronal activity or no observable change in the signal due to the compensation of the HbO2:HbR ratio. However, concentration change is in favor of the HbO2, thanks to the flood of oxygenated blood driven by the CBF and washout of HbR. This situation was presented by Malonek and Grinvald with a popular quotation "watering the entire garden for the sake of one thirsty flower." [19].

Post stimulus undershoot (PSU) is negative deviation of the signal intensity from the baseline, following the positive BOLD response. PSU response begins to be

prominent about 6 seconds after the peak and continues up to 30 seconds after the stimulus offset. PSU can be treated as the indicator of HbR accumulation. Thus, it can be explained by rapid return of CBF to its baseline while there is a delayed return of CBV. Alternative hypothesis and various theories can be found in the literature [20, 21].

4.1.2 Pre–Processing of fMRI Analysis

Analysis of the fMRI BOLD signal acquired during a stimulus driven paradigm is typically conducted by utilizing a unit response model, namely hemodynamic response function (HRF) (Figure 4.1). Aim of the HRF is to identify variance of the BOLD signal while detecting neuronal activity which is correlated with the paradigm. In this sense HRF must hold a background in the physiology of the neuronal processes and act like a transfer function between neuronal activity and BOLD signal. Besides, in order to construct postulated BOLD time course successfully, the model must have sufficient variability. However, a large part of the variance in the BOLD signal does not arise from the neuronal activity but from the technical limitations. Thus there is a pre–processing part in order to overcome drawbacks of the fMRI scan and increase signal to noise ratio (SNR).

First step of the pre–processing stage is the motion correction. MR machine acquires the data from the predefined spatial location regardless of the content. Even the head of the subject was fixed; it is not possible to prevent the movement of it during the scan. Thus location of a tissue in the space and the corresponding voxel of the acquired volume might change. Movement of the head in the acquired volume is corrected by the rigid body transformation. This transformation is limited to the translations (in X, Y, or Z direction) and rotations (over X, Y, or Z axis). The motion correction or in other words spatial realignment algorithm tries to minimize the square of distance between the source and the target images. After the correction in spatial domain, second step is generally the correction in the time domain which is the slice timing correction. It is a fact that every slice in a functional EPI volume has a different

time point, since scanning each slice takes some time. If the order of slices is regular–up then there would be a sampling time gap between lower and upper slices in the order of seconds. It is important to shift the postulated or real BOLD time course based on this time gap and acquisition order, especially in the event related fMRI experiments or if the model is not sufficiently flexible. Next step is used as a spatial filtering by means of smoothing. Smoothing process has the tendency to blur images by eliminating details. In this sense, smoothing emphasize background or wide spread signal changes which is dependent to the properties of the spatial filter. Smoothing algorithm averages each voxel with its neighbors by using a weighting matrix defined by a 3D Gaussian kernel. The amount of smoothing is given by the full width at half maximum (FWHM) parameter of the Gaussian kernel. FWHM parameter must be decided based on the expected spatial scale of the hemodynamic changes while considering the loss of resolution. In the case of the small spatial scale, limited degree of smoothness should be selected however the smoothness needs to be greater than the voxel size [22].

After the pre–processing stage, a model of the expected BOLD signal during the experiment is created by using multiple regressors in a general linear model (GLM).

4.1.3 General Linear Model (GLM) and Statistical Analysis

General framework of the model based fMRI data analysis includes three main parts. First part is the model specification, second is the parameter estimate, and the last part is the statistical inference. General linear model is the most common way and the core model of functional data analysis. It is the linear combination of the predictor variables which represent effects of interests and confounds. GLM helps us to give the meaning of BOLD signal changes correlated linearly with predictor or explanatory variables. Since it is not clear that which anatomical region(s) will respond to which experimental condition, conducting same analysis for all voxels will give estimated results with different weights for each voxel and condition (mass–univariate approach). Results of fMRI analysis are the activation maps derived from these estimated weights

by contrasting and statistical inference (thresholding).

BOLD time series of a given voxel is the serial observations of consecutive dynamic EPI scans during an fMRI session. In an example, 100 dynamic EPI scans (volumes) in an fMRI session means 100 samples of BOLD time series of each voxel (volume x element) in the brain. This data can be express as a vector y_i, $i = 1 : N$, where N is the total number of volumes, one taken every few seconds, or samples corresponding to specific time points. Response model is the weighted sum of "regressors" which is the combination of explanatory variables of the data, and the residual (zero mean) error. Each regressor can be modeled as separate vectors x_{ik}, $k = 1 : K$, where K is the total number of regressors in the model. Weights of regressors are the unknown β_k parameter which can be referred to as regression parameters or effect size, unique to each regressor. β_0 is a constant corresponding to the mean value of time series. e_i is the noise of the fMRI data (Eq.4.1).

$$\begin{aligned} y_1 &= \beta_0 + \beta_1 x_{11} + \beta_2 x_{12} + \ldots + \beta_K x_{1K} + e_1 \\ y_2 &= \beta_0 + \beta_1 x_{21} + \beta_2 x_{22} + \ldots + \beta_K x_{2K} + e_2 \\ &\vdots \\ y_N &= \beta_0 + \beta_1 x_{N1} + \beta_2 x_{N2} + \ldots + \beta_K x_{NK} + e_N \end{aligned} \tag{4.1}$$

Vector and matrix notation of Equation 4.1 is

$$Y = X\beta + e \tag{4.2}$$

All measured data (time course) of one voxel are grouped into Nx1 vector Y. The NxK matrix X is design matrix including modeled effects or explanatory variables. Regression parameters are grouped into Kx1 vector β. Noise terms are grouped into

Nx1 vector e. Since β_0 is the mean value, it can be subtracted from the data before GLM analysis or can be inserted into the variables: X and β.

Parameter estimate which can be define as the estimation of model parameters (β) is the next step of GLM analysis. This estimation process is to find the parameters that allow the best fit to the observations (maximum likelihood) because there are far more unknown variables than equations. In this sense, aim is to minimize the sum of square difference (Eq.4.3) between the observations and the model by using ordinary least squares. This difference (S) minimizes when the gradient vector or derivative with respect to β is zero.

$$S = \sum_i e^2 = \sum_i (Y - X\beta)^2 \tag{4.3}$$

We can derive normal equations by rearrangements in the derivative of equation 4.3. Matrix notation of normal equations and least square estimates can be written as:

$$\begin{aligned} X^T Y &= (X^T X)\hat{\beta} \\ \hat{\beta} &= (X^T X)^{-1} X^T Y \end{aligned} \tag{4.4}$$

where $\hat{\beta}$ represent estimated model parameters.

Critical assumption in this part is the Gaussian distribution of the noise (e). However, there are lots of factors that produce residuals such as thermal noise, cardiac and respiratory rhythms, unmodelled brain activities, and spontaneous activities of intrinsic networks. Thus in practice, the data without any stimulation is temporally autocorrelated. As a processing state this autocorrelation can be cancelled out by using pre–whitening temporal filter or pre–colouring. Alternatively, there are Bayesian strategies dealing with this problem in the literature.

After fitting GLM to the BOLD time series of the voxels, estimated weights

of the explanatory variables are achieved. However, finding a non–zero value is not enough to evaluate results for the significance. Since the parameter estimates of β are calculated from the noisy fMRI data, level of significance must be defined according to a valid statistical manner. Parameter estimates of β most frequently represented by T–statistics:

$$t = \frac{\hat{\beta}}{std(\hat{\beta})} \tag{4.5}$$

In equation 4.5, $std(\hat{\beta})$ is the standard deviation or uncertainty. Increase of parameter estimate relative to its uncertainty increases significance of T–statistic, t. However, in order to state that null hypothesis ($\beta = 0$) is rejected, T–statistic must be compared with the distribution of T–statistics for the desired level of confidence. It is assumed that the distribution of the noise is Gaussian (normal distribution) in fMRI data. Thus p–value can be calculated easily. However statistical inference is not such simple.

Significance of a single explanatory variable could be evaluated by aforementioned procedure. However, there are typically more than one condition in an fMRI experimental paradigm as described in the following text. Besides, relations among the explanatory variables might be the answer of the formulated hypothesis. In most cases, answers to the main question of the experiment necessitate combining different regressors of the model representing different conditions based on the paradigm design. At this point, linear combination of parameter estimates is defined as contrast. Contrast vector c and parameter estimates of β are the vectors with the same size (P x 1) and their multiplication gives contrast of parameter estimates. For example, if finding the difference between two conditions is the aim of contrast ($\beta_1 - \beta_2$), transpose of column vector $c = [1 \ -1 \ 0 \ 0 \ \ldots \ 0]$ and column vector $\beta = [\beta_1 \ \beta_2 \ \beta_3 \ \beta_4 \ \ldots \ \beta_P]$ should be multiplied ($c^T\beta = \beta_1 - \beta_2$).

Similarly, T–statistic can be derived by dividing the contrast with its standard

deviation:

$$t = \frac{c^T \hat{\beta}}{\sqrt{var(c^T \hat{\beta})}} \tag{4.6}$$

In the equation 4.6, variance of contrast and estimated variance of noise are defined as follows:

$$\begin{aligned} var(c^T \hat{\beta}) &= \hat{\sigma}^2 c^T (x^T x)^{-1} c \\ \hat{\sigma}^2 &= \frac{(\hat{e}^T \hat{e})}{(J-P)} \\ \hat{e} &= Y - X\hat{\beta} \end{aligned} \tag{4.7}$$

where, $\hat{e}$ is the estimated error term.

In order to find p–value, T–statistic is compared with distribution of the T–statistics having J–P degrees of freedom, where J is the number of time points (N), and P is the number of parameters (Rank(X)). Additionally, the formula of the t–value (Eq.4.6) gives one–sided results. That is to say, the contrast of the difference $\beta_1 - \beta_2$ searches for the cases in which β_1 is higher than β_2. In order to search for higher β_2 a different contrast should be defined $c^T = [-1\ 1]$.

Alternative combinations of parameter estimates or contrasts give answers to different questions. For instance, contrast of $c^T = [1\ 1]$ can be used to find significance of the average $\beta = ((\beta_1 + \beta_2)/2)$. It is important to note that this contrast example does not represent the union of two conditions $(\beta_1 \cup \beta_2)$. If ones concern is for finding the union of conditions, then $c^T = [1\ 1]$ is not the correct contrast for the answer. In order to investigate significance of conditions together but in a separate manner, F–tests should be introduced with two contrasts: [1 0] representing β_1 and [0 1] representing β_2.

F–tests can be used to answer such kind of questions: "Is there any contrast in a set of contrasts significantly different from zero?" As can be understood, there are more than one contrast and they are tested for significance simultaneously. There is

an F–test contrast matrix, c, of size PxK with contrasts in its columns. Calculation of F–statistic, f, can be made by contrast matrix c:

$$f = \frac{\hat{\beta}^T c(\hat{\sigma}^2 c^T (x^T x)^{-1} c)^{-1} c^T \hat{\beta}}{K} \tag{4.8}$$

where, K is the number of contrasts.

In the F–test null hypothesis states that all the contrasts are zero ($c^T\beta = 0$). Besides, F–statistic is F–distributed with degrees of freedom K and $N-P$. Additionally, F–test is not sensitive to the directionality of the contrasts. For instance, [1 0] and [−1 0] give the same result. In this sense, two tailed t–test can be conducted by using F–test.

Results of T–test or F–test are three dimensional (3D) statistical maps or SPMs. At this point, a simple inference method can be used to detect significance threshold (u) in order to reject null hypothesis (t>u) namely voxel–wise inference. Due to the mass univariate strategy of the fMRI data analysis, spatial information of 3D voxel data is not taken into account. In this context, cluster–wise inference methods were introduced as an alternative to voxel–wise inference. Cluster–wise inference uses a cluster–forming threshold (u_c) to define binary map and searches for the clusters including more than k voxels. In other words statistical test is performed for each cluster and null hypothesis is rejected in the case of cluster size bigger than k. Both methods are applicable for different situations. Friston et al. presented theoretical power analysis of distributed activations and showed that cluster level inference is more powerful than voxel level inference. On the other hand, localization power is higher in the voxel level inference compared to cluster level inference. Actually, cluster-wise inference is more common than voxel-wise inference because of the spreading effect of spatial smoothing.

Statistical inference methods control the allowed risk of false positives for a single measurement. However number of false positive results is increased by the number of multiple tests or measurements. As an example, if the allowed risk of false positives is $\alpha = 0.05$ in an fMRI experiment typically measuring 20000 brain voxels, then 1000

false positive active voxels would be expected. Since this situation is not acceptable, false positives should be controlled over all voxels or clusters. The standard measure is the probability of making one or more false positives among all tests, familywise error (FWE) rate. Bonferroni correction is a famous FWE rate control method. In this method FWE–corrected P–value threshold is determined by dividing FWE rate by the number of tests. In our example FWE–corrected new α will be 0.0000025 in the case of $\alpha_{FWE} = 0.05$. Bonferroni correction is the most conservative method to control FWE rate. On the other hand, spatial smoothing procedure makes the voxel data close to their neighbors. However, there is not any concern about the similarity among the tests in Bonferroni correction. Thanks to the random field theory (RFT), FWE is controlled while considering effect of spatial smoothing procedure.

Meaning of the spatial smoothness in RFT is the increase of spatial dependence of the tests while decreasing the resolution. This situation introduces a new definition RESEL (resolution element) instead of voxel (volume element). RESEL count of a volume can be calculated by FWHM parameter of spatial smoothing and the number of voxels, I.

$$RESEL_{count} = \frac{I}{(FWHM_x FWHM_y FWHM_z)} \tag{4.9}$$

RFT states FWE corrected voxel–wise inference for Z-statistic images as follows:

$$P_{vox}^{FWE}(z) = RESEL_{count}(2\pi)^{-2}(z^2 - 1)exp(\frac{-z^2}{2}) \tag{4.10}$$

As can be seen in the equation 4.10, if we want to have lower P–values without significant change in z, we have to decrease RESEL count which implies increase in the level of smoothing. Similarly, if the smoothness of the data is low, z values must be high for significance due to the exponential term.

There are assumptions in the RFT. First of all, the distribution of the activities in the brain is assumed to be Gaussian. Besides, smoothness of the data is assumed to be sufficient, constant and have an exact FWHM value. It is not possible to verify these

assumptions. Moreover, RFT is still a quite conservative method. Thus, alternative methods are developed by many groups.

4.2 Visually Driven Thalamo–Cortical Oscillations: Implications from Temporal Frequency Response Characteristics of LGN and V1 Using FMRI

Visual stimuli at various temporal frequencies have been used extensively as a convenient tool in order to investigate the frequency response of the visual system [23, 24, 25]. Differentiation of the output to visual input with a certain temporal frequency (or in a particular frequency band) from those to the remaining stimulation frequencies is regarded to reflect the temporal frequency selectivity hence the intrinsic tuning of the visual system.

As thalamo–cortical loops are one major source of oscillatory neuronal activities in the brain, determination of the frequency characteristics of the lateral geniculate nucleus (LGN) and the primary visual cortex (V1) is essential in order to evaluate the temporal frequency selectivities of the visual system. LGN is the main source of visual information for V1 and the main target nucleus of optic tract which receives 90% of the retinal outputs [5]. On the other hand, proportion of the retinal inputs among total synapses in LGN is 30–40% in the primates [26], which implies that majority of the inputs are extraretinal and have a modulatory effect rather than being the driver [27]. In addition to the synapses of the LGN interneurons and of thalamic reticular nucleus, V1 is the structure with largest number of synapses in LGN carrying feedback signals from the cortex to thalamus [26]. Therefore, LGN is an important site for the modulatory effects on visual input and therefore can play an important role in the temporal frequency tuning of the visual system. Although LGN has a relatively small volume, its activities can still be measured in fMRI [28, 29, 30].

There are various fMRI studies reporting BOLD activity changes due to the

temporal stimulation frequencies [31, 32, 33, 34, 35, 36, 37, 38]. However, presented results do not formulate a consensus due to several reasons. One of them is the probable confounding effect of the spatial properties of the patterned stimuli used. This seems to be a common problem with the studies that used retinotopic mapping scans for identifying V1 region [31, 33, 39]. Their contradictory results on temporal frequency characteristics probably depend on the various spatial properties of the visual stimuli that were used to activate the V1 region. Therefore, possible interaction among temporal and spatial frequency [40] should be taken into consideration while comparing the results. Furthermore, these studies reported BOLD responses at only three or four temporal frequencies with limited overlap while defining frequency response characteristics of V1.

Another reason of conflicting results might be the definition of the region of interest (ROI). Studies creating ROI with limited number of active voxels in V1 [34, 35, 38] have reported increasing BOLD response with increasing temporal frequency that reaches a peak around 6–10 Hz continuing with a plateau. In contrast, studies calculating BOLD response in a broader area covering V1 and extra–striatal areas reported a band pass response with a peak at approximately 8 Hz [36, 37].

A common disadvantage of all these studies except the one by Singh et al. [37] is the logarithmic sampling of temporal frequencies because of the obligation to use integer multiples of the refreshing period of the raster screens used.

In order to overcome these drawbacks, we used diffuse light stimuli without any spatial pattern and contrast to avoid potentially confounding effects of spatial frequency which may result in incorrectly derived conclusions about the effects of the temporal stimulation frequency on the BOLD response. Besides, LED light sources have been used that have no limitations concerning the selection of stimulation frequencies unlike screens with constant refresh rates. This allowed us to use a large number of temporal frequencies (13) for investigation of the temporal frequency characteristics of the visual system. Additionally, we used the intersection area of the functional and template anatomical masks for ROI definition. Individual functional mask of each subject was

created by using the activation area at all stimulation frequencies. Finally, LGN and V1 BOLD activities in response to a wide range of temporal frequencies (6–46 Hz) of diffuse visual flickers are reported. The frequency range included frequencies above the flicker fusion frequency of the retina (30 Hz), because earlier electrophysiological studies reported steady–state fluctuations at stimulation frequency also for stimuli far above this frequency [23].

4.2.1 ROI Based Functional MRI Data Analysis and Results

Thirty five healthy volunteers (20 females, 15 males, mean age = 25.60 $\pm$ 3.87 years) out of forty were recruited for this study after giving informed consent. Data of five subjects were not used in the analysis due to the non significant LGN activity.

Pre–processing steps of fMRI data were performed by using the SPM5 software package [41] for Matlab (The Mathworks, Inc.). Motion correction and spatial smoothing with a Gaussian kernel of FWHM 8 mm were applied. All functional data sets were spatially normalized into a standard space (MNI152, 2mm) prior to performing general linear model (GLM) analysis, which is widely used to obtain stimulus related hemodynamic activations. For this purpose a design matrix was created using boxcar model of visual stimulation which was convolved with a synthetic model of the hemodynamic response function, its time and dispersion derivatives, and the motion correction parameters. A high–pass temporal filtering with a cut–off of 128 s was applied.

In the first stage, a single subject multi–session fixed–effects GLM analysis was performed in order to investigate the single and combined effects of different temporal frequencies. Parameter estimates ('beta' images) and SPM{t} maps of each visual stimulation frequency for each subject were generated.

In this study, ROIs were defined as binary masks resulting from the intersection area of the functional and the structural regions. Subject specific functional ROIs were derived from the thresholded ($p<0.05$, uncorrected) results of the fixed–effects

multi–session GLM analysis including all 13 stimulation frequencies. Besides, structural ROIs were defined by registering standard template ROIs extracted from two separate probabilistic atlases for LGN and V1.

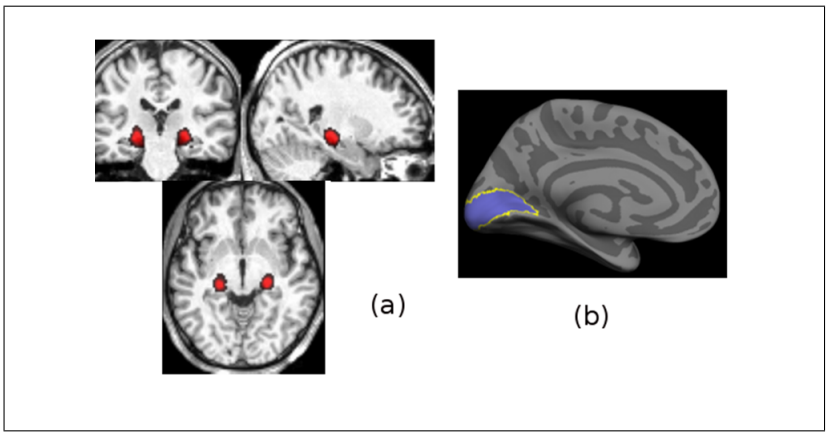

Figure 4.2 (a) Structural template for LGN and (b) Structural template for V1, overlay on average cortical folding pattern of all subjects.

In order to define structural LGN ROI in the MNI space, the cytoarchitectonic probabilistic map for lateral geniculate body [42] from the Jülich histological atlas implemented in FMRIB Software Library [43] was thresholded at p=0.01 (Figure 4.2-a). However, primary visual cortex exhibits a folding pattern which allows surface–based registration thus decreases prediction error compared to probabilistic atlases in volumetric coordinates [44]. Therefore, structural V1 ROI was defined by implementing spatial probability map of V1 derived from cortical folding patterns (Figure 4.2-b) [45]. In order to apply surface–based registration method, high resolution structural images were processed using the FreeSurfer software package [46, 47].

Subject specific LGN and V1 masks (Figure 4.3) were used to extract average 'beta'–values (parameter estimates) of each visual stimulation frequency. Parameter estimate images of 13 different stimulation frequencies which were the output of GLM analysis were multiplied with subjects own binary LGN and V1 masks. Averaged 'beta'–values were calculated separately for LGN and V1 for each stimulation frequency. Since 'beta'–values might display a high intersubject variability, average 'beta'–values of each subject were normalized across stimulation frequencies by dividing each frequency response by the maximum response. In the final stage, repeated

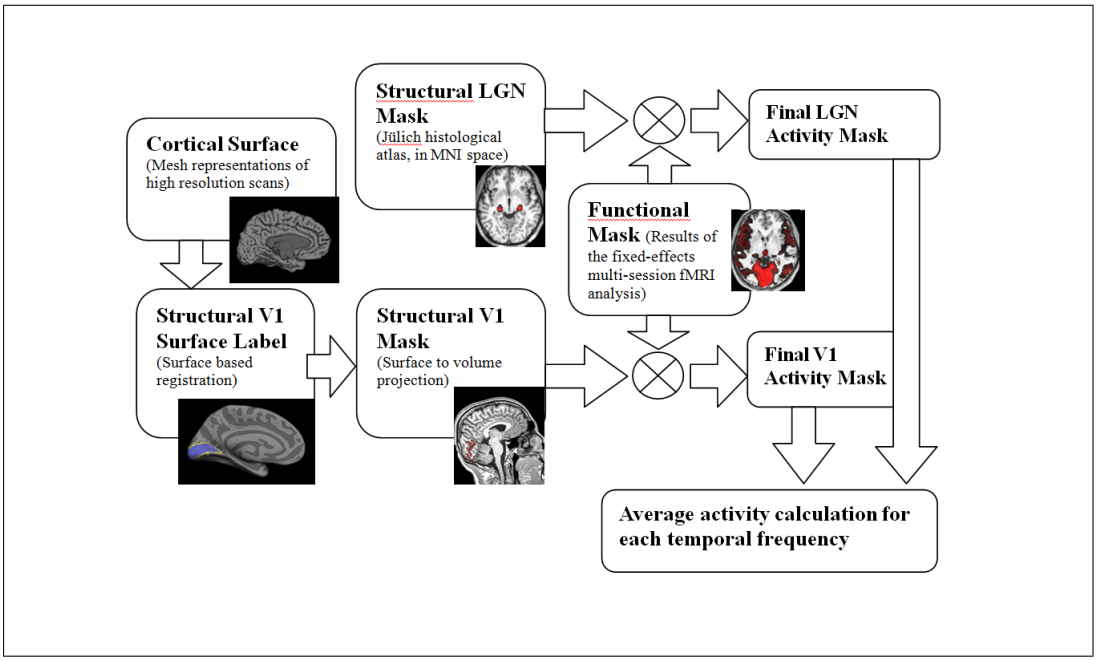

Figure 4.3 Simplified block diagram of the analysis to create V1 and LGN masks.

measures ANOVA (SPSS 21.0) was carried out to compare responses among various stimulation frequencies and ROIs.

Additionally, the similarities/dissimilarities between the frequency characteristics of V1 and LGN were studied. For each subject, the correlation coefficients were computed between the frequency characteristics of both ROIs, and the resulting correlation coefficients of all subjects were exposed to one–sample t–test to test whether they significantly deviate from 0.

For a sample subject, average pre–processed BOLD time series of the voxels in the V1 mask are shown in Figure 4.4. BOLD signal intensity change to visual stimulation was calculated relative to the first rest period of each recording corresponding to first 10 TRs (scans). After this, three consecutive stimulus and rest periods were averaged. It is obvious that the level of BOLD response depends on the stimulation frequency. In the same region of interest, average BOLD percent change is decreasing with increasing stimulation frequency. Besides, a separation of transient and sustained BOLD components can also be observed with a steeper decrease of the sustained activity (plateau) than the decrease of transient on– and off–responses with increasing

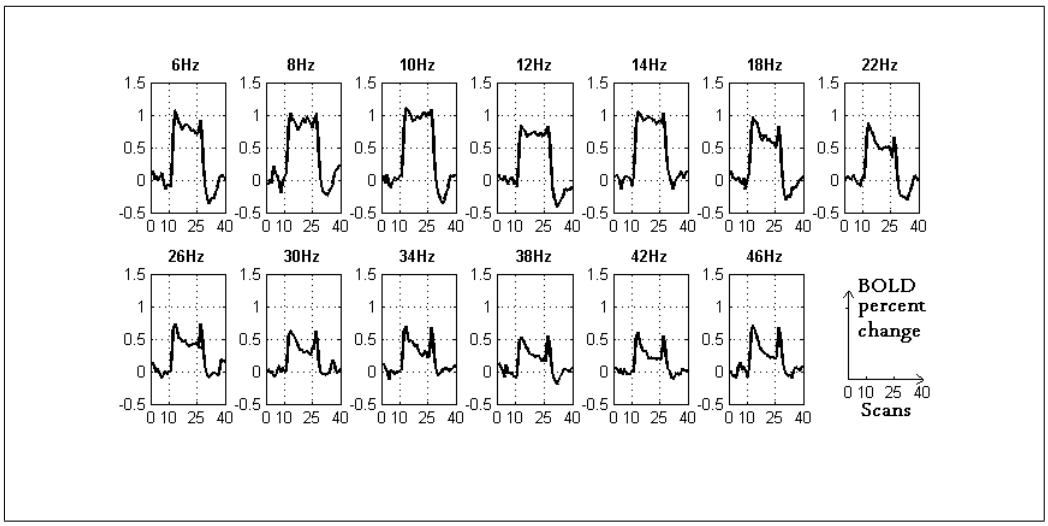

Figure 4.4 Average BOLD percent change time courses of V1 of a sample subject for thirteen different visual stimulation frequencies.

stimulation frequency. Although attempts have been made to model the transient components of the BOLD response, there are no clear definitions of them yet [48]. Therefore, in the present study we preferred not to arbitrarily define various time windows for each transient but referred to the canonical hemodynamic response function to quantify the overall activity at various stimulation frequencies.

BOLD activations of a sample subject were projected on to the pial surface of his own anatomical image in Figure–4.5. Activities are the unmasked SPM{t} maps derived from the GLM analysis. Threshold value (± 3.00) was selected arbitrarily in order to visualize spatial activity distribution more clearly. It can be stated that the extend of the significant BOLD activities is changing with stimulation frequency. There is also a narrowing of the activated area with increasing frequency towards the central visual field.

In order to evaluate frequency dependencies of the LGN and V1 activations, we first carried out repeated measures ANOVA including both the "ROI" (2 areas: LGNs and V1) and "stimulation frequency" (13 levels: 6, 8, 10, 12, 14, 18, 22, 26, 30, 34, 38, 42 and 46 Hz) as within–subject factors. Main effect of ROI was non–significant, pointing to that the mean activation levels were comparable for active voxels of both

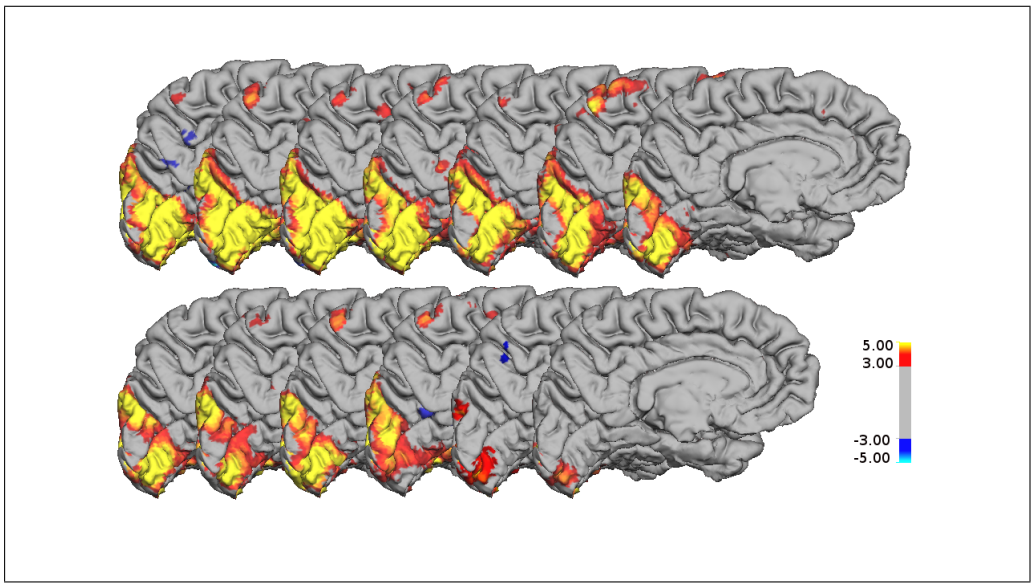

Figure 4.5 Spatial extend of BOLD activation (SPMt maps) with various temporal frequencies for a sample subject with an arbitrary threshold value ($|t| \geq 3.00$) for representation. First row and second row, from left to right represent responses to temporal frequencies from 6 Hz to 22Hz and from 26 Hz to 46 Hz respectively.

LGN and V1. On the other hand, both the overall effect of the "stimulation frequency" ($F(12, 408)=13.56$; $p<0.001$) and the effect of "ROI x stimulation frequency" interaction ($F(12, 408)=17.11$, $p<0.001$) were significant. These findings point out that, although both LGN and V1 activations get smaller with increasing stimulation frequency, their rate of decrease are significantly different. This effect can be clearly observed in Figure 4.6 in terms of a very steep decrease in the strength of V1 activations compared with the relatively smaller change of intensity in LGN response.

In a second stage, the frequency dependency of LGN and V1 were analyzed with separate repeated measures ANOVAs with a single within–subject factor "stimulation frequency". In this case, main effect of frequency was significant for V1 activations ($F(7.15, 243.14)=32.60$, $p<0.001$, Greenhouse–Geisser corrected), while it was non–significant for LGN activations ($F(12, 408)=1.30$, $p=0.21$). These post–hoc analyses revealed that the frequency dependent difference between both structures (significant ROI x stimulation frequency interaction) is pre–dominantly due to stronger decrease of V1 activity with increasing stimulation frequency. To investigate mean activation levels of LGN and V1 for each stimulation frequency separately, post hoc paired T–

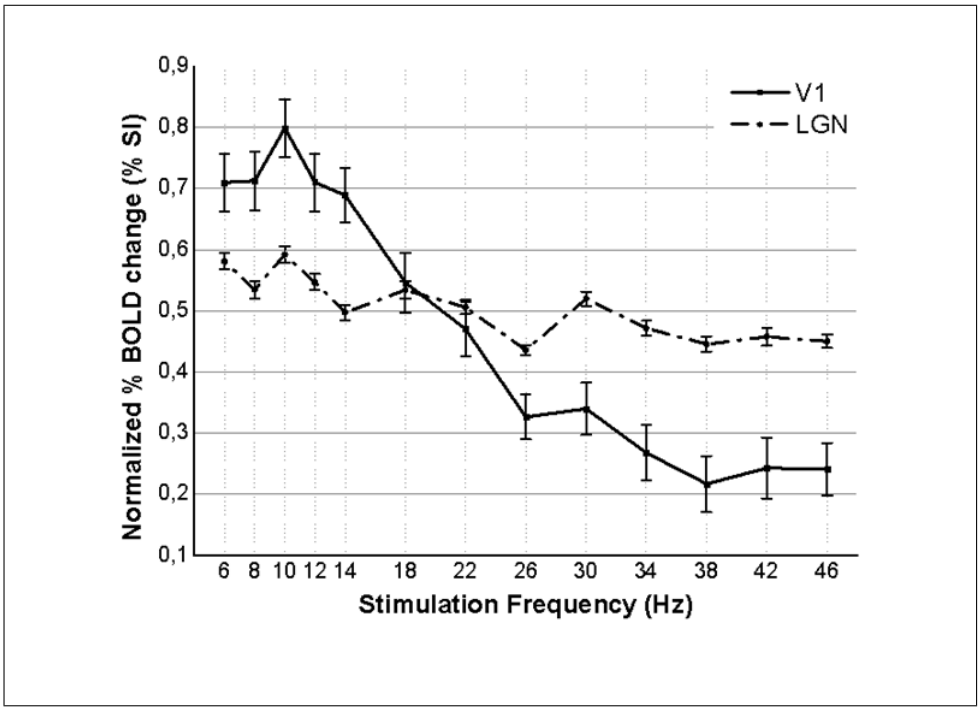

Figure 4.6 Grand average (N=35) frequency characteristics curves of V1 (solid line) and LGN (dashed line) obtained by measuring the normalized activations ('beta'–values) in response to thirteen visual stimulation frequencies (mean ± SE).

Tests between LGN and V1 at each frequency were computed. Significant differences were found for the frequency levels lower than 18 Hz and higher than 22 Hz. This result implies that, V1 activations are significantly higher than LGN activations in the 6–14 Hz frequency band, and significantly lower than LGN activations in the 26–46 Hz frequency band (Table 4.1).

Correlation coefficients between LGN and V1 activations were also computed for each subject in order to test the existence of any correlation among the frequency response characteristics of both ROIs. Mean value and standard deviation of correlation coefficients among subjects were 0.4389 ± 0.315, which correspond to a significant correlation at group level ($p<0.001$). Despite the proven difference of the decay of V1 response with increasing frequency in comparison to that of the LGN response, significant correlation between LGN and V1 responses reflects the similarity of the local peaks of their overall frequency characteristics, which are observed around 10, 20, 30 and 40 Hz (Figure 4.6).

Table 4.1
Temporal frequency wise mean difference between the activation levels of V1 and LGN.

Stimulation Frequency	6 Hz	8 Hz	10 Hz	12 Hz	14 Hz	**18 Hz**	**22 Hz**	26 Hz	30 Hz	34 Hz	38 Hz	42 Hz	46 Hz
Mean Difference	-0,13	-0,18	-0,21	-0,16	-0,19	-0,01	0,04	0,11	0,18	0,20	0,23	0,21	0,21
Standard Deviation	0,28	0,31	0,21	0,31	0,31	0,25	0,20	0,24	0,31	0,28	0,29	0,24	0,22
T–value	-2,68	-3,38	-5,75	-3,13	-3,64	-0,29	1,05	2,65	3,37	4,31	4,72	5,22	5,63
Significance (2–tailed)	0,01	0,00	0,00	0,00	0,00	**0,78**	**0,30**	0,01	0,00	0,00	0,00	0,00	0,00

4.2.2 Correlated LGN & V1 BOLD Responses

LGN does not demonstrate monotonously changing or stable average activation among various stimulation frequencies, but a slight decay of activation with increasing stimulation frequencies with local peaks around 10, 20, 30 and 40 Hz, which probably emphasize the frequency selective response characteristic. There are few fMRI studies reporting temporal frequency response characteristics of the LGN [49, 31, 33] compared to a high number of studies on the visual cortices [50, 51, 34, 52, 35, 36, 37, 53, 54].

Kastner et al. [31] investigated LGN responses at temporal frequencies of 0.25, 3.75, and 10 Hz (corresponding to reversal rates of 0.5, 7.5, and 20 Hz) by using checkerboard stimuli of high contrast (100%) and found similar activities at 3.75 and 10 Hz and significantly smaller activities at 0.25 Hz stimulation pointing to a high–pass characteristic. On the other hand, Mullen et al. [33], in a study based on contrast reversal of achromatic radial sine–wave gratings (0.5 cpd) at 2, 8, and 16 Hz showed that LGN response was significantly smaller at 16 Hz with respect to 8 Hz for high–contrast stimuli, and significantly smaller at 16 Hz with respect to 2 Hz for low contrast stimuli pointing to a low–pass characteristic. This discrepancy between the results depends mainly on the limited overlap of stimulation frequencies. Although these studies have extensively studied the effects of stimulus contrast and the differences

between the processing of chromatic and achromatic stimuli, the conclusions about the temporal frequency characteristics of the LGN are non–comparable and limited due to this fact. In the present study, by relying on the sensitivity of the visual system to higher frequencies in the achromatic domain and by using diffuse LED light, we could sample a much wider range of temporal frequencies with a finer frequency sampling, which gave more detailed information about the temporal frequency characteristics of LGN. This enabled us to describe global and local maxima in addition to a general low–pass trend in the temporal frequency characteristics of LGN.

The local peaks of V1 responses are mostly similar to those of LGN responses yielding a significant correlation. This finding is in line with the results of both Kastner et al. [31] and Mullen et al. [33] although their reports on the correlatedness of LGN and V1 activities rely on only 3 stimulation frequencies. The high correlation we observed within a wide range of stimulation frequencies from 6 to 46 Hz with 4 local peaks in both structures might point to preferred signal transmission frequencies in the thalamo–cortical circuitry of the visual system at these temporal frequencies. Although present results are not able to explain whether these selectivities are generated by one of the structures or stem from other structures connected with any one of them, we can tentatively claim that these specific tuning frequencies play a role in thalamo–cortical interaction in the visual system. The presence of similar maxima in EEG responses and local field potentials of the visual system [23, 24, 25] further support this view.

4.2.3 Low–pass Character of the V1 Activity

However, rapid decay of response intensities in V1 with increasing stimulation frequencies is not accompanied with a similar decrease in the BOLD signal of the LGN. Considering that the BOLD signal is mainly driven by the synaptic rather than the spiking activity of the investigated brain volume [2], the strong decay of V1 BOLD activity although the LGN activity does not change as strongly with stimulation frequency suggests the role of the local circuitry of V1 and maybe other neuronal projections from higher visual areas to V1 in this specific response characteristics. Assuming

that the LGN input to V1 does not decrease but rather fluctuates around a constant level with increasing frequencies, one can explain the low–pass effect observed in the V1 BOLD responses rather as the result of higher extra–synaptic input to V1 at lower stimulation frequencies. This might depend either on local network of V1 to be able to produce stronger inputs to higher cortical areas or on stronger feedback to V1 from extra–striatal areas. However, we can conclude that the selectively stronger activation for lower temporal frequencies first emerges in V1. There are also studies reporting different V1 response characteristics other than a significant decrease. Possible reasons why there is no consensus in the literature are discussed further in the following topics. Considering differentiations among experimental setups and analyzing techniques is a useful point of view while discussing discrepant results.

4.2.4 Spatial Contrast in Stimuli

Main dissociation among studies is related to the existence of the reversing spatial pattern (checkerboard, ring, horizontal or radial gradings, etc.) in addition to the temporal frequency of the stimulus. Actually there is a positron emission tomography (PET) study conducted by Fox and Raichle [55] showing that the response curves of regional cerebral blood flow (rCBF) percent change as a function of temporal frequency were nearly identical for flashing light and reversing checkerboard stimuli. There are number of BOLD fMRI studies using similar stimulation setup with flickering light and agreeing closely with PET results [51, 52, 53]. However, there are some critical properties of their setup which hinder us to make a general conclusion about the similarity of the outputs. Firstly, the stimuli were not achromatic but monochromatic (diffuse red light) thus activates parvocellular pathways while (L–cone input) suppressing activation of magnocellular pathway [56]. In this sense we can speculate that the similarity does not cover responses of acromatic stimulation. Likewise, there are clues in the recent literature concerning separate BOLD responses of the chromatic and achromatic stimuli as a function of stimulation frequency [49, 57, 33]. Secondly, duration of the flash stimuli was constant (5 ms) thus luminance was linearly related to the flashing stimulus rate. On the other hand, luminance of the reversing checkerboard was con-

stant. Effect of the increase in illumination accompanies with the flashing stimuli while the spatial frequency effect accompanies with checkerboard stimuli. Moreover, Mirzajani et al. [40] conducted an fMRI study showing possible effects of spatial frequency on the temporal frequency response. As a result, spatial frequency parameter of the stimuli may introduce modulatory effects on the temporal frequency tuning.

In our study, there is no spatial pattern or contrast. Besides, visual stimulations with different frequencies were compatible to each other regarding the mean light intensity and total time of visual field illumination, in other words duty cycle of flashing light stimuli was 50%, thus exposure of light was identical for each temporal frequency.

4.2.5 Effect of ROI Definition in V1 Response

Another topic is the way of ROI creation in V1, which is one of the main components directly influencing the results. In the literature, ROI selection technique shows variability which seems to be able to explain different conclusions to some extent. These techniques can be classified into three main groups; those using limited number of significantly active voxels in V1, those using a broader significantly active area by adding extra–striatal areas beside V1, and those using retinotopic mapping scan to define borders of V1 and significantly active voxels within V1.

Studies using limited number of highest active voxels within ROIs in V1 focused frequently on the wave characteristics of the BOLD signal rather than the frequency response characteristics of the visual cortex. Parkes et al. [35] presented checker board stimuli at temporal frequencies of 4, 6, 7.5, 10, 12, 15, 20 Hz at a fixed duration of 16.7 ms during 10 s with and without a slight jitter, and investigated the effect of the periodicity of the stimuli. They defined the activation threshold not based on the level of significance, but in order to get 10 cm^3 ROI. In the most active ROI, the normalized BOLD responses to periodic stimuli were increased up to 7.5 Hz, and it became stationary for the rest. As discussed earlier, fixed duration for stimulation causes intensity increase in higher frequencies, thus pure temporal frequency related change might not

be presented. Wan et al. [54] used radial checkerboard with stimulation frequencies at 0.5, 1.0, 4.0, 8.0, and 16.0 Hz during 4 s. Average hemodynamic impulse responses of visual stimuli were calculated for activated areas within a very small (6–mm spherical, about 4 voxels) volume centered on maximally active voxel which was detected by conjunction analysis of all frequencies. They conclude that response increase stopped at 8 Hz stimulation and decreased at 16 Hz stimulation. However, statistically significant difference was between high (4–16 Hz) and low (0.5–1 Hz) frequency groups, and the decrease at 16 Hz was non–significant. Short activation period (4 s) also implies that the results reflect mostly transient characteristics, since it does not allow enough time for the BOLD signal maximize. Muthukumaraswamy and Singh [34] averaged fMRI data across all temporal frequency conditions (0, 1, 6, 10, 15 Hz) for each subject to find the spatial peak. They reported that the BOLD response modulation in this peak increased up to 6 Hz and displayed a plateau between 6–15 Hz. They used reversing square–wave vertical gratings and found similar results for spatial frequencies 3 cpd (cycles/degree), and 0.5 cpd. Finally, there is a correspondence between presented results of these studies using a ROI that covers a limited number of active voxels at V1. There is an increase in BOLD signal change with frequency increase and a peak value in the 6–10 Hz band, which finally continues with a plateau. Among studies that use ROIs of significantly active voxels in the visual cortex covering V1 and extrastriate area, Singh et al. [37] used checkerboard illuminated with 1 ms flashing light at 2, 4, 6, 8, 10, 12 Hz, and found a band pass response which has a peak at approximately 8 Hz. Interestingly, they calculated the fMRI signal strength by multiplying the average BOLD percent change with the number of active voxels detected and applied simple correlation analysis. Besides, Rosa et al. [36] found an inverted U–shaped frequency response which has a peak at 7.5 Hz and sharp drop above 15 Hz while presenting checkerboard stimulation (reversing) at the frequencies of 2, 3.75, 5, 6, 7.5, 10, 15, 30 Hz. They used general linear model (GLM) analysis, and results of fixed–effects group analysis were reported for a visual cortex ROI which is common for all subjects. Despite the differences in the applied techniques, results are quite similar for both studies, which show a band pass response peak at approximately 8 Hz.

As can be seen, identification of the visual areas is the most critical step which

might change the results dramatically. There is no significant BOLD activity decrease with increasing frequency in the case of limited ROI of V1. Besides, there is a band bass response of BOLD activity in the case of broader region of visual cortex. It is obvious that the average activity of a limited number of voxels does not represent the response of a structure as a whole. In this sense, ROI definition must be limited to cortical regions such as V1 thus retinotopic mapping scan seems to be a good option for defining borders of V1. On the other hand, voxels that are not significantly active could not be the indicator of the response properties of V1. There might be sub areas in the V1 that may have temporal frequency selective BOLD response. Presence of domains for low (0.75 Hz) and high (15 Hz) temporal frequency visual inputs in the human V1 at a submillimeter resolution supports this view [58]. At this point, retinotopic mapping might not be sufficient, additional ROI restrictions might be necessary. Moreover, retinotopic mapping scans uses spatial and temporal frequencies which will introduce adaptation. Singh et al. faced with a similar situation and excluded 5 Hz from their data [39].

We decided to use subject specific ROI definition method beyond those defined by retinotopic scan and preferred to use intersection area of functional and structural borders. Functional area represents subject specific significantly active area of all stimulation frequencies by using proper contrast in the GLM design. Besides, subject specific structural area defined by a surface based method using template cortical folding pattern. It has been shown that there is a good correspondence between the borders of V1 defined by retinotopic functional scan and by high resolution anatomical scan which can visualize cortical striation consistent with the stria of Genari [59]. As a result, we aimed to avoid from the aforementioned disadvantage of additional retinotopic functional scan and used structural border of V1.

4.2.6 Transient and Sustained BOLD Responses

Another interesting aspect of this study is about the time series of the BOLD response which were presented in figure 4.4. Existence of the transient and sustained

components of the BOLD signal, which do not represent similar decrease with increasing stimulation frequency, can be seen clearly. Uludağ used an 8 Hz flickering black–and–white radial checkerboard in order to stimulate only one hemifield during 20 seconds and showed a separate activity of the phasic (transient) network covering interestingly both hemispheres [48]. His study supports the view of separate transient and sustained networks. Besides, Horiguchi et al. used achromatic high and low luminance levels each lasting 24 sec for stimulation and defined transient and sustained responses as two separate temporal channels which have a balance varying with eccentricity [60]. In other words, from the central visual field to periphery, BOLD response comprises transient pattern more than sustained one. More recently, Sun et al. used black/white checkerboard whose contrast was reversed at 0.17, 0.75, 2, 4, 8, or 15 Hz during a brief exposure (3 seconds) and conclude that the transient BOLD response depended very little on the reversal frequency [61]. As can be seen, there is a growing body of evidence about the separate temporal BOLD response types emerging at spatially different or overlapping areas. Discarding this separation may hide the effects of temporal frequency and be misleading if the duration of the stimulus is very short. In the following study transient and sustained BOLD responses were separated and the weights of temporal BOLD components depend on the stimulation frequency were reported.

4.3 Temporal Frequency Dependent Response Characteristics of Transient and Sustained BOLD Components in The Primary Visual Area

Functional MRI with blood oxygenation level–dependent (BOLD) contrast has been used to derive information about the intensity of the neuronal activation beyond the localization of the activations. To some extent, quantification of the neuronal activity via BOLD intensity brings assumptions about the linear neurovascular coupling. Clarifying coupling/uncoupling mechanism between oxygen metabolism (CMRO2) and blood flow (CBF) in the proposed biomechanical coupling models is necessary for more

reliable conclusions [62, 63]. Actually, there are inhibitory, excitatory, and combined oscillation based mechanisms revealed by electrophysiological data, and effects of them on the BOLD responses and the model outputs are questionable and should be considered as an important aspect [64]. Instead of a constant hemodynamic response function (HRF) and neurovascular coupling model, flexible extended models are necessary for the sake of false negative activations of BOLD fMRI experiments [65]. At this point, speculation about possibility of the neurovascular coupling (CBF/CMRO2) being the source of information about the balance of inhibitory and excitatory neuronal activity might be a good example of this point of view in the literature [66].

BOLD response to a stimulation represents a well–known pattern (HRF) with a number of transient components that have been reported previously [67]. However static HRF dictates a constant response intensity for all components in the general linear model analysis of the fMRI data. Especially overshoots of the BOLD response at block transitions of the stimulation period (phasic) are promising candidates for addressing different cognitive perspectives of the response [68, 60, 48]. In this sense, exploring transient BOLD responses is crucial not only for neurovascular coupling models but also for different perspectives of cognitive processes.

In this study, we decided to separate transient BOLD responses and quantify their differences by using steady state visual stimulation which allows to discuss state based response differentiations and effects of inhibitory and excitatory balance of neural networks.

4.3.1 Analysis of BOLD Components and Results

Subject recruitment and data acquisition procedure are same as the previous work since the same data set of forty subjects was used in the presented study.

FMRI data processing was carried out using FEAT (FMRI Expert Analysis Tool) Version 5.98, part of FSL (FMRIB's Software Library, www.fmrib.ox.ac.uk/fsl).

The following pre–statistics processing was applied; motion correction using MCFLIRT [69]; slice–timing correction using Fourier–space time–series phase–shifting; non–brain removal using BET [70]; spatial smoothing using a Gaussian kernel of FWHM 8.0mm; grand–mean intensity normalisation of the entire 4D dataset by a single multiplicative factor; highpass temporal filtering (Gaussian–weighted least–squares straight line fitting, with sigma=45.0s). Time–series statistical analysis was carried out using FILM with local autocorrelation correction [71]. Single subject, multi–session analysis was carried out using a fixed effects model, by forcing the random effects variance to zero in FLAME (FMRIB's Local Analysis of Mixed Effects) [72, 73, 74]. Z (Gaussianised T/F) statistic images were thresholded using clusters determined by $Z>2.3$ and a (corrected) cluster significance threshold of $P=0.05$ [75].

Occipital lobe region of MNI 2mm probability atlas which is distributed with FSL was used as standard template. MNI occipital probability atlas was binarized to produce template occipital mask for ROI analysis. Besides, multi–session Z statistic results of each subject were binarized to create functional mask. Final mask of each subject was achieved by multiplying functional mask and template occipital mask. However, all voxels of the final mask are not active at each session since the subject–based multi–session analysis results represents average significance among sessions. Thus, selecting large number of voxels in the session level may include non–significant voxels and lower the average activity. Moreover, spatial locations of the activities might represent variable transient effects [60]. In order to fix the effect of spatial extend on the response of transients and achieve maximum response, number of voxels in the subject mask was limited more conservatively to 300 voxels by increasing threshold of multi–session Z statistics. Z statistic images were, therefore binarized for most active 300 voxels in the occipital cortex. Finally, combined functional and template mask of each subject was covering 300 voxels in the occipital cortext which was the most active voxels of multi–session Z statistic images.

Final masks of each subject were in the MNI standard space while the time series data were in the subject's own anatomical space. In order to find mask for each session in the subjects own space, final mask were registered to average functional

image of each session. Average BOLD time series data were achieved by multiplication of pre–processed functional images with registered mask and spatial averaging of time series data.

Baseline level of BOLD signal was calculated by averaging second half of first rest period which covers 5 samples. Remaining three active and rest time period couples were averaged in order to increase signal to noise ratio. Percentage change of BOLD signal from baseline was calculated for each subject and stimulation session according to the equation 4.11.

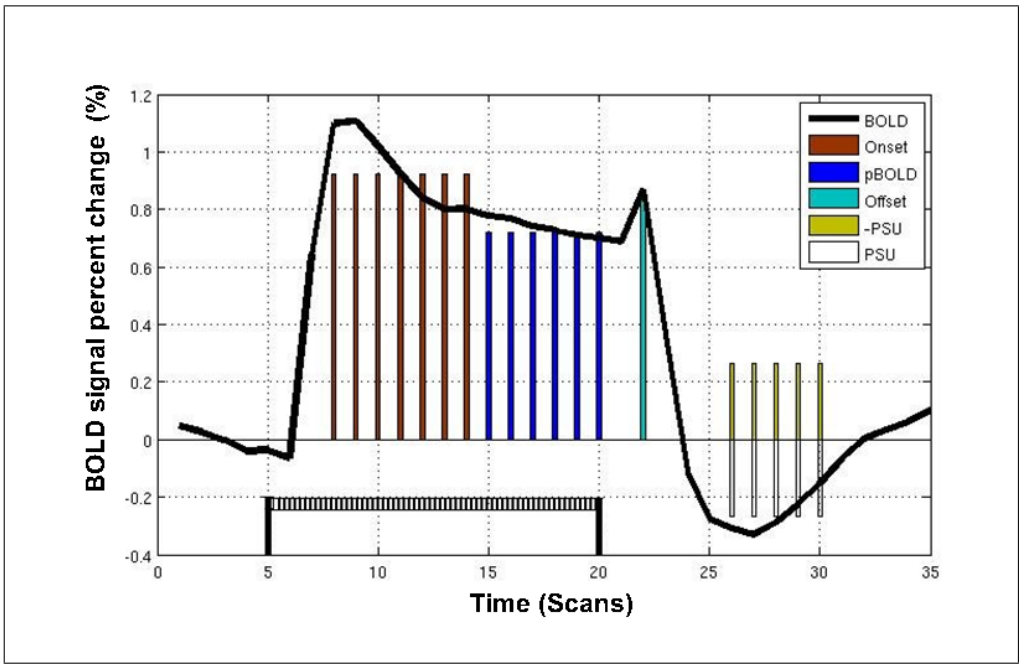

Figure 4.7 Example BOLD time series of a stimulation block. First five samples were excluded. Visual stimulation period is shown at the bottom of the figure (between 5–20 samples). In order to calculate Onset, pBOLD, Offset and PSU values, samples that are shown with different color bars are used.

$$PercentBOLD(t) = \frac{BOLD(t) - \sum_{i=6}^{10} BOLD(i)}{\sum_{i=6}^{10} BOLD(i)} \tag{4.11}$$

where, BOLD is the time series data and $i = 1, 2, ..., 100$ is the sample index.

Four different transient were calculated by averaging samples; early positive BOLD (early pBOLD), late positive BOLD (late pBOLD), post–stimulus overshoot

(PSO), post–stimulus undershoot (PSU) (Figure 4.7). In the literature, the time to peak of BOLD signal during stimulation is reported approximately 4–8 seconds after the stimulus onset [67]. We therefore excluded first 2 samples of the BOLD signal which covers 5.962 seconds of stimulation period while quantifying positive BOLD periods. Total stimulation period was 44.715 s which includes 15 samples of BOLD signal. After excluding first two samples, early and late periods of positive BOLD signal were calculated by averaging next 7 samples and last 6 samples of stimulation period separately. Time period of early and late positive BOLD was 20.867 s and 17.886 s respectively. Due to the low sampling frequency, post–stimulus overshoot was defined as the peak value of the BOLD signal after the end of the stimulation period. Post–stimulus peak value was quantified with the second sample which is 5.962 seconds after the end of the stimulation. Post–stimulus undershoot was calculated by averaging 5 samples which are in the middle one–third of the rest period. Total rest period was 44.715 seconds and PSU was started 14.905 seconds after the stimulus offset.

Repeated measures ANOVA (SPSS 21.0) was carried out to compare responses among various stimulation frequencies and transients.

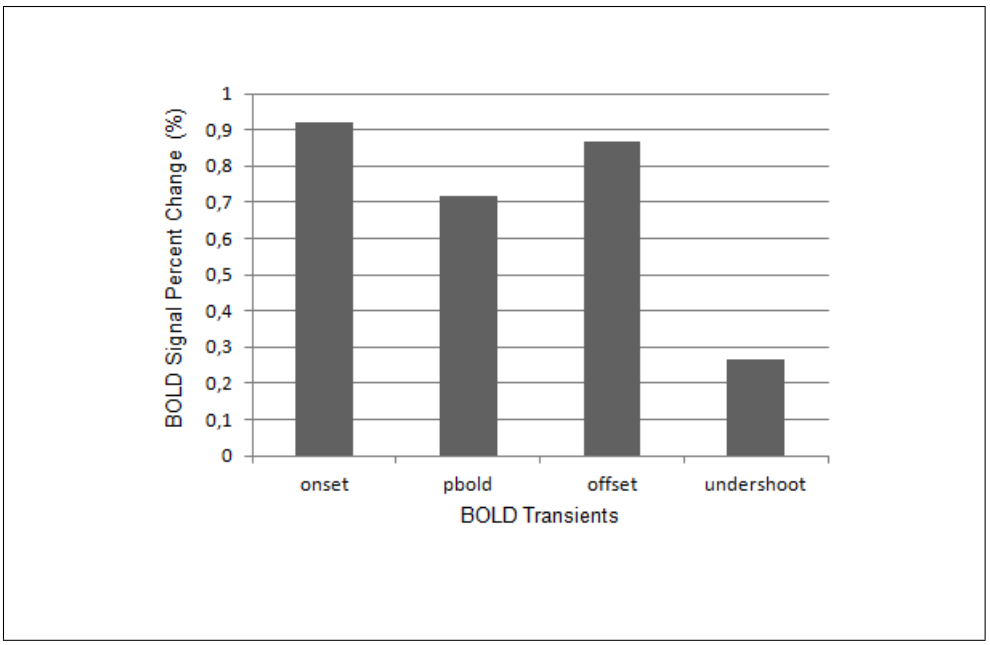

Figure 4.8 Grand average percent change of BOLD transients.

Figure 4.8 displays a bar graph with four components each for a different BOLD

transient, which represents the subject and frequency average of percentage change of BOLD signal intensity. Besides, figure 4.9 shows the subject average of BOLD percentage change for four different BOLD transients versus stimulation frequency.

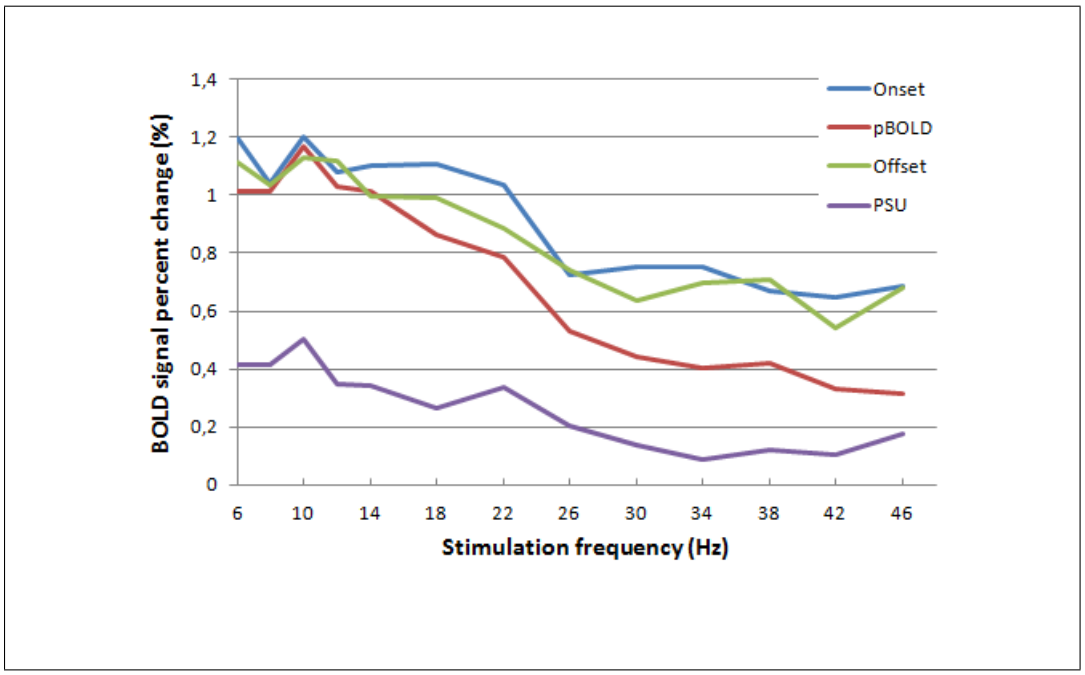

Figure 4.9 Percent change of BOLD transients for different stimulation frequencies.

In order to evaluate frequency dependency and interactions of BOLD transients, we carried out repeated measures ANOVAs. The ANOVAs had the within–subject factor frequencies (13 frequencies: 6, 8, 10, 12, 14, 18, 22, 26, 30, 34, 38, 42 and 46 Hz) and a group factor transients (4 transients: early pBOLD, late pBOLD, PSO, PSU). Main effects of transients ($F(3,117)=92.99$; $p<0.001$, Greenhouse Geisser corrected), and frequency ($F(12,468)=19.13$; $p<0.001$, Greenhouse Geisser corrected) were significant, as was the interaction of transient x frequency ($F(36,1404)=1.97$; $p<0.05$, Greenhouse Geisser corrected). This result is indicating a strong frequency dependent change in transients of BOLD signal besides existence of distinguishable BOLD transients. Moreover, frequency dependent change is significantly different among them. These results allow us to use ANOVA for the pair wise statistics of BOLD transients.

In the pair wise statistics of BOLD transients, we carried out six separate repeated measure ANOVAs for the six combinations of two BOLD transients out of

four. The ANOVAs had the within–subject factor frequencies (13 frequencies: 6, 8, 10, 12, 14, 18, 22, 26, 30, 34, 38, 42 and 46 Hz) and group factor transients (2 out of 4 transients: early pBOLD, late pBOLD, PSO, PSU). Main effects of transients were significant for early pBOLD, late pBOLD ($F(1, 39) = 54.83$; $p < 0.001$), early pBOLD, PSU ($F(1, 39) = 112.67$; $p < 0.001$), late pBOLD, PSO ($F(1, 39) = 20.46$; $p < 0.001$), late pBOLD, PSU ($F(1, 39) = 102.66$; $p < 0.001$), PSO, PSU ($F(1, 39) = 129.69$; $p < 0.001$). Notably, the main effect of transients was not significant for the early pBOLD, PSO combination ($F(1, 39) = 2.34$; NS), indicating similarity of their amplitude while late pBOLD was significantly different from early pBOLD and PSO. Main effects of frequency were significant for all transient couples; early pBOLD, late pBOLD ($F(12, 468) = 13.83$; $p < 0.001$), early pBOLD, PSO ($F(12, 468) = 8.51$; $p < 0.001$), early pBOLD, PSU ($F(12, 468) = 20.07$; $p < 0.001$), late pBOLD, PSO ($F(12, 468) = 13.32$; $p < 0.001$), late pBOLD, PSU ($F(12, 468) = 30.66$; $p < 0.001$), PSO, PSU ($F(12, 468) = 14.64$; $p < 0.001$). The interaction of transient x frequency was significant for transient couples including late pBOLD; early pBOLD, late pBOLD ($F(12, 468) = 7.44$; $p < 0.001$), late pBOLD, PSO ($F(12, 468) = 3.61$; $p < 0.001$), late pBOLD, PSU ($F(12, 468) = 3.16$; $p < 0.005$), showing that frequency dependent change of the amplitude was a property that differentiate late pBOLD from other BOLD transients. Besides, the interaction of transient x frequency was not significant for early pBOLD, PSO ($F(12, 468) = 1.07$; NS), early pBOLD, PSU ($F(12, 468) = 0.935$; NS), PSO, PSU ($F(12, 468) = 0.729$; NS).

4.3.2 Discussion about the Differential Responses of BOLD Transients

In order to discuss frequency dependent activations of primary visual cortex, analyzing BOLD responses in more detail by means of its components, might be a good next step. Using ideal hemodynamic response function (HRF) brings us to an assumption that well known BOLD transients react to the visual stimulus with different frequencies similarly. However, this is not the case. It has been shown that frequency response characteristics of BOLD transients are not coupled strictly to the stimulation but may reflect separate underlying neuronal processes. Deriving model

stimulus response by using HRF and stimulus pattern omits underlying neuronal events thus explaining biomechanical processes became more difficult. Without using HRF, information that the BOLD signal carry can be more accessible.

Without using ideal HRF, we were able to find significantly different dynamics of BOLD transients with changing stimulation frequency. Especially, separation of onset and offset responses from pBOLD with increasing frequencies is an important finding. We can separate these transients not only with their visual stimulation frequency characteristics but also their features in the BOLD time course. Transient onset and offset overshoot signals are phasic responses, while sustained pBOLD is tonic [48]. Phasic BOLD transients are decreasing their responses more slowly than tonic BOLD response with increasing stimulation frequencies. Intensity loss of tonic BOLD response implies the higher dependency of it to the effects of stimulation frequency increase.

Visual stimulation frequency increase may cause the transformation of neuronal processes by which inhibitory inter–neurons start to play a more dominant role. In this sense, suppression of tonic response might be originated from the increase in the effectiveness of specialized inhibitory local networks.

5. SIMULTANEOUS EEG/fMRI ANALYSIS OF THE RESONANCE PHENOMENA IN STEADY STATE VISUAL EVOKED RESPONSES

5.1 Source of EEG Signal and EEG Oscillations

EEG signal is produced by pyramidal neurons which have a dendritic tree formation oriented perpendicular to the scalp surface and their cell bodies (soma) are located in layers 5 and 6 of cerebral cortex. Besides, source of EEG signal is post synaptic potentials of the apical dendrites which create a current flow in the extracellular medium and constitute a dipolar source–sink configuration[3].

Surface electrodes could record current flow if there is a synchronization and summation of neuronal activation produced by large number of neurons [76]. Because signal intensity is very low due to the electrical properties of the structures (glial cells, meninx, scalp, scull) between EEG source and electrode. Moreover, conducting volume decreases the spatial resolution besides the intensity of the EEG signal. In other words, each electrode could detect EEG signal of all possible generators and artifact sources such as eye, muscle, electrode movements [77].

5.1.1 EEG Oscillations

EEG signal represents oscillations and resonating activities at various frequency bands (Table 5.1). These oscillations can be classified as three groups based on their source of initiation.

Table 5.1
Oscillations of EEG signal.

Name	Frequency Band
Delta	0.1–4 Hz
Theta	4–8 Hz
Alpha	8–13 Hz
Beta	13–30 Hz
Gamma	30–80 Hz

5.1.2 Spontaneous (Ongoing) EEG Oscillations

Spontaneous (ongoing) rhythmic activities constitute the core of EEG signal throughout the human life. Although, there is a hypothesis about the close correlation between vital activities of the neurons and the origin of spontaneous oscillations, it was presented that ongoing EEG oscillations manifest significant changes with cognitive functions, cognitive disorders, lesions, circle of the sleep, and neural development [3].

Spontaneous delta (0.1–4 Hz) rhythm is seen in adults in deep sleep (Non–rapid eye movement – NREM, sleep–stage 4), under anesthesia, and in coma (state of unconsciousness). Theta (4–8 Hz) oscillation is seen in sleep (NREM sleep stage 2–3), in meditation, and during creative moods beside abnormal situations. Alpha (8–13 Hz) wave is seen in relax and closed eyes condition and is the posterior dominant rhythm. In the case of high level of alertness and attention, low amplitude beta (13–30 Hz) and gamma (30–80 Hz) oscillations are emerged in the EEG trace [24].

Discovery of EEG signals and the pioneer findings about alpha rhythm are the most famous achievements of Hans Berger in 1929. He reported that dominant 10 Hz activity during the period of eyes closed was decreased and replaced with a faster and lower intensity wave, beta, when the subjects open their eyes. This demonstrates not only the existence of EEG oscillations but also relatedness with cognitive state.

Higher signal amplitude during the resting state and eyes closed condition than the signal amplitude during the cognitive processes implies that increased EEG amplitude could not be direct representative of increased neuronal activity. Similarly, high amplitude low frequency delta oscillations during specific phases of the sleep could not be explained by the increased cognitive processes. Synergistic activities of the signal generators is the key point while evaluating amplitude increase of the EEG. Synchronization of the neuronal networks and resonance of signal generators at the same frequency increase EEG amplitudes. In a similar manner, deep electrode recordings suggest that ongoing oscillations with low intensity and high frequency, namely beta and gamma, are produced by synchronization of local neuronal groups [78].

It has been known that inhibitory interneurons are affective in synchronization process of gamma frequency oscillations represented by local networks [78]. Besides, long–range synchrony of large scale networks is pronounced by excitatory connections composing low frequency oscillations [79, 80, 81].

5.1.3 Event Related Oscillations

Event related measurements are conducted to explore effects of experimental stimulus on EEG signal. Temporal variations of EEG time course can be seen as a response to the internal or external stimuli and is named as event related potentials (ERPs). However, there are high amplitude spontaneous oscillations which are accompanied with ERPs, and might not be stimulus mediated or evoked responses. Therefore, basic approach for separating ERP signal is time domain averaging of many EEG epocs (time windows) which are temporarily locked to the stimulus onset. The aim of averaging is to cancel out background activity which is assumed to be random and uncorrelated with the stimulus [82, 83].

Amplitude and phase of oscillations are also modulated due to the cognitive or sensory stimulation. As a result of phase resetting and/or amplitude modulation, event related oscillations (EROs) are emerged. It was proposed that EROs provide

basic connectivity for the association and communication processes of the brain [11]. In this context, increase of synchronization (amplitude increase) and desynchronization (amplitude decrease) help us to investigate intrinsic processes of the brain.

5.1.4 Steady State Visually Evoked Potentials (SSVEPs)

Steady state evoked potentials (SSEPs) are EEG signals having particular amplitude and phase response during repetitive stimulation period which does not allow to return to resting state and constitutes a steady state [25]. Since the time domain signal is stationary, SSEPs are preferably summarized by the power and phase spectrums in the frequency domain.

There is a complex relation between the temporal frequency of the stimulus and power of the SSEP response at that frequency. In the case of visual stimulation, three local maxima of the steady state visual evoked potential (SSVEP) are reported in the low (6–12 Hz), medium (15–25 Hz), and high (30–60 Hz) frequency bands [25]. Additionally, it was proposed that selective responses correspond to different visual pathways which can be separated by their sensitivity to the color, frequency, and contrast of the stimuli [25]. Another study investigating resonance phenomenon in visual cortex reported similar selectivity to certain resonance frequencies around 10, 20 and 40 Hz in the frequency band of 1–100 Hz, with a fine sampling with 1 Hz steps [23].

Visual stimulation with a particular temporal or spatial frequency results in an SSVEP frequency spectrum with peaks at the fundamental and harmonics (integer multiple) of the stimulation frequency. For instance, 8 Hz stimulus induces not only fundamental response at 8 Hz but also at 16 Hz (first harmonic), at 24 Hz (second harmonic), and so on. Also, it has been shown by many researchers that even if the flicker frequency is very high (80 Hz) and discrimination of flicker is not available to consciousness, it is possible to record SSVEP at the stimulation frequency [23, 84].

5.2 Simultaneous EEG/fMRI and Neuro–vascular Coupling

Combined EEG and fMRI studies show great promise to develop a more comprehensive understanding of the neural basis of behavior, including brain function and dysfunction [10]. Understanding the neural basis of brain functioning requires knowledge about the spatial and temporal aspects of information processing. FMRI and EEG are two techniques widely used to noninvasively investigate human brain function. EEG signals recorded on the scalp surface represent electrical perspective of the neuronal activity while fMRI BOLD contrast depends primarily on blood oxygenation in turn reflects metabolic activity in the tissue [85]. Neither of these technologies alone, however, can provide the information necessary to understand the spatio–temporal aspects of information processing in the human brain. FMRI yields highly localized measures of brain activation, with a good spatial resolution (about 2–5 mm) but since hemodynamic response is indirect and slow motion result of neuronal activity, temporal resolution significantly longer (about 5–8 s) than the time needed for most perceptual and cognitive processes [86]. EEG has the necessary temporal resolution to study the dynamics of brain function, but its poor spatial resolution precludes identification of underlying neural sources. FMRI and EEG therefore represent complementary imaging techniques, and combining information from them is a particularly useful way to examine the spatial and temporal dynamics of brain processes [10].

Even though EEG has existed for more than eight decades and relatively young fMRI for more than two decades [12, 13, 14], the concurrent use of both methods has been established only in the last couple of years. This is mainly because of several technical challenges, when combining both methods (i.e., electromagnetic induction on EEG electrodes by the changing magnetic field of MR machine) [87]. Many important neuroscience groups are now working on combination of EEG & fMRI and construction of reliable and valid models [67, 88, 89, 90, 91, 92, 93, 94]. However, a reliable electrovascular coupling model which fully describes connectivity between neuronal activity representations on EEG and hemodynamic response could not be proposed yet.

5.2.1 The Relation Between EEG and fMRI Signals

Relationship between BOLD signal and neuronal activations could be examined in different scales via multi–unit spiking activity (MUA), local field potentials (LFPs), and EEG, alternatively excitation–inhibition networks (EIN) and activation–deactivation point of views are also possible. While, multi–unit activity represents action potentials of related area, local field potentials represent synaptic inputs and intracortical processes conducted with inter–neurons. Initially, both MUA and LFPs seemed to be correlated with BOLD response, although in a recent study, strong coupling between LFPs and changes in tissue oxygen concentration in the 25–60 Hz frequency range which persisted even in the absence of spikes has been observed in cat primary visual cortex [95].

Similarly, in concurrent electrophysiology and fMRI experiments in the visual system of monkeys, it has been found that LFPs are better predictors of the BOLD response rather than MUA, especially in the 40–130 Hz (beta and gamma) frequency range (Figure 5.1) [2]. These results imply that the BOLD signals reflect input activity and intracortical processes rather than pyramidal cell output activity [96]. In other words, all of these observations suggest that the presynaptic (population of excitatory or inhibitory) elements of the axon terminals are the sites of enhanced metabolic activity, and that these might be the elements driving fMRI signals [97].

Although it proved very useful in characterizing the response properties of local structures (as in LPFs), the method clearly falls short of providing information on spatiotemporal cooperativeness and on the global, associational operations performed by neuronal networks [98]. At this point, scalp EEG represents operations of global neuronal networks and also reflects synaptic inputs, similar to beta and gamma frequency bands of the LFPs it can be assumed that EEG needs to be correlated with BOLD signal. Many papers published based on the assumption that sources of EEG and event related potentials (ERPs) coincide with the highly activated areas on fMRI [99, 38]. However, modeling the correlation between electrophysiological processes and increase in metabolic activity with such a simple way is problematic [90, 87]. EEG amplitudes

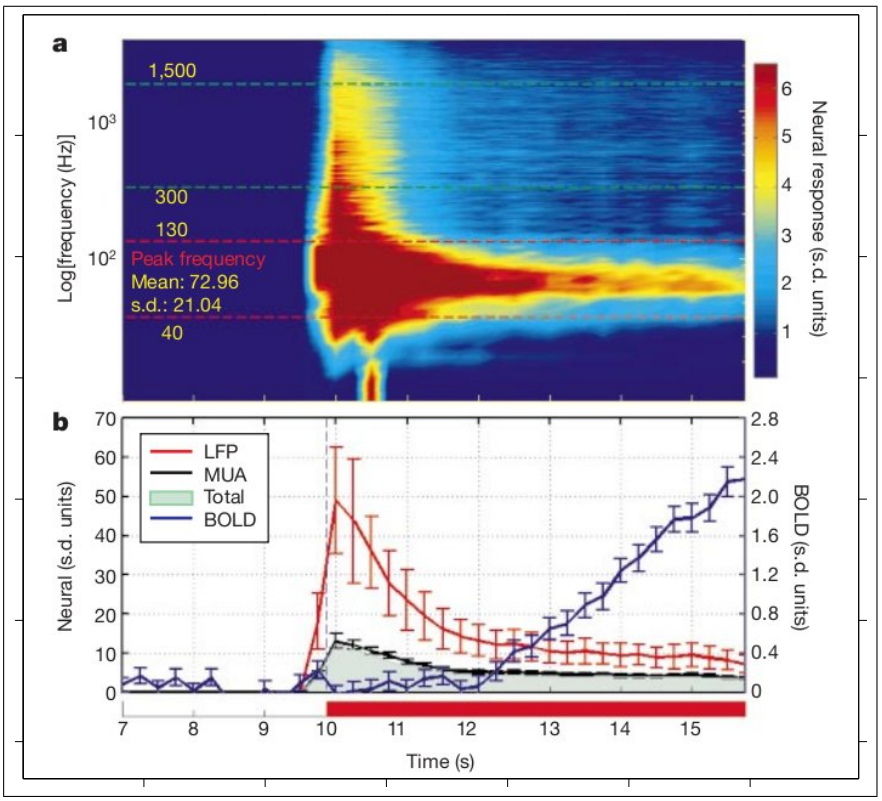

Figure 5.1 Time–dependent frequency analysis for population data. a, Spectrogram of the first 6 s of the neural response averaged over all data collected during 24, 12.5, 12 and 6 s of stimulus presentation (10 monkeys, 619 experiments). Colour encodes the reliability of signal change for each frequency. Red and black dashed lines show the LFP and MUA frequency bands, respectively. b, Mean LFP (red), MUA (black) and total (green surface) neural response (average across all frequencies), together with the BOLD signal (blue). Error bars are 1 s.d. [2].

represent not the summation of the neuronal activations but the synchronization of a global neuronal network [11]. Neuronal synchronization in a single voxel as seen by local field potential measurements might not be enough to produce significant difference in EEG signal. In this context, Henning et al. proposed that neurovascular coupling model developed based on local field potentials is not applicable for EEG based non-invasive electrophysiological measurements. In their work, visual evoked potentials (VEPs) and BOLD signal correlation were investigated during visual movement perception. Neuronal activity without synchronization increased BOLD signal but in VEP measurements which is also an EEG based technique it could not produce detectable signal change [100]. On the other hand, BOLD signal might also be blind to EEG oscillations an example of this might be the failure across studies to identify an average cortical BOLD signal pattern which is positively correlated with alpha power [87]. This is an expected statement since significance of the BOLD signal is evaluated by

comparing with the baseline signal intensity (at rest). Even at rest a default mode neuronal network is dynamically active in the brain. Without significant increase in the BOLD signal of each single voxel, electrical synchronization of many voxels in other words nonuniform activity of a neuronal population could provide measurable changes in EEG [101]. Moreover, while alpha oscillations are positively correlated with thalamic BOLD activity there is a negative correlation was reported with occipital–parietal areas by multiple studies [102, 89, 103, 104, 105]. Above mentioned evidences emphasize that EEG and fMRI do not measure identical responses and can be blind each other but reflect complementary information.

5.2.2 Hardware and Artifact Reduction in Simultaneous Acquisition

EEG–fMRI integration strategies for the analysis of brain state fluctuations started to use simultaneous acquisition more dominantly over separate and interleaved acquisition. Because, different stages of the vigilance and variations of acting manner makes the objective assessment of the results difficult for the recordings of EEG and fMRI in separate sessions. Effect of adaptation for perceptual and cognitive experiments, effect of different positions of subjects (generally upright in EEG and supine in fMRI) on physiological responses and finally environmental differences (noise of MR machine) are other criticisms on separate recordings [106]. In spite of early studies based on separate recordings, integration strategies applicable for simultaneous acquisition will be discussed in the next part. Before that recent advances in hardware and artifact reduction which makes simultaneous acquisition possible will be mentioned. Significant improvements have been made fallowing the first reported EEG recording inside an MR scanner by Ives and colleagues [107]. Difficulties basically due to the environmental properties of MR room during an fMRI scan. Static high magnetic field, rapid changing imaging gradients, radio frequency (RF) excitations, vibration and finally motion make the EEG recording challenging for hardware and achieving sufficient signal quality.

High magnetic field hinders the use of standard EEG amplifiers consist of fer-

romagnetic materials in the MR room. On the other hand transferring signals far from measuring location to the amplifier increases artifacts despite the reduced field strength, because motion artifacts increases under the inhomogeneity of the gradient field. Preferably, short lead guides are placed parallel to the z axis of the scanner around which the gradient switching occurs, the signal is amplified and digitized very close to the measuring site (proximity of the bore magnet) by MR compatible amplifiers and digital signal is carried to the recording location by fiber–optic cables [15].

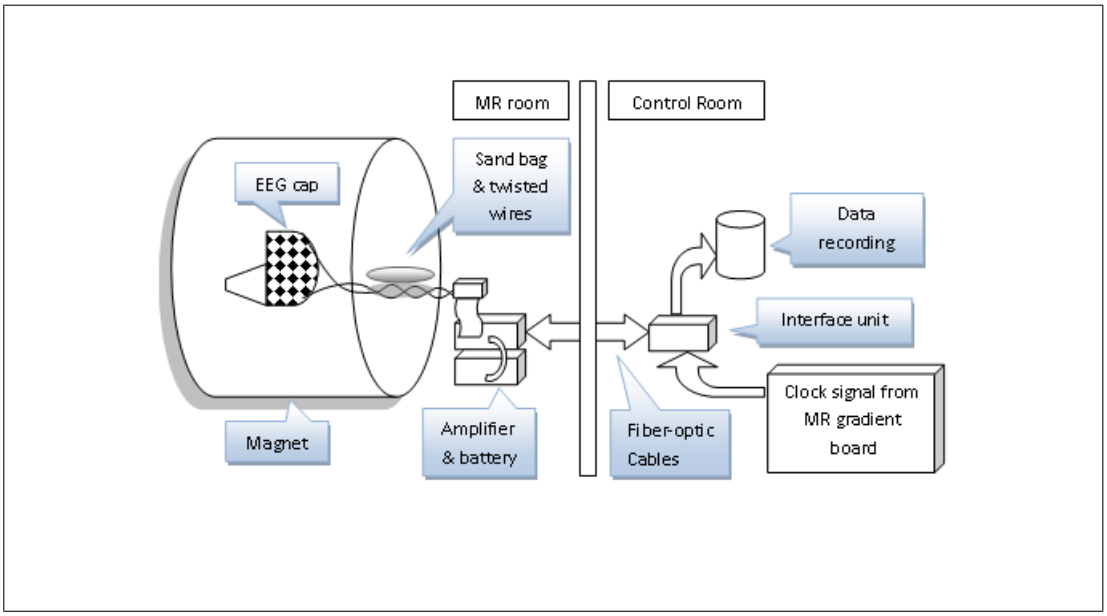

Figure 5.2 Schematic presentation of a modern EEG/fMRI setup.

Recent MR compatible EEG amplifier systems are free of ferromagnetic materials (mostly copper, gold or carbon), use short leads and could be placed inside the MR room. Specifications of these amplifiers also satisfies, high amplitude of measured signal in order not to attenuate (± 3.2 mV to ± 325 mV), high sampling frequency to partially catch the slew rate of imaging gradients (5000 Hz) switchable high input impedance (10 MΩ/10 GΩ) for the safety issues [87]. Additionally, for the sake of signal quality using a vacuum head cushion, tape, bandage or electrode cap to keep wires in a optimized predefined position, twisting of all wires to cancel induced fields each other out, avoiding loops and immobilize wires via sandbags are other artifact reduction strategies in the literature (Figure 5.2) [108, 109]. Finally, synchronization (phase–locking) of EEG sampling with the MR gradient board clock signal by using additional components,

effectively improves performance of the artifact reduction methods and eliminates the necessity for over–sampling of the EEG signal [110].

Despite the optimized hardware designs in an EEG–fMRI setup, artifacts still occur in the range of physiological EEG frequency spectrum. Defining artifact sources clearly is the key point for artifact reduction algorithms. Artifact caused by the magnetic field changes and RF excitation, which induce current on EEG leads is referred as imaging or gradient artifact. Gradient artifact is stationary over time but has the largest amplitude (about 1000 times higher than EEG signals) [15]. The ballistocardiogram (BCG), or pulse artifact is caused by pulsations of the scalp arteries [16]. The BCG artifact is higher but close to the amplitude range of EEG signal (up to 200 μV at 3T), spatially and temporally unstable. Most of the BCG power lies in the frequency range of 1–10 Hz, waveforms are often similar to interictal spikes and varies between EEG channels, within and between subjects [111]. This second type of artifact is more challenging because of its unpredictable nature. Both of them add linearly to the EEG signal.

Basic principle of the first gradient artifact reduction methods is to find an average template of artifact waveform and subtract it from the measured signal [15]. Template waveform is achieved by averaging the EEG signal for each MR image acquisition period (for each TR). MR and EEG synchronization is very crucial for this step because even a small drift in detection of the period onsets, due to the low EEG resolution or time delay, results in inaccurate template generation, residual gradient induced spikes after correction and finally unsuccessful artifact reduction. Synchronize EEG sampling and fMRI scanning using a sole clock is an alternative but modification of both systems is not possible in many situations [112]. Good results have been obtained by subtraction of the average template followed by adaptive noise canceling (ANC) even in the absence of the slice timing signals by using adaptive FIR method [15, 54]. FMRI artifact slice template removal (FASTR) algorithm similarly uses subtraction of local artifact templates and decomposes residuals using Principal Component Analysis (PCA) finally ANC filtering [113]. Infomax Independent Component Analysis (ICA) is another technique to find most correlated components with artifact template [114].

It has to bear in mind that, template generation technique is based on the rationale that the average EEG signal, time–locked to the each TR period, is zero and imaging artifact waveform does not fluctuate.

BCG artifact reduction methods are very similar those mentioned for gradient artifacts. Period onsets for template is marked by QRS or "R–peak" detection methods and using an additional ECG electrode. Because of the non–stationary nature of BCG artifacts, a sliding average approach with or without additional weighting is beneficial [16, 109]. Besides, indirect measure of the BCG waveform by using a piezoelectric motion sensor located over the temporal artery has been proposed [115]. This method correlates motion sensing signal and EEG by adaptive Kalman filtering. Temporal PCA has also been used to remove BCG artifact [108]. Advantage of this technique is the slight BCG artifact variations can be tolerated. There is a detailed and comparative study about the performance of artifact removing algorithms in the literature [111].

5.2.3 EEG & fMRI Data Fusion Methods

Integration strategies can be classified in to two main approaches. Firstly, the earlier and the widely accepted and used approach is based on giving the prior information (prediction and constraints) of one modality to the other. This technique necessitates the initial processing of EEG or fMRI data thus can be named as asymmetrical analysis approach. Secondly, symmetrical approach is based on the fusion of both data by constructing a general forward model [87].

Asymmetrical approach includes two different perspectives: i) fMRI constrained source estimation of electrophysiological data; ii) EEG informed (in time or frequency domain) prediction of fMRI activations.

Since, inverse problem solutions are problematic basically concerning uniqueness, using fMRI activation sites to constrain solution space could be beneficial in the finding of ERP source estimation more precisely and approximation of functional

connectivity [116]. However, hard constraint may cause severe distortions or elimination of meaningful EEG sources when there are distinct mismatches between the fMRI activations and the EEG estimates. Adjustable weighting of fMRI information in a priori source covariance matrix was proposed with simulated data without excluding the non–fMRI source locations [117]. Another technique which is automatically adjusts the strength of fMRI constraint according to the mismatch level was suggested [118]. The relevance of fMRI–derived prior information characterized by Bayesian theory is more promising because the weighting is determined by data itself [119]. Additionally, it has been showed that anatomical and functional constraints in the weighting of solution space by using weighted minimum norm method can improve accuracy of the solution [120]. Besides, it has to be kept in mind that the two modalities do not measure identical phenomena. These methods are useful and reliable when the approximate locations of the ERP sources are known [10]. That's why this type of approach has a limited effectiveness among EEG/fMRI integration strategies.

EEG–informed fMRI can be applied in pathological brain activity such as interictal epileptiform activity (IEA) and endogenous brain oscillations which is conducted under uncontrolled experimental conditions such as relaxed wakefulness or sleep [87]. The electrophysiological signal is tried to correlate with variance of fMRI BOLD signal during the analysis. IEA or sleep spindles are used to mark period or onset of events on the fMRI signal [121, 122, 123, 124]. In this sense method can be defined as a forward model from EEG data to fMRI [87]. EEG frequency domain correlation with fMRI signal fluctuations can be done besides aforementioned time domain based correlations [125, 126, 127]. Beyond that, single trial ERP data has been used to generate predictors of fMRI activity [128, 129, 130, 88, 131, 132]. This approach is an example of paradigm controlled experiment since ICA parameters of EEG, P300 or N100 amplitude and/or latency is convolved with hemodynamic response function and is used directly in the GLM stage of fMRI analysis.

Symmetrical fusion approaches is aimed at utilizing both electrical and hemodynamic measurements simultaneously and symmetrically in spatio–temporal assessment of brain function [133, 87]. This technique requires explicit definition of common neu-

ronal processes that elicits both EEG and fMRI data. Current advances are settled on neuronal mass model (NMM) in this field [134, 135, 136, 137, 91, 64]. As a conclusion, cross–modal analysis of dynamic coupling using complementary information from EEG and fMRI within the framework of nonlinear system identification is an important issue and must further be developed.

5.3 Simultaneous EEG/fMRI Analysis of the Resonance Phenomena in Steady State Visual Evoked Responses

Although functional neuroimaging technologies such as PET or fMRI have made it possible to localize the brain activations with a high precision in the 3 dimensional space, electroencephalogram (EEG) as a non–invasive measurement technique of brain electrical activity is still one of the important tools for investigating human brain function under physiological and pathological conditions [138]. Beyond the easy and comfortable application using inexpensive equipments, the continuing importance of EEG based measurements depends mainly on the high temporal resolution of the EEG signal in the millisecond range, while the hemodynamic or metabolic activities measured with fMRI and PET suffer from a poor temporal resolution due to the slower temporal dynamics of the vascular and metabolic responses, which indirectly reflect neuronal activity changes [10].

In fact, EEG is also an indirect signal of the cortical neuronal activity, because it represents the spatial sum of the post–synaptic potentials generated on the cortical pyramidal cells. The volume conduction in the brain tissue and in–homogenous electrical conductances of the tissues between the EEG generators and the scalp lead further to blurring of the signal, which makes it almost impossible to directly relate the EEG signal with the neuronal activity within the cortex. On the other hand, the spatial summation of the post–synaptic activity in the brain volume–conductor that builds the biophysical basis of the measurement of neuro–electric signals from the scalp, offers EEG the special property of representing the local and large–scale synchronizations

within and among neuronal groups [81]. In other words, the EEG amplitude represents the level of neuronal synchronicity but not the level of the non–synchronized neuronal activity [139]. Such synchronization patterns in the EEG can either be observed as transient waveforms such as epileptic spikes or in the form of spontaneous, evoked or induced rhythms in various frequency bands [76].

One of the synchronized states in the EEG that can be well–controlled by the external events is the steady–state evoked potential produced by trains of stimuli with an inter–stimulus interval (ISI) shorter than needed for the complete processing of a single stimulus [25]. While the EEG response to a single stimulus decays in hundreds of milliseconds, regular oscillatory responses are obtained by driving the brain with stimulus trains with shorter ISIs, which is also used to obtain the photic driving response in clinical EEG [140]. Such steady–state stimulation has been mostly applied in the visual modality, and EEG oscillations at the stimulation frequency could be observed with flickering light up to 100 Hz frequency, when EEG segments were averaged phase–locked to the stimuli [23]. The spectral analysis of the averaged steady–state visual evoked potentials (SSVEP) reveals mainly peaks at the stimulation frequency and its harmonics.

The stability of the SSVEPs across trials and subjects makes them a suitable tool for the investigation of the visual system. Furthermore, the well–defined frequency spectra of the SSVEPs make them less prone to EEG artifacts, as SSVEPs can be efficiently quantified by measuring the amplitudes of the spectral peaks at the stimulation frequency and its harmonics by excluding the effects of the artifacts occurring at other frequency ranges. Because of these properties some research groups developed SSVEP based techniques also for measuring cognitive processes [141], where the modulation of the amplitude or phase of the SSVEPs produced by repetitive stimuli in the background of the task–related event were used as measures of cognitive processes under study [142, 143].

Studies measuring the SSVEPs with systematically varying flicker frequencies have shown that their amplitudes do not change uniformly or monotonously with chang-

ing stimulation frequencies [23, 25]. The reproducible pattern of the frequency characteristics of SSVEPs shows a clear peak around 10 Hz and additional local maxima around 20, 40 and 80 Hz. While these frequencies have been pragmatically used to obtain large SSVEP responses [143], it is important to understand the neuronal mechanism lying behind this phenomenon to effectively use SSVEPs for testing sensory or cognitive functions. Various studies have argued that the peaks in the SSVEP frequency characteristics represent resonant behavior of damped neuronal oscillators in the sensory system [23, 144], while for the scalp recorded data these peaks could also have other explanations such as different positions and orientations of the respective dipoles to the scalp surface. However, a study carried out in the cat brain with intracranial electrodes supported the resonance hypothesis by showing similar spectral peaks in the local field potentials (LFP) in visual sensory areas 17 and 18 [24]. According to the authors, these spectral characteristics represent the behavior of strongly damped oscillators, which are tuned to different frequency bands and get entrained to variable extents at a large range of stimulation frequencies. Therefore, periodic activation with stimuli matching the frequency preference of these tuned oscillators is expected to reveal resonance phenomena which can be observed as global and local peaks in the SSVEP frequency characteristics. The simultaneous EEG/fMRI measurement allows to test the resonance hypothesis about the selective increases in SSVEP amplitudes at certain stimulation frequencies in human subjects. While EEG as a measure sensitive to the synchronicity of neuronal activity would catch the resonance phenomena at the tuning frequencies of the neuronal oscillators with large SSVEP amplitudes, blood oxygen level dependent (BOLD) signal of the fMRI, which depends on the metabolic demand of both synchronously and non–synchronously activated neuronal populations [2], would change independent of the synchronization level. An inverse correlation between the EEG amplitudes and BOLD response is already shown for spontaneous alpha rhythm that represents a synchronized state of cortical neuronal activity [89, 105]. Such frequency–dependent changes in the coupling between EEG and hemodynamic signal during steady–state visual responses may shed light on the neuronal mechanisms responsible for the SSVEP generation and visual perception. This study aims to analyze the neuronal dynamics in the visual sensory system that lead to the SSVEPs by investigating their BOLD counterparts obtained through visual stimulation at various

frequencies [14]. For this purpose, flickering light was used to stimulate visual areas at systematically varying frequencies between 6 and 46 Hz, and the correlations between SSVEP amplitudes and the BOLD responses were computed for 3 different frequency ranges, which showed different levels of correlation between both signals.

5.3.1 EEG Pre–processing

After eliminating the epochs with eye and muscle artifacts manually, EEG was down–sampled to 1kHz and averaged over non–overlapping epochs of 1 s duration along the 3 stimulation blocks for each stimulation frequency (Figure 5.3). The amplitude spectra of the averaged SSVEPs were then obtained by computing the magnitudes of the Fast Fourier Transforms (FFT) of the repetitive SSVEP signals. As the amplitude spectra of the SSVEPs obtained with all stimulation frequencies contained peaks at the stimulation frequency (fundamental frequency) and at least its first and second harmonics, the SSVEPs at each stimulation frequency were quantified by adding the amplitudes at the stimulation frequency and its first and second harmonics. Because the topographical pattern was clearly occipital, mean amplitudes of the O1, Oz, and O2 electrodes were used in further analyses.

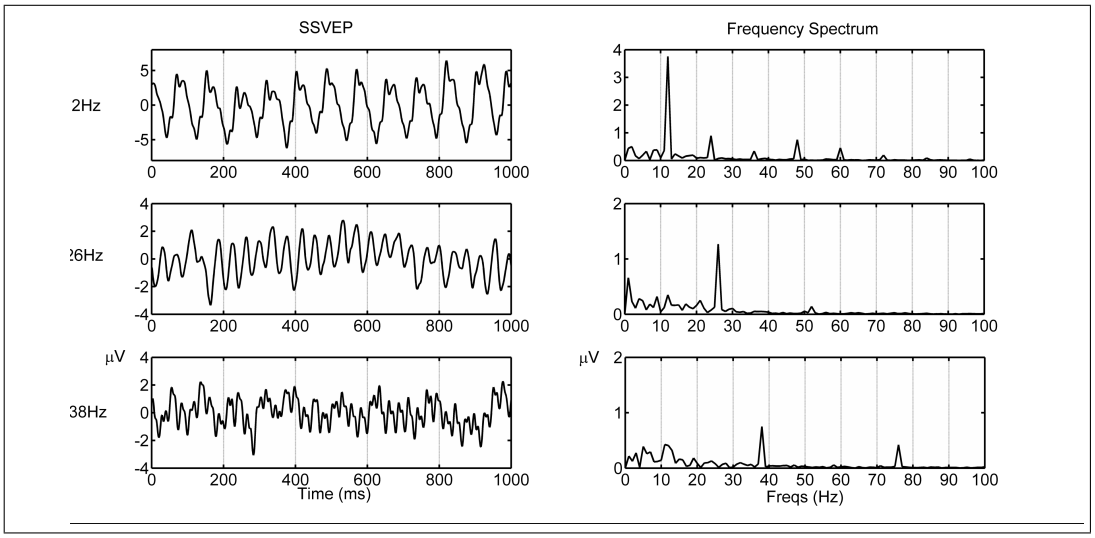

Figure 5.3 Left column: Sample SSVEPs of a typical subject obtained with three different stimulation frequencies. Right column: The frequency spectra of the SSVEPs showing peaks at the stimulation frequencies and their harmonics.

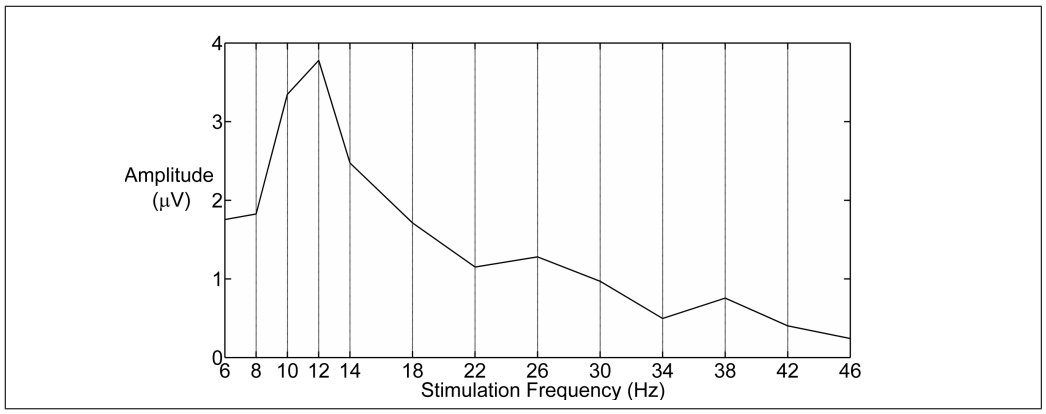

Figure 5.4 The SSVEP amplitudes of a subject quantified as the sum of the spectral peaks at the stimulation frequency and its first and second harmonics at 13 visual stimulation frequencies. Average amplitudes from the O1, Oz and O2 channels have been used for SSVEP–informed fMRI analysis.

The individual SSVEP frequency characteristics were then obtained by plotting the SSVEP amplitudes vs. stimulation frequencies for each subject (Figure 5.4).

5.3.2 EEG informed fMRI processing

Software tools within FSL (FMRIB's Software Library, FMRIB, Oxford, UK) were used in fMRI data processing [145]. Data were pre–processed prior to performing general linear model (GLM) analysis. Motion correction, slice timing correction, non–brain removal, spatial smoothing using a Gaussian kernel of FWHM 8.0 mm, grand–mean intensity normalization of the entire 4D dataset, high–pass temporal filtering (Gaussian–weighted least–squares straight line fitting, with sigma=45.0 s) were applied [69].

In the first stage, GLM time series analysis with local autocorrelation correction was applied in order to find BOLD related signal changes discriminating the visual stimulation periods from the rest periods [71]. For this, basic boxcar model which is convolved with the double–gamma hemodynamic response function (HRF) was used with its temporal derivative in the design matrix.

In the second stage, higher–level single subject multi–session GLM analysis was

applied using random–effects analysis for specific ranges of stimulation frequencies to combine analysis of previous level and integrate it with SSVEP derived data [72]. The frequency ranges were defined according to the peaks in the frequency characteristics of the SSVEP responses that represent SSVEP amplitude changes vs stimulation frequencies. After the analysis of the SSVEP frequency characteristics of 40 subjects, the sessions were grouped into 3 frequency ranges with a SSVEP amplitude maximum in each of them. These frequency ranges roughly corresponded to the alpha (6–12 Hz), beta (14–26 Hz) and gamma (30–46 Hz) bands of the EEG. The amplitude patterns of the SSVEP responses of each subject across 4 (alpha: 6,8,10,12 Hz and beta: 14,18,22,26 Hz) or 5 (gamma: 30,34,38,42,46 Hz) different stimulation frequencies were used as SSVEP derived fMRI regressors. To model only fMRI activity correlated with the SSVEP amplitudes, mean of the amplitudes representing the common response to all stimulation frequencies in the frequency band was removed, and a zero–mean vector was obtained for each frequency band of each subject. Parameter estimates (PEs) of the first–level fMRI analysis were then modeled in the design matrix with a vector of ones representing mean fMRI activation in the whole frequency band and a zero–mean SSVEP derived fMRI regressor as an additional covariate representing the SSVEP correlated visual stimulation effects in the fMRI. By this means, mean fMRI activations and SSVEP correlated fMRI activations were obtained for each subject and frequency band. In the third stage, multi–subject single–band group average GLM (one–sample t–test) design was setup and performed to test the consistency of the fMRI and SSVEP informed fMRI results obtained in the 2nd stage across 40 subjects. Gaussian Random Fields (GRF) theory based maximum height thresholding with a (corrected) significance threshold of $P<0.05$ was employed for Z (Gaussianised T/F) statistic images [75]. Average and EEG correlated Z statistic images were registered to standard space (MNI152) [69].

5.4 SSVEP results

The total number of 1 s epochs obtained during the 3 visual stimulation blocks at each stimulation frequency was 132 (3 x 44 s), and after artifact removal the mini-

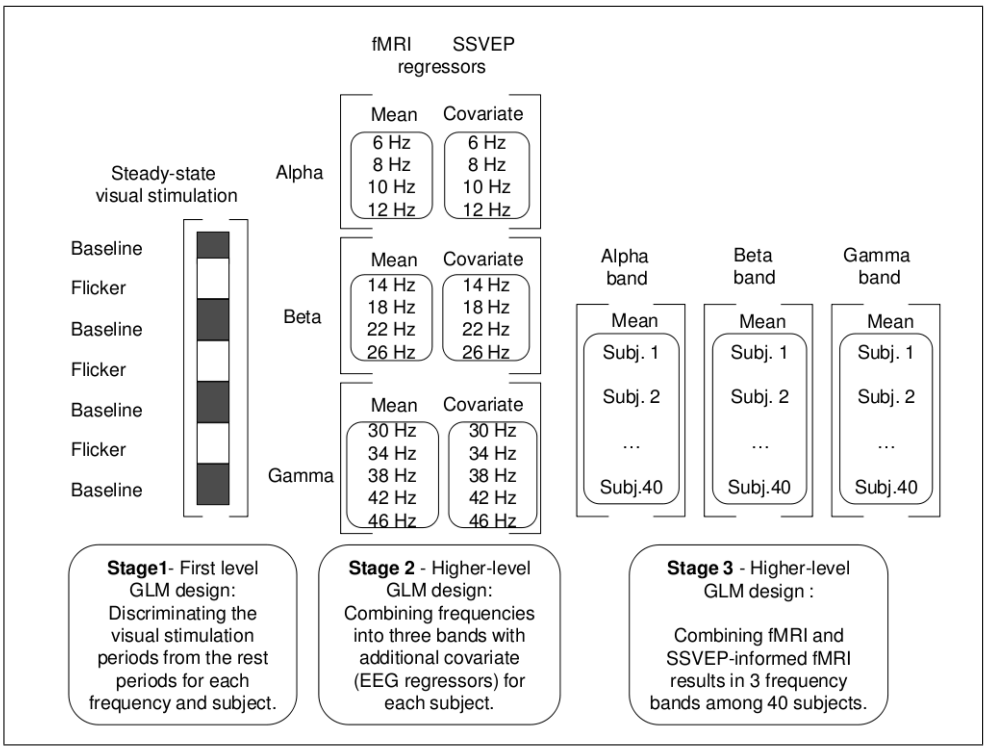

Figure 5.5 Short description of the SSVEP–informed fMRI analysis.

mum number of usable epochs was 108 among the 40 subjects. The averaged SSVEP responses displayed clear oscillatory patterns phase–locked to the visual stimuli and the frequency spectra of the responses showed peaks at the stimulation frequency and its harmonics (Figure 5.3). As spectral peaks could be observed at least up to the 2nd harmonic for all stimulation frequencies, the representative SSVEP amplitudes for each stimulation frequency were obtained by adding the amplitudes at the fundamental frequency (stimulation frequency) and its 1st and 2nd harmonics.

Figure 5.4 displays the SSVEP amplitudes of one subject at each of the 13 stimulation frequencies. Although the exact peak frequencies had a variability among the subjects, the general pattern of visual SSVEP amplitudes across the stimulation frequencies consisted of a global maximum around 10 Hz and secondary local maxima around 20 and 40 Hz in line with the findings of previous studies [23].

5.5 fMRI and SSVEP–informed fMRI results

In the first stage of the three–level analysis of fMRI data, the voxels with significantly higher BOLD responses during the visual stimulation compared with the rest period were obtained separately for each stimulation frequency in each subject.

In the second–stage of the analysis, the main aim was to investigate the correlation between the fMRI activations and the SSVEP amplitudes at different stimulation frequencies. Considering that the generation of the 3 main amplitude maxima observed in the SSVEP frequency characteristics might depend on different mechanisms, the full spectrum of visual stimulation frequencies was divided into 3 ranges according to the location of the peaks, so that each of the 40 subjects had a peak in each of these frequency bands. The resulting frequency ranges were 6–12 Hz, 14–26 Hz and 30–46 Hz, which roughly corresponded to the alpha, beta and gamma frequency bands of the EEG.

Second–stage analysis gathered together the results of the first–stage analysis for each of these 3 frequency bands at the single–subject level. To obtain the fMRI activations which are correlated with the SSVEP amplitude changes across the different stimulation frequencies within each band independent of the fMRI activations that are common among the different stimulation frequencies, two regressors were used in the GLM design. The first one consisted of the same weighting factor, 1, for each stimulation frequency, while the second regressor stemming from the SSVEP amplitudes to the same stimulation frequencies was transformed to a zero–mean vector by removing the mean.

The third–stage, which tested the consistence of the findings of the second stage among 40 subjects resulted in fMRI activation maps that are common for all stimulation frequencies in each of the 3 bands (Figure 5.6) and that are correlated with the pattern of change of the SSVEP amplitudes among the different frequencies in each frequency range (Figure 5.7).

Mean fMRI activity that is independent of the SSVEP amplitudes (Figure 5.6) shows, that in all 3 bands the lateral geniculate nuclei, the primary visual cortex (BA17) and visual association areas (BA18 and BA19) were active. In general the level of activity decreased slightly with increasing frequencies. Additional activations were observed in the precuneus and bilateral in the hippocampi and dorso-lateral prefrontal cortices (BA46 and BA47).

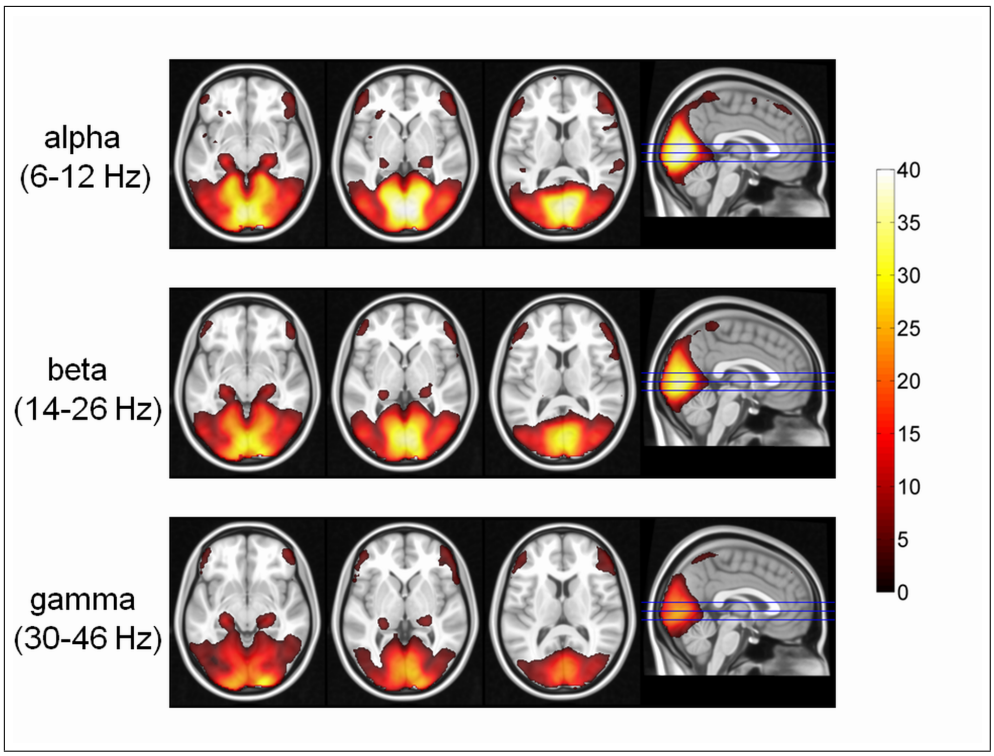

Figure 5.6 Mean fMRI activation maps of 40 subjects obtained with visual stimulation in the alpha, beta and gamma frequency ranges. Colors represent the Z (Gaussianised T/F) scores. For all frequency bands, significant BOLD increase were observed in the primary (BA17) and secondary visual areas (BA18 and BA19), bilateral dorsolateral prefrontal cortices (BA46 and BA47), bilateral hippocampi (left column), LGN (2nd column) and precuneus (right column).

The fMRI activity maps that were correlated with the SSVEP amplitude changes across the different stimulation frequencies within each frequency band, while a significant correlation was obtained in the primary visual area (BA17) and lingual gyri (BA19) for the beta band, and in a limited area of the primary visual cortex for the gamma band (Figure 5.7).

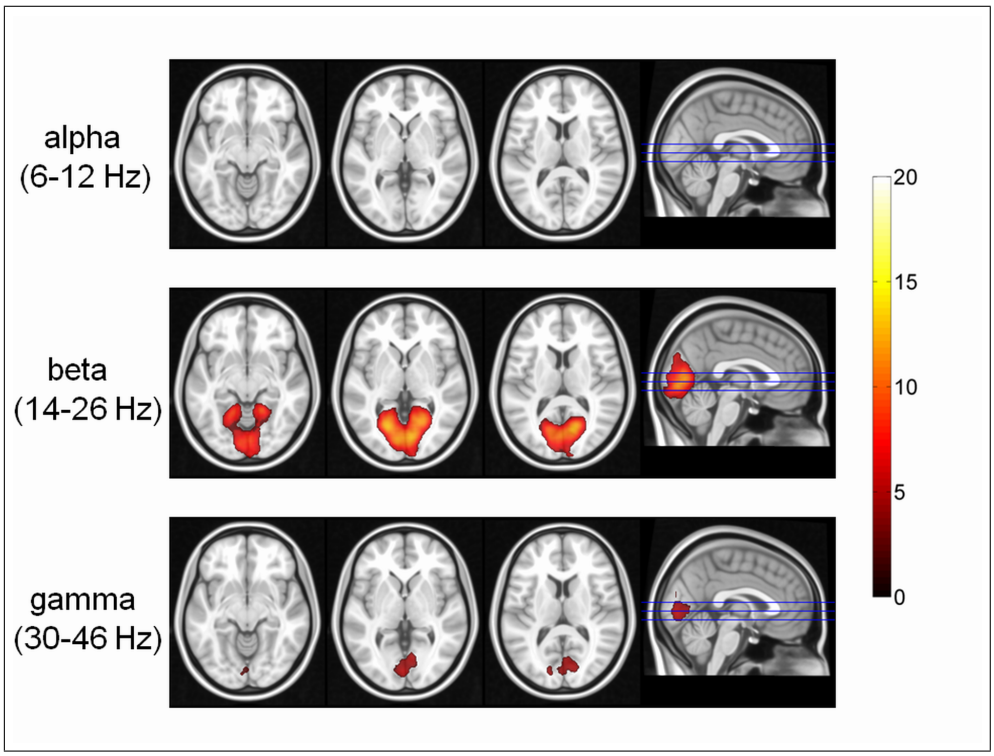

Figure 5.7 SSVEP correlated fMRI activation maps of 40 subjects obtained with visual stimulation in the alpha, beta and gamma frequency ranges. The maps are based on the significantly correlated change of the BOLD responses with SSVEP amplitudes across the different visual stimulation frequencies in each frequency band. Colors represent the Z (Gaussianised T/F) scores. For the beta band, BOLD responses in the primary visual cortex (BA17) and lingual gyri (BA19) showed a significant correlation with SSVEP amplitudes, while for the gamma band an SSVEP-correlated BOLD response could only be observed in the primary visual cortex.

5.6 Discussion

The strength of the present study is that it is the first study that recorded simultaneous EEG/fMRI responses with steady–state visual stimulation at systematically varying stimulation frequencies between 6 and 46 Hz in a large group (40) of subjects to obtain reliable information about the neural events generating the steady–state visual evoked responses. The change of SSVEP amplitudes along the stimulation frequencies revealed individual variability in the peak frequencies among the subjects, but the presence of three amplitude maxima around 10, 20 and 40 Hz was the common finding for all 40 subjects. This result is in accordance with earlier studies on SSVEP frequency characteristics [23, 24, 25].

In the present study, BOLD responses during steady–state visual stimulation

revealed significant increases in primary sensory and association areas of vision and in the thalamus (LGN) when visual stimulation periods were compared with the rest periods. Although a slight decrease in the strength of this hemodynamic response was observed with increasing stimulation frequency, the same areas were active along the whole range of stimulation frequencies. Also some weaker activations were observed in the precuneus, bilateral hippocampi and prefrontal cortices. We will first focus on the activities recorded in the visual areas, but these latter activations will also be shortly discussed.

The presence of clear oscillatory SSVEP responses in the EEG in–line with significant increases of BOLD responses for all stimulation frequencies shows that there is a high temporal correlation between both electrophysiological and hemodynamic responses in terms of the signal change during stimulation periods compared with the rest periods. This finding is in accordance with the EEG/fMRI results reported by Rosa an coworkers [36], who showed a high temporal correlation between the EEG spectral parameters and the BOLD response during steady–state visual stimulation with checkerboard reversal rates of 2, 3.75, 5, 6, 7.5, 10, 15, and 30 Hz. However, this study pooled all stimulation frequencies and did not compare the responses in both modalities among the different stimulation frequencies, which is the main focus of the present work. For the analysis of the correlations between the SSVEP and BOLD responses among different stimulation frequencies, we divided the whole range of 13 visual stimulation frequencies into 3 frequency ranges, because the common finding was that each subject's SSVEP frequency characteristics contained a peak in each of the 3 frequency ranges, 6–12 Hz, 14–26 Hz and 30–46 Hz, which roughly correspond to alpha, beta and gamma frequency bands of the EEG. A further reason for the analysis of responses at different stimulation frequencies in 3 sub–bands was that the SSVEP frequency characteristics showed strongly decreasing amplitudes with increasing stimulation frequencies after a global peak around 10 Hz. Therefore, analysis of the correlations between the fMRI activations and the SSVEP amplitudes along the whole range of 13 stimulation frequencies would mainly reflect the effects in the lower frequencies and any normalization procedure to overcome this problem would introduce an arbitrary bias to the data. The 3 bands allowed to analyze the correlations between

both modalities through responses of comparable amplitudes.

We found no correlation between the SSVEP and BOLD responses for the stimulation frequencies between 6 and 12 Hz (alpha range), while there was a significant correlation in the primary visual cortex (BA17) and lingual gyri (BA19) for the stimulation frequencies between 14 and 26 Hz (beta range) and a significant correlation in a limited part of the primary visual area (BA17) for frequencies between 30 and 46 Hz (gamma range). This pattern of correlations is especially interesting, because the global maximum of the SSVEP amplitudes is consistently obtained around 10 Hz, where no cross–frequency correlation was present between EEG and fMRI. Based on previous results in animal subjects, which show that the BOLD response in a cortical volume is correlated with the synaptic activity measured in the form of local field potentials [2], this finding suggests that the strong peak of the SSVEP in the alpha band does not depend on an increase of the total synaptic activity compared with visual stimulation at other frequencies in the frequency band. This finding is in favor of the hypothesis that the global peak of the SSVEP amplitudes reflects the resonance of oscillators tuned to this frequency, because the repetitive stimulation at this frequency yields strongly synchronized neuronal activity without a net increase in the total synaptic activity. The report by Parkes and coworkers [35] on the reduced BOLD response obtained with periodic stimulation compared with stimuli delivered with a latency jitter supports this view in terms of a reduced metabolic demand for the entrainment of neuronal oscillators into a rhythmic pattern. Hence, resonant entrainment of the neuronal oscillator leads to large amplitudes in the scalp recorded EEG, which is sensitive to neuronal synchronicity, while BOLD signal, which is mainly sensitive to the total amount of synaptic activity, does not show any significant change compared with the stimuli at non–resonant frequencies. Such discrepancy between the SSVEP and BOLD response at the resonant frequency is especially plausible if the inter–neurons within the investigated cortical volume do not play a role in the resonating circuitry, and therefore their synaptic work does not contribute to the BOLD response generated in the cortical volume. The modeling study by Robinson and coworkers [146], which shows that resonant behavior near the alpha peak both in the spontaneous EEG and in SSVEP can be explained by the cortico–thalamic loop delays, supports this point.

Furthermore, a number of studies, which reported a negative correlation between the BOLD activity and the EEG alpha power in the occipital cortex [89, 147, 105] also support the finding that high amplitude alpha oscillations do not require a high metabolic rate in the cortex. The same does not hold for secondary SSVEP peaks observed within the beta and gamma frequency ranges. In the beta band, a strong correlation is observed between the SSVEP and the hemodynamic response in a large part of the primary visual area and partially in the secondary visual area BA19. This contrast compared with the alpha peak could be explained by either an increased synaptic input to the visual cortex from the thalamus at the beta and gamma peak frequencies, which would increase the BOLD signal in–line with the SSVEP peak, or again by a resonance of a neuronal oscillator but this time consisting of a local neuronal network with significant contribution of inhibitory or excitatory inter–neurons within the cortical volume, which would increase the metabolic demand and therefore BOLD response in the investigated area. Which of these two possible mechanisms holds true for the beta and gamma SSVEP peaks needs further investigation by analyzing the possible changes in effective connectivity between the LGN and the primary visual area across the stimulation frequencies in the beta and gamma frequency ranges. However, in vitro evidence for the cortex that the interplay between excitatory pyramidal cells and inhibitory inter–neurons is essential for the generation of oscillatory activities within beta and gamma frequency ranges [148, 149] suggests that the latter mechanism might be responsible of the correlation between the SSVEP and BOLD responses at beta and gamma peaks. At this point, we would like to pronounce that even the presence of a linear relationship between the electrophysiological and hemodynamic signal does not dictate that the observed electrophysiological phenomenon reflects a simple summation of the synaptic activity, but the increased synaptic activity within the investigated cortical volume might be necessary for the phase–locking of the neuronal oscillators, which would yield the change in the surface–recorded EEG response. The spatial restriction of the SSVEP–correlated BOLD activity in the gamma range compared with the beta range is in accordance with EEG results that show the role of the beta oscillations in building functional interactions between more spatially distant regions of the central nervous system, while gamma oscillations build rather local patches of synchrony. In general, the localization of the SSVEP correlated BOLD activations both in beta and

gamma ranges were in accordance with previous studies about the generators of the SSVEPs [150].

The contrasting results obtained in alpha vs. beta and gamma ranges in the present study are in accordance with the results of an earlier study of our group that investigated BOLD transients obtained with steady–state visual stimuli between 1 and 44 Hz [50]. BOLD response typically consists of three transients; the initial dip, the positive BOLD (PBOLD) and the post–stimulus undershoot (PSU), which have been explained by the balloon model of the dynamics of blood flow and oxygenation changes during brain activation [20] or the independent change of model components under specific conditions [151]. Later, a biophysical model of the coupling between neuronal activity and the balloon model was proposed, which showed that increases in excitatory activity amplify both the PBOLD and the PSU, whereas increasing the inhibitory activity evokes decrease in the PBOLD signal without altering the PSU [64]. The results by Emir and coworkers [50] revealed that PBOLD and PSU were correlated during visual stimulation between 1 and 13 Hz suggesting that they might be attributed to exclusively excitatory inputs from a distant source [81]. However, the PBOLD and PSU were uncorrelated between 13 and 44 Hz, possibly because of the significant contribution of the inhibitory inter–neurons within the cortex in the neuronal responses produced within this frequency range. The same mechanism might explain the present results about the alpha vs beta and gamma oscillations in the following manner: The synchronizing long–range excitatory input to the cortex at the alpha peak does not lead to a significant increase in the cortical metabolic rate resulting in uncorrelated SSVEP and PBOLD changes, while the resonance of the neuronal oscillators that operate in the beta and gamma frequency ranges requiring interaction of the local inhibitory and excitatory neurons leads to increased energy demand in the cortical volume leading to correlated increases in SSVEP and PBOLD responses.

An earlier study with the similar aim to investigate human cerebral activation during steady–state visual evoked responses [152] as in the present study, applied EEG and regional cerebral blood flow (rCBF) measurements with positron emission tomography (PET) in separate sessions. The authors reported a SSVEP amplitude maximum

at 15 Hz. On the basis that the primary visual cortex rCBF follows an activation pattern similar to the SSVEP amplitudes among stimulation frequencies at 5, 10, 15, 25 and 40 Hz, the authors concluded that the SSVEP peak corresponds to a true activation of neuronal clusters in primary visual cortex and is not a phase summation effect. First of all, the global SSVEP peak frequency reported in this study does not correspond to that in other SSVEP studies [23, 25] and in the present study, possibly because of the different stimulation conditions. The authors used stroboscopic flashes, which leads to increasing mean luminance with increasing stimulation frequency. This problem was overcome by both Herrmann [23] and in the present study by using LED light sources with 50% due time, such that the mean intensity of the light remained constant across stimulation frequencies. Additionally, it is well described before studies [23, 25] and in the present study, that the SSVEP amplitude maxima are not exactly at the same frequency for all subjects. Regarding the present results for example, SSVEP amplitude maximum can be obtained at stimulation frequencies between 8 and 12 Hz for different subjects. Therefore, the grand–average SSVEP frequency characteristics show rather broad peaks compared with the individual ones. Probably, this is the reason, why Pastor and coworkers [152] sampled the rCBF measurements at only 5 different stimulation frequencies of 5, 10, 15, 25 and 40 Hz, which were chosen according to the SSVEP peaks in their EEG sessions. This low sampling of stimulation frequencies may be the reason why the authors did not observe the non–linear effect we obtained in the alpha frequency range, which we sampled with stimuli at 6, 8, 10 and 12 Hz. Furthermore, the correlation of the rCBF measurements from the subjects with a regressor consisting of the grand–average SSVEP amplitudes in contrast to the individual correlations we computed might also explain the discrepancy between the results.

There are two other studies that investigated the relationship between SSVEP and fMRI measurements and reported that the relationship between both responses is a linear one [37, 54]. The first one [37] recorded EEG and fMRI responses in separate sessions using a checkerboard illuminated with flashes of 1 ms duration at 2, 4, 6, 8, 10 and 12 Hz, and found a SSVEP peak at 8 Hz in 7 of 8 subjects and at 6 Hz in one subject. These SSVEP peaks that roughly correspond to the maximal hemodynamic

responses both in PET or fMRI studies [55, 35] resulted in a high correlation between SSVEP and BOLD signals. However, atypical SSVEP peaks at 6–8 Hz instead of the expected peak around 8–12 Hz and the uncorrected mean light intensity due to the 1 ms flashes at different frequencies makes it questionable, whether the linear relationship depends on the intensity or the frequency of the applied visual stimuli. The thick MRI slices of 10 mm might also be responsible for the discrepant results compared with the present study. The other study by Wan and coworkers [54] used radial checkerboard stimuli at 0.5, 1, 4, 8 and 16 Hz, which cannot exclude the presence of the non–linear relationship between SSVEP and BOLD responses we observed between 6 and 12 Hz.

A straightforward interpretation of the activations of the bilateral hippocampi, dorso–lateral prefrontal cortices and precuneus during the steady–state visual stimulation is hard, however, there are a range of studies, which report that the SSVEP responses in frontal electrodes are sensitive to tasks related with executive functions and working memory [144, 142, 143], which have been mostly investigated by superimposing the task–related stimuli on a sinusoidally modulated light at 13 Hz. These studies implicitly show that there are neuronal generators in the prefrontal regions which oscillate at the visual stimulation frequency. How these areas are coupled with the visual areas in terms of oscillatory activities and whether oscillations at the stimulation frequency or its sub–harmonics are obtained with higher stimulation frequencies needs further investigation. However, a sub–sampling of the visual information in higher areas might be expected in the light of the results reported on the theta–gamma coupling during visual perception [79]. The activation of these areas during the passive visual stimulation condition in the present study might depend on the self–instructed attempt of the subjects to judge the stimulation rate or a self–instructed working memory condition to predict the end of the flicker period which was constant along the whole experiment.

Additionally, information gained from the SSVEP/fMRI analyses in the present study, which overcame the temporal registration problem between both modalities by obtaining electrophysiological signals that are stationary for the duration of the slower BOLD response, might be extrapolated to the EEG/fMRI analysis of the transient event–related potentials (ERPs): More reliable and consistent correlations between

electrophysiological and fMRI responses can be expected, when the EEG/fMRI analyses are carried out on evoked or induced oscillations in separate frequency bands instead of a search for correlations between the time–domain peak amplitudes or latencies of ERPs with the BOLD response.

6. CONCLUSION

In this dissertation research, we have investigated human early visual system's dependency on the temporal frequency of the visual input by using BOLD fMRI. BOLD responses of LGN and V1 were investigated in a wide frequency range (6–46 Hz) with a fine frequency sampling (13 frequencies). LGN data revealed local peaks on a background of a non-significant decrease in BOLD response with increasing frequency. V1 activity also displayed similar local maxima with a global peak in the range of 8-12 Hz but a rapid, significant decrease of BOLD response with increasing frequency, which became especially steeper in the range of 14-26 Hz. Although the rate of decrease of V1 response was significantly higher than that of LGN, their frequency characteristics curves showed a high correlation due to the similar local maxima and minima of BOLD responses in both structures.

Despite the fact that present results are not able to explain whether these selectivities for local maxima and minima are generated by one of the structures (LGN and V1) or stem from other structures connected with any one of them, we can tentatively claim that these specific tuning frequencies play a role in thalamo–cortical interaction in the visual system. Thus, high correlation might point to preferred signal transmission frequencies in the thalamo–cortical circuitry of the visual system. Besides, strong decay of response intensities in V1 with increasing stimulation frequencies is not accompanied with a similar decrease in the BOLD signal of the LGN. Considering that the BOLD signal is mainly driven by the synaptic rather than the spiking activity of the investigated brain volume [2], the strong decay of V1 BOLD activity although the LGN activity does not change as strongly with stimulation frequency suggests the role of the local circuitry of V1 and maybe other neuronal projections from higher visual areas to V1 in this specific response characteristics. Assuming that the LGN input to V1 does not decrease but rather fluctuates around a constant level with increasing frequencies, one can explain the low-pass effect observed in the V1 BOLD responses rather as the result of higher extra–synaptic input to V1 at lower stimulation frequen-

cies. This might depend either on local network of V1 to be able to produce stronger inputs to higher cortical areas or on stronger feedback to V1 from extra–striatal areas. However, we can conclude that the selectively stronger activation for lower temporal frequencies first emerges in V1.

Another interesting finding presented in this dissertation research is about the BOLD components and their dependency to the temporal frequency parameter of the visual stimulation. Existence of the transient (tonic) and sustained (phasic) components of the BOLD signal, which do not represent similar decrease with increasing stimulation frequency, can be seen clearly. We can claim that visual stimulation frequency increase may cause the transformation of neuronal processes by which inhibitory inter–neurons start to play a more dominant role. In this sense, suppression of tonic response might be originated from the increase in the effectiveness of specialized inhibitory local networks.

In the final stage, simultaneous EEG/fMRI measurement allowed us to test resonance phenomena by combining both modalities based on giving the prior information of SSVEP amplitudes to the fMRI. In this sense, steady state visually evoked potentials (SSVEPs) are used as covariate in the GLM analysis of fMRI data. What is more, whole range of visual stimulation frequencies (6–46 Hz) are introduced to the GLM analysis in three separate frequency ranges corresponding to alpha (6–12 Hz), beta (14–26 Hz), and gamma (30–46 Hz) bands. Therefore, SSVEP correlated BOLD images are reported in 3 bands separately. We found no correlation for the stimulation frequencies in the alpha range, while there was a significant correlation in the beta and gamma range.

In conclusion, our results show a non–linear relationship between the surface recorded SSVEP amplitudes and the BOLD response of the visual cortex at stimulation frequencies around the alpha band, which supports the view that resonance at the tuning frequency of the alpha oscillator in the visual system is responsible for the global amplitude maximum of the SSVEP around 10 Hz. The SSVEP/BOLD relationships at secondary amplitude maxima of the SSVEP are linear, which however does not

exclude the possibility that they also represent resonances with significant contribution of the cortical inter–neurons to the phase–coupling of neuronal oscillators. In short, the surface–recorded SSVEPs display a frequency–selective non–linear relationship with the BOLD response, hence do not reflect a simple summation of the synaptic activity in the cortex as proposed in earlier studies [37, 54, 152]. Present work further shows that scalp–recorded EEG and fMRI reflect different aspects of the neuronal activity, hence cannot be simply fused to increase the temporal or spatial resolution of each other in many instances. However, the complementary information in each modality can efficiently answer basic questions regarding specific phenomena in each modality.

APPENDIX A. PUBLICATIONS RELATED TO THE THEME OF THE PHD THESIS

1. **Bayram, A.**, Z. Bayraktaroğlu, E. Karahan, B. Erdoğan, B. Bilgiç, M. Özker, I. Kaşıkçı, A. D. Duru, A. Ademoğlu, C. Öztürk, K. Arıkan, N. Tarhan, and T. Demiralp, "Simultaneous EEG/fMRI Analysis of the Resonance Phenomena in Steady-State Visual Evoked Responses," *Clinical EEG and Neuroscience*, Vol. 42, no. 2, pp. 98-106, 2011.

2. **Bayram, A.**, A. Ademoğlu, E. Karahan, B. Bilgiç, A. D. Duru, N. Tarhan , and T. Demiralp, "Visual stimulation frequency dependent changes in bold transients," *Frontiers in Human Neuroscience Conference Abstract: XI International Conference on Cognitive Neuroscience (ICON XI)*, 2011.

3. Demiralp, T., **A. Bayram**, E. Karahan, B. Bilgiç, N. Tarhan, and A. Ademoğlu, "Frequency response characteristics of lateral geniculate nucleus and primary visual cortex," *Frontiers in Human Neuroscience Conference Abstract: XI International Conference on Cognitive Neuroscience (ICON XI)*, 2011.

4. Karahan, E., M. Özker, B. Erdoğan, Z. Bayraktaroğlu, **A. Bayram**, C. Öztürk, A. Ademoğlu, and T. Demiralp, "Steady state visual evoked potential informed fMRI analysis for alpha, beta and gamma bands," *16th Annual Meeting of the Organization for Human Brain Mapping*, (Barcelona), pp. 818 MT–PM, 2010.

5. **Bayram, A.**, B. Bilgiç, A. B. Arslan, B. Baran, O. Tanrıdağ, and T. Demiralp, "Crossmodal interaction with the auditory modality affects the BOLD response to visual stimuli," *Frontiers in Human Neuroscience Conference Abstract: 10th International Conference on Cognitive Neuroscience*, 2008.

6. Erdoğan, B., Z. Bayraktaroğlu, **A. Bayram**, B. Bilgiç, and T. Ölmez, "Artifact reduction performance of different algorithms for simultaneous recordings of EEG and fMRI," *Frontiers in Human Neuroscience Conference Abstract: 10th International Conference on Cognitive Neuroscience*, 2008.

REFERENCES

1. Uhlhaas, P. J., and W. Singer, "Neural synchrony in brain disorders: relevance for cognitive dysfunctions and pathophysiology.," *Neuron*, Vol. 52, pp. 155–68, Oct. 2006.

2. Logothetis, N. K., J. Pauls, M. Augath, T. Trinath, and A. Oeltermann, "Neurophysiological investigation of the basis of the fMRI signal," *Nature*, Vol. 412, pp. 150–7, July 2001.

3. Niedermeyer, E., and F. Lopes Da Silva, *Electroencephalography: Basic Principles, Clinical Applications, and Related Fields*, Lippincott Williams & Wilkins, 5th ed., 2005.

4. Laufs, H., J. L. Holt, R. Elfont, M. Krams, J. S. Paul, K. Krakow, and A. Kleinschmidt, "Where the BOLD signal goes when alpha EEG leaves," *NeuroImage*, Vol. 31, pp. 1408–1418, July 2006.

5. Gazzaniga, M. S., R. B. Ivry, and G. R. Mangun, *Cognitive Neuroscience: The Biology of the Mind*, W W Norton & Co Inc, 2002.

6. Hannula, D. E., D. J. Simons, and N. J. Cohen, "Imaging implicit perception: promise and pitfalls," *Nat Rev Neurosci*, Vol. 6, pp. 247–255, Mar. 2005.

7. Purves, D., *Neuroscience, Fourth Edition*, Sinauer Associates, Inc., 4th ed., 2007.

8. Horton, J. C., and D. L. Adams, "The cortical column: a structure without a function.," *Philosophical transactions of the Royal Society of London. Series B, Biological sciences*, Vol. 360, pp. 837–862, 2005.

9. Freeman, W. J., M. D. Holmes, B. C. Burke, and S. Vanhatalo, "Spatial spectra of scalp EEG and emg from awake humans.," *Clinical neurophysiology : official journal of the International Federation of Clinical Neurophysiology*, Vol. 114, pp. 1053–68, June 2003.

10. Menon, V., and S. Crottazherbette, "Combined EEG and fMRI studies of human brain function," *International Review of Neurobiology*, Vol. 66, no. 05, pp. 291–321, 2005.

11. Başar, E., M. Schürmann, T. Demiralp, C. Başar-Eroğlu, and A. Ademoğlu, "Event-related oscillations are 'real brain responses' – wavelet analysis and new strategies," *International Journal of Psychophysiology*, Vol. 39, pp. 91–127, Jan. 2001.

12. Bandettini, P. A., E. C. Wong, R. S. Hinks, R. S. Tikofsky, and J. S. Hyde, "Time course epi of human brain function during task activation.," *Magnetic resonance in medicine : official journal of the Society of Magnetic Resonance in Medicine / Society of Magnetic Resonance in Medicine*, Vol. 25, pp. 390–7, June 1992.

13. Kwong, K. K., J. W. Belliveau, D. A. Chesler, I. E. Goldberg, R. M. Weisskoff, B. P. Poncelet, D. N. Kennedy, B. E. Hoppel, M. S. Cohen, and R. Turner, "Dynamic magnetic resonance imaging of human brain activity during primary sensory stimulation.," *Proceedings of the National Academy of Sciences of the United States of America*, Vol. 89, pp. 5675–9, June 1992.

14. Ogawa, S., D. W. Tank, R. Menon, J. M. Ellermann, S. G. Kim, H. Merkle, and K. Ugurbil, "Intrinsic signal changes accompanying sensory stimulation: functional brain mapping with magnetic resonance imaging.," *Proceedings of the National Academy of Sciences of the United States of America*, Vol. 89, pp. 5951–5, July 1992.

15. Allen, P. J., O. Josephs, and R. Turner, "A method for removing imaging artifact from continuous EEG recorded during functional MRI," *NeuroImage*, Vol. 12, pp. 230–239, Aug. 2000.

16. Allen, P. J., G. Polizzi, K. Krakow, D. R. Fish, and L. Lemieux, "Identification of EEG events in the MR scanner: The problem of pulse artifact and a method for its subtraction," *NeuroImage*, Vol. 8, pp. 229–239, Oct. 1998.

17. Biswal, B. B., "Resting state fMRI: a personal history.," *NeuroImage*, Vol. 62, pp. 938–44, Aug. 2012.

18. Hathout, G. M., B. Varjavand, and R. K. Gopi, "The early response in fMRI: a modeling approach.," *Magnetic resonance in medicine : official journal of the Society of Magnetic Resonance in Medicine / Society of Magnetic Resonance in Medicine*, Vol. 41, pp. 550–4, Mar. 1999.

19. Malonek, D., and A. Grinvald, "Interactions between electrical activity and cortical microcirculation revealed by imaging spectroscopy: implications for functional brain mapping.," *Science*, Vol. 272, pp. 551–4, Apr. 1996.

20. Buxton, R. B., E. C. Wong, and L. R. Frank, "Dynamics of blood flow and oxygenation changes during brain activation: The balloon model," *Magnetic Resonance in Medicine*, Vol. 39, no. 6, pp. 855–864, 1998.

21. van Zijl, P. C. M., J. Hua, and H. Lu, "The BOLD post-stimulus undershoot, one of the most debated issues in fMRI.," *NeuroImage*, Vol. 62, pp. 1092–102, Aug. 2012.

22. Friston, K. J., W. Penny, C. Phillips, S. Kiebel, G. Hinton, and J. Ashburner, "Classical and bayesian inference in neuroimaging: theory.," *NeuroImage*, Vol. 16, pp. 465–83, June 2002.

23. Herrmann, C. S., "Human EEG responses to 1-100 hz flicker: resonance phenomena in visual cortex and their potential correlation to cognitive phenomena.," *Experimental brain research*, Vol. 137, pp. 346–53, Apr. 2001.

24. Rager, G., and W. Singer, "The response of cat visual cortex to flicker stimuli of variable frequency.," *The European Journal of Neuroscience*, Vol. 10, pp. 1856–77, May 1998.

25. Regan, D., *Human brain electrophysiology: evoked potentials and evoked magnetic fields in science and medicine.*, New York: Elsevier, 1989.

26. Casagrande, V. A., G. Sáry, D. Royal, and O. Ruiz, "On the impact of attention and motor planning on the lateral geniculate nucleus.," *Progress in Brain Research*, Vol. 149, pp. 11–29, Jan. 2005.

27. Sherman, S. M., and R. W. Guillery, "On the actions that one nerve cell can have on another: distinguishing 'drivers' from 'modulators'.," *Proceedings of the National Academy of Sciences of the United States of America*, Vol. 95, pp. 7121–6, June 1998.

28. Büchel, C., R. Turner, and K. Friston, "Lateral geniculate activations can be detected using intersubject averaging and fMRI," *Magnetic Resonance in Medicine*, Vol. 38, pp. 691–694, Nov. 1997.

29. Chen, W., T. Kato, X.-H. Zhu, J. Strupp, S. Ogawa, and K. Uğurbil, "Mapping of lateral geniculate nucleus activation during visual stimulation in human brain using fMRI," *Magnetic Resonance in Medicine*, Vol. 39, pp. 89–96, Jan. 1998.

30. Fujita, N., H. Tanaka, M. Takanashi, N. Hirabuki, K. Abe, H. Yoshimura, and H. Nakamura, "Lateral geniculate nucleus: anatomic and functional identification by use of MR imaging.," *American Journal of Neuroradiology*, Vol. 22, pp. 1719–26, Oct. 2001.

31. Kastner, S., D. H. O'Connor, M. M. Fukui, H. M. Fehd, U. Herwig, and M. a. Pinsk, "Functional imaging of the human lateral geniculate nucleus and pulvinar.," *Journal of Neurophysiology*, Vol. 91, pp. 438–48, Jan. 2004.

32. Kastner, S., K. A. Schneider, and K. Wunderlich, "Beyond a relay nucleus: neuroimaging views on the human LGN.," *Progress in Brain Research*, Vol. 155, pp. 125–43, Jan. 2006.

33. Mullen, K. T., B. Thompson, and R. F. Hess, "Responses of the human visual cortex and lgn to achromatic and chromatic temporal modulations: an fMRI study.," *Journal of Vision*, Vol. 10, pp. 1–19, Jan. 2010.

34. Muthukumaraswamy, S. D., and K. D. Singh, "Spatiotemporal frequency tuning of BOLD and gamma band MEG responses compared in primary visual cortex.," *NeuroImage*, Vol. 40, pp. 1552–60, May 2008.

35. Parkes, L. M., P. Fries, C. M. Kerskens, and D. G. Norris, "Reduced BOLD response to periodic visual stimulation," *NeuroImage*, Vol. 21, pp. 236–243, Jan. 2004.

36. Rosa, M. J., J. Kilner, F. Blankenburg, O. Josephs, and W. Penny, "Estimating the transfer function from neuronal activity to BOLD using simultaneous EEG-fMRI.," *NeuroImage*, Vol. 49, pp. 1496–509, Jan. 2010.

37. Singh, M., S. Kim, and T.-S. Kim, "Correlation between BOLD-fMRI and EEG signal changes in response to visual stimulus frequency in humans," *Magnetic Resonance in Medicine*, Vol. 49, no. 1, pp. 108–114, 2003.

38. Wan, X., J. Riera, K. Iwata, M. Takahashi, T. Wakabayashi, and R. Kawashima, "The neural basis of the hemodynamic response nonlinearity in human primary visual cortex: Implications for neurovascular coupling mechanism," *NeuroImage*, Vol. 32, no. 2, pp. 616–625, 2006.

39. Singh, K. D., a. T. Smith, and M. W. Greenlee, "Spatiotemporal frequency and direction sensitivities of human visual areas measured using fMRI.," *NeuroImage*, Vol. 12, pp. 550–64, Nov. 2000.

40. Mirzajani, A., N. Riyahi-Alam, M. A. Oghabian, H. Saberi, and K. Firouznia, "Spatial frequency modulates visual cortical response to temporal frequency variation of visual stimuli: an fMRI study.," *Physiological measurement*, Vol. 28, pp. 547–54, May 2007.

41. Ashburner, J., "SPM: a history.," *NeuroImage*, Vol. 62, pp. 791–800, Aug. 2012.

42. Bürgel, U., K. Amunts, L. Hoemke, H. Mohlberg, J. M. Gilsbach, and K. Zilles, "White matter fiber tracts of the human brain: three-dimensional mapping at microscopic resolution, topography and intersubject variability.," *NeuroImage*, Vol. 29, pp. 1092–105, Feb. 2006.

43. Jenkinson, M., C. F. Beckmann, T. E. J. Behrens, M. W. Woolrich, and S. M. Smith, "FSL," *NeuroImage*, Vol. 62, pp. 782–90, Aug. 2012.

44. Hinds, O. P., N. Rajendran, J. R. Polimeni, J. C. Augustinack, G. Wiggins, L. L. Wald, H. Diana Rosas, A. Potthast, E. L. Schwartz, and B. Fischl, "Accurate prediction of v1 location from cortical folds in a surface coordinate system.," *NeuroImage*, Vol. 39, pp. 1585–99, Mar. 2008.

45. Fischl, B., N. Rajendran, E. Busa, J. Augustinack, O. Hinds, B. T. T. Yeo, H. Mohlberg, K. Amunts, and K. Zilles, "Cortical folding patterns and predicting cytoarchitecture.," *Cerebral cortex*, Vol. 18, pp. 1973–80, Aug. 2008.

46. Dale, A. M., B. Fischl, and M. I. Sereno, "Cortical surface-based analysis. i. segmentation and surface reconstruction," *NeuroImage*, Vol. 9, no. 2, pp. 179–194, 1999.

47. Fischl, B., M. I. Sereno, and A. M. Dale, "Cortical surface-based analysis. ii: Inflation, flattening, and a surface-based coordinate system," *NeuroImage*, Vol. 9, no. 2, pp. 195–207, 1999.

48. Uludağ, K., "Transient and sustained BOLD responses to sustained visual stimulation.," *Magnetic resonance imaging*, Vol. 26, pp. 863–9, Sept. 2008.

49. D'Souza, D. V., T. Auer, H. Strasburger, J. Frahm, and B. B. Lee, "Temporal frequency and chromatic processing in humans: an fMRI study of the cortical visual areas," *Journal of vision*, Vol. 11, no. 8, pp. 1–17, 2011.

50. Emir, U. E., Z. Bayraktaroğlu, C. Öztürk, A. Ademoğlu, and T. Demiralp, "Changes in BOLD transients with visual stimuli across 1-44 hz.," *Neuroscience letters*, Vol. 436, pp. 185–8, May 2008.

51. Hagenbeek, R. E., S. A. R. B. Rombouts, B. W. van Dijk, and F. Barkhof, "Determination of individual stimulus–response curves in the visual cortex.," *Human brain mapping*, Vol. 17, pp. 244–50, Dec. 2002.

52. Ozus, B., H. L. Liu, L. Chen, M. B. Iyer, P. T. Fox, and J. H. Gao, "Rate dependence of human visual cortical response due to brief stimulation: an event-related fMRI study.," *Magnetic resonance imaging*, Vol. 19, pp. 21–5, Jan. 2001.

53. Thomas, C. G., and R. S. Menon, "Amplitude response and stimulus presentation frequency response of human primary visual cortex using BOLD EPI at 4 T," *Magnetic Resonance in Medicine*, Vol. 40, pp. 203–209, Aug. 1998.

54. Wan, X., K. Iwata, J. Riera, M. Kitamura, and R. Kawashima, "Artifact reduction for simultaneous EEG/fMRI recording: Adaptive FIR reduction of imaging artifacts," *Clinical Neurophysiology*, Vol. 117, pp. 681–692, Mar. 2006.

55. Fox, P. T., and M. E. Raichle, "Stimulus rate determines regional brain blood flow in striate cortex.," *Annals of neurology*, Vol. 17, pp. 303–5, Mar. 1985.

56. Chase, C., A. Ashourzadeh, C. Kelly, S. Monfette, and K. Kinsey, "Can the magnocellular pathway read? evidence from studies of color," *Vision Research*, Vol. 43, pp. 1211–1222, May 2003.

57. Mullen, K. T., S. O. Dumoulin, and R. F. Hess, "Color responses of the human lateral geniculate nucleus: selective amplification of s-cone signals between the lateral geniculate nucleno and primary visual cortex measured with high-field fMRI.," *The European Journal of Neuroscience*, Vol. 28, pp. 1911–23, Nov. 2008.

58. Sun, P., K. Ueno, R. A. Waggoner, J. L. Gardner, K. Tanaka, and K. Cheng, "A temporal frequency-dependent functional architecture in human v1 revealed by high-resolution fMRI.," *Nature neuroscience*, Vol. 10, pp. 1404–6, Nov. 2007.

59. Bridge, H., S. Clare, M. Jenkinson, P. Jezzard, A. J. Parker, and P. M. Matthews, "Independent anatomical and functional measures of the v1/v2 boundary in human visual cortex.," *Journal of vision*, Vol. 5, pp. 93–102, Jan. 2005.

60. Horiguchi, H., S. Nakadomari, M. Misaki, and B. A. Wandell, "Two temporal channels in human v1 identified using fMRI.," *NeuroImage*, Vol. 47, pp. 273–80, Aug. 2009.

61. Sun, P., J. Guo, S. Guo, J. Chen, L. He, and S. Fu, "BOLD signal change and contrast reversing frequency: an event-related fMRI study in human primary visual cortex.," *PloS one*, Vol. 9, p. e99547, Jan. 2014.

62. Blockley, N. P., V. E. M. Griffeth, and R. B. Buxton, "A general analysis of calibrated BOLD methodology for measuring CMRO2 responses: comparison of a new approach with existing methods.," *NeuroImage*, Vol. 60, pp. 279–89, Mar. 2012.

63. Buxton, R. B., "Dynamic models of BOLD contrast.," *NeuroImage*, Vol. 62, pp. 953–61, Aug. 2012.

64. Sotero, R. C., and N. J. Trujillo-Barreto, "Modelling the role of excitatory and inhibitory neuronal activity in the generation of the BOLD signal," *NeuroImage*, Vol. 35, pp. 149–165, Mar. 2007.

65. Gonzalez-Castillo, J., Z. S. Saad, D. A. Handwerker, S. J. Inati, N. Brenowitz, and P. A. Bandettini, "Whole-brain, time-locked activation with simple tasks revealed using massive averaging and model-free analysis.," *Proceedings of the National Academy of Sciences of the United States of America*, Vol. 109, pp. 5487–92, Apr. 2012.

66. Buxton, R. B., V. E. M. Griffeth, A. B. Simon, and F. Moradi, "Variability of the coupling of blood flow and oxygen metabolism responses in the brain: a problem for interpreting BOLD studies but potentially a new window on the underlying neural activity.," *Frontiers in neuroscience*, Vol. 8, p. 139, Jan. 2014.

67. Buxton, R. B., K. Uludag, D. J. Dubowitz, and T. T. Liu, "Modeling the hemodynamic response to brain activation," *NeuroImage*, Vol. 23, no. Supplement 1, pp. S220–S233, 2004.

68. Fox, M. D., A. Z. Snyder, D. M. Barch, D. a. Gusnard, and M. E. Raichle, "Transient BOLD responses at block transitions.," *NeuroImage*, Vol. 28, pp. 956–66, Dec. 2005.

69. Jenkinson, M., P. Bannister, M. Brady, and S. Smith, "Improved optimization for the robust and accurate linear registration and motion correction of brain images," *NeuroImage*, Vol. 17, pp. 825–841, Oct. 2002.

70. Smith, S. M., "Fast robust automated brain extraction," *Human Brain Mapping*, Vol. 17, pp. 143–155, Nov. 2002.

71. Woolrich, M. W., B. D. Ripley, M. Brady, and S. M. Smith, "Temporal autocorrelation in univariate linear modeling of FMRI data," *NeuroImage*, Vol. 14, pp. 1370–1386, Dec. 2001.

72. Beckmann, C. F., M. Jenkinson, and S. M. Smith, "General multilevel linear modeling for group analysis in fMRI," *NeuroImage*, Vol. 20, pp. 1052–1063, Oct. 2003.

73. Woolrich, M. W., T. E. J. Behrens, C. F. Beckmann, M. Jenkinson, and S. M. Smith, "Multilevel linear modelling for fMRI group analysis using Bayesian inference," *NeuroImage*, Vol. 21, pp. 1732–1747, Apr. 2004.

74. Woolrich, M., "Robust group analysis using outlier inference," *NeuroImage*, Vol. 41, pp. 286–301, June 2008.

75. Worsley, K. J., "Statistical analysis of activation images," in *Functional MRI: An Introduction to Methods*, Oxford University Press, USA, 1 ed., 2001.

76. Başar, E., M. Schürmann, C. Başar-Eroğlu, and T. Demiralp, "Selectively distributed gamma band system of the brain.," *International Journal of Psychophysiology*, Vol. 39, pp. 129–35, Jan. 2001.

77. Onton, J., and S. Makeig, "Information-based modeling of event-related brain dynamics.," *Progress in brain research*, Vol. 159, pp. 99–120, Jan. 2006.

78. Whittington, M. A., and R. D. Traub, "Interneuron diversity series: inhibitory interneurons and network oscillations in vitro.," *Progress in brain research*, Vol. 26, pp. 676–82, Dec. 2003.

79. Demiralp, T., Z. Bayraktaroglu, D. Lenz, S. Junge, N. A. Busch, B. Maess, M. Ergen, and C. S. Herrmann, "Gamma amplitudes are coupled to theta phase in human EEG during visual perception.," *International Journal of Psychophysiology*, Vol. 64, pp. 24–30, Apr. 2007.

80. Nunez, P. L., "Neocortical dynamics of macroscopic-scale EEG measurements.," *IEEE Engineering in Medicine and Biology Magazine*, Vol. 17, no. 5, pp. 110–7, 1998.

81. Nunez, P. L., and R. B. Silberstein, "On the relationship of synaptic activity to macroscopic measurements: does co-registration of EEG with fMRI make sense?," *Brain Topography*, Vol. 13, no. 2, pp. 79–96, 2000.

82. Başar, E., T. Demiralp, M. Schürmann, C. Başar-Eroğlu, and A. Ademoğlu, "Oscillatory brain dynamics, wavelet analysis, and cognition.," *Brain and language*, Vol. 66, pp. 146–83, Jan. 1999.

83. Başar, E., *EEG-brain dynamics: relation between EEG and brain evoked potentials*, Elsevier/North-Holland Biomedical Press, 1980.

84. Lyskov, E., V. Ponomarev, M. Sandström, K. H. Mild, and S. Medvedev, "Steady-state visual evoked potentials to computer monitor flicker.," *International Journal of Psychophysiology*, Vol. 28, pp. 285–90, May 1998.

85. Ogawa, S., R. S. Menon, D. W. Tank, S. G. Kim, H. Merkle, J. M. Ellermann, and K. Ugurbil, "Functional brain mapping by blood oxygenation level-dependent contrast magnetic resonance imaging. a comparison of signal characteristics with a biophysical model," *Biophysical Journal*, Vol. 64, pp. 803–12, Mar. 1993.

86. Horwitz, B., K. J. Friston, and J. G. Taylor, "Neural modeling and functional brain imaging: an overview," *Neural Networks*, Vol. 13, no. 8-9, pp. 829–846, 2000.

87. Laufs, H., J. Daunizeau, D. Carmichael, and A. Kleinschmidt, "Recent advances in recording electrophysiological data simultaneously with magnetic resonance imaging," *NeuroImage*, Vol. 40, pp. 515–528, Apr. 2008.

88. Debener, S., M. Ullsperger, M. Siegel, and A. K. Engel, "Single-trial EEG/fMRI reveals the dynamics of cognitive function," *Trends in cognitive sciences*, Vol. 10, pp. 558–563, Dec. 2006.

89. Goldman, R. I., J. M. Stern, J. Engel, and M. S. Cohen, "Simultaneous EEG and fMRI of the alpha rhythm," *Neuroreport*, Vol. 13, pp. 2487–92, Dec. 2002.

90. Henning, S., K.-D. Merboldt, and J. Frahm, "Task- and EEG-correlated analyses of BOLD MRI responses to eyes opening and closing," *Brain Research*, Vol. 1073-1074, pp. 359–364, Feb. 2006.

91. Sotero, R. C., and N. J. Trujillo-Barreto, "Biophysical model for integrating neuronal activity, EEG, fMRI and metabolism," *NeuroImage*, Vol. 39, no. 1, pp. 290–309, 2008.

92. Strobel, A., S. Debener, B. Sorger, J. C. Peters, C. Kranczioch, K. Hoechstetter, A. K. Engel, B. Brocke, and R. Goebel, "Novelty and target processing during an auditory novelty oddball: a simultaneous event-related potential and functional magnetic resonance imaging study," *Neuroimage*, Vol. 40, no. 2, pp. 869–883, 2008.

93. Thaerig, S., N. Behne, J. Schadow, D. Lenz, H. Scheich, A. Brechmann, and C. S. Herrmann, "Sound level dependence of auditory evoked potentials: Simultaneous EEG recording and low-noise fMRI," *International Journal of Psychophysiology*, Vol. 67, no. 3, pp. 235–241, 2008.

94. Vanni, S., J. Warnking, M. Dojat, C. Delon-Martin, J. Bullier, and C. Segebarth, "Sequence of pattern onset responses in the human visual areas: an fMRI constrained VEP source analysis," *NeuroImage*, Vol. 21, pp. 801–817, Mar. 2004.

95. Viswanathan, A., and R. D. Freeman, "Neurometabolic coupling in cerebral cortex reflects synaptic more than spiking activity," *Nature Neuroscience*, Vol. 10, pp. 1308–12, Oct. 2007.

96. Logothetis, N. K., "What we can do and what we cannot do with fMRI," *Nature*, Vol. 453, pp. 869–78, June 2008.

97. Logothetis, N. K., "The ins and outs of fMRI signals," *Nat Neurosci*, Vol. 10, pp. 1230–1232, Oct. 2007.

98. Logothetis, N. K., and J. Pfeuffer, "On the nature of the BOLD fMRI contrast mechanism," *Magnetic Resonance Imaging*, Vol. 22, no. 10, pp. 1517–1531, 2004.

99. Dale, A. M., and E. Halgren, "Spatiotemporal mapping of brain activity by integration of multiple imaging modalities," *Current Opinion in Neurobiology*, Vol. 11, no. 2, pp. 202–208, 2001.

100. Henning, S., K.-D. Merboldt, and J. Frahm, "Simultaneous recordings of visual evoked potentials and BOLD MRI activations in response to visual motion processing," *NMR in Biomedicine*, Vol. 18, no. 8, pp. 543–552, 2005.

101. Amit, D. J., and S. Romani, "Search for fMRI BOLD signals in networks of spiking neurons," *European Journal of Neuroscience*, Vol. 25, pp. 1882–1892, Mar. 2007.

102. Feige, B., K. Scheffler, F. Esposito, F. Di Salle, J. Hennig, and E. Seifritz, "Cortical and subcortical correlates of electroencephalographic alpha rhythm modulation.," *Journal of neurophysiology*, Vol. 93, pp. 2864–72, May 2005.

103. Goldman, R., J. Stern, J. Engel, and M. Cohen, "Tomographic mapping of alpha rhythm using simultaneous EEG/fMRI," *NeuroImage*, Vol. 13, p. 1291, June 2001.

104. Gonçalves, S. I., J. C. de Munck, P. J. W. Pouwels, R. Schoonhoven, J. P. A. Kuijer, N. M. Maurits, J. M. Hoogduin, E. J. W. Van Someren, R. M. Heethaar, and F. H. Lopes Da Silva, "Correlating the alpha rhythm to BOLD using simultaneous EEG/fMRI: inter-subject variability.," *NeuroImage*, Vol. 30, pp. 203–13, Mar. 2006.

105. Moosmann, M., P. Ritter, I. Krastel, A. Brink, S. Thees, F. Blankenburg, B. Taskin, H. Obrig, and A. Villringer, "Correlates of alpha rhythm in functional magnetic resonance imaging and near infrared spectroscopy," *NeuroImage*, Vol. 20, pp. 145–158, Sept. 2003.

106. Herrmann, C. S., and S. Debener, "Simultaneous recording of EEG and BOLD responses: a historical perspective," *International Journal of Psychophysiology*, Vol. 67, pp. 161–168, Mar. 2008.

107. Ives, J., S. Warach, F. Schmitt, R. Edelman, and D. Schomer, "Monitoring the patient's EEG during echo planar MRI," *Electroencephalography and Clinical Neurophysiology*, Vol. 87, pp. 417–420, Dec. 1993.

108. Bénar, C.-G., Y. Aghakhani, Y. Wang, A. Izenberg, A. Al-Asmi, F. Dubeau, and J. Gotman, "Quality of EEG in simultaneous EEG-fMRI for epilepsy," *Clinical Neurophysiology*, Vol. 114, pp. 569–580, Mar. 2003.

109. Goldman, R. I., J. M. Stern, J. Engel, and M. S. Cohen, "Acquiring simultaneous EEG and functional MRI," *Clinical Neurophysiology*, Vol. 111, pp. 1974–1980, Nov. 2000.

110. Mandelkow, H., P. Halder, P. Boesiger, and D. Brandeis, "Synchronization facilitates removal of MRI artefacts from concurrent EEG recordings and increases usable bandwidth," *NeuroImage*, Vol. 32, pp. 1120–1126, Sept. 2006.

111. Grouiller, F., L. Vercueil, A. Krainik, C. Segebarth, P. Kahane, and O. David, "A comparative study of different artefact removal algorithms for EEG signals acquired during functional MRI," *NeuroImage*, Vol. 38, pp. 124–37, Oct. 2007.

112. Anami, K., T. Mori, F. Tanaka, Y. Kawagoe, J. Okamoto, M. Yarita, T. Ohnishi, M. Yumoto, H. Matsuda, and O. Saitoh, "Stepping stone sampling for retrieving artifact-free electroencephalogram during functional magnetic resonance imaging," *NeuroImage*, Vol. 19, pp. 281–295, June 2003.

113. Niazy, R., C. Beckmann, G. Iannetti, J. Brady, and S. Smith, "Removal of fMRI environment artifacts from EEG data using optimal basis sets," *NeuroImage*, Vol. 28, pp. 720–737, Nov. 2005.

114. Jung, T.-P., S. Makeig, C. Humphries, T.-W. Lee, M. J. Mckeown, V. Iragui, and T. J. Sejnowski, "Removing electroencephalographic artifacts by blind source separation," *Psychophysiology*, Vol. 37, pp. 163–178, Mar. 2000.

115. Bonmassar, G., P. L. Purdon, I. P. Jääskeläinen, K. Chiappa, V. Solo, E. N. Brown, and J. W. Belliveau, "Motion and ballistocardiogram artifact removal for interleaved recording of EEG and EPs during MRI," *NeuroImage*, Vol. 16, no. 4, pp. 1127–1141, 2002.

116. Babiloni, F., F. Cincotti, C. Babiloni, F. Carducci, D. Mattia, L. Astolfi, A. Basilisco, P. Rossini, L. Ding, Y. Ni, J. Cheng, K. Christine, J. Sweeney, and B. He, "Estimation of the cortical functional connectivity with the multimodal integration of high-resolution EEG and fMRI data by directed transfer function," *NeuroImage*, Vol. 24, pp. 118–131, Jan. 2005.

117. Liu, A. K., J. W. Belliveau, and A. M. Dale, "Spatiotemporal imaging of human brain activity using functional MRI constrained magnetoencephalography data: Monte Carlo simulations.," *Proceedings of the National Academy of Sciences of the United States of America*, Vol. 95, pp. 8945–50, July 1998.

118. Im, C.-H., Z. Liu, N. Zhang, W. Chen, and B. He, "Functional cortical source imaging from simultaneously recorded ERP and fMRI," *Journal of Neuroscience Methods*, Vol. 157, no. 1, pp. 118–123, 2006.

119. Daunizeau, J., C. Grova, J. Mattout, G. Marrelec, D. Clonda, B. Goulard, M. Pelegrini-Issac, J.-M. Lina, and H. Benali, "Assessing the relevance of fMRI-based prior in the EEG inverse problem: a bayesian model comparison approach," *IEEE Transactions on Signal Processing*, Vol. 53, pp. 3461–3472, Sept. 2005.

120. Phillips, C., M. D. Rugg, and K. J. Friston, "Anatomically informed basis functions for EEG source localization: combining functional and anatomical constraints.," *NeuroImage*, Vol. 16, pp. 678–95, July 2002.

121. Gotman, J., "Epileptic networks studied with EEG-fMRI.," *Epilepsia*, Vol. 49 Suppl 3, pp. 42–51, Jan. 2008.

122. Gotman, J., E. Kobayashi, A. P. Bagshaw, C.-G. Bénar, and F. Dubeau, "Combining EEG and fMRI: a multimodal tool for epilepsy research.," *Journal of magnetic resonance imaging : JMRI*, Vol. 23, pp. 906–20, June 2006.

123. Hawco, C. S., A. P. Bagshaw, Y. Lu, F. Dubeau, and J. Gotman, "BOLD changes occur prior to epileptic spikes seen on scalp EEG.," *NeuroImage*, Vol. 35, pp. 1450–8, May 2007.

124. Jann, K., R. Wiest, M. Hauf, K. Meyer, C. Boesch, J. Mathis, G. Schroth, T. Dierks, and T. Koenig, "BOLD correlates of continuously fluctuating epileptic activity isolated by independent component analysis.," *NeuroImage*, Vol. 42, pp. 635–48, Aug. 2008.

125. Khader, P., T. Schicke, B. Röder, and F. Rösler, "On the relationship between slow cortical potentials and BOLD signal changes in humans," *International Journal of Psychophysiology*, Vol. 67, pp. 252–261, Mar. 2008.

126. de Munck, J., S. Gonçalves, L. Huijboom, J. Kuijer, P. Pouwels, R. Heethaar, and F. Lopes Da Silva, "The hemodynamic response of the alpha rhythm: An EEG/fMRI study," *NeuroImage*, Vol. 35, pp. 1142–1151, Apr. 2007.

127. Scheeringa, R., M. C. Bastiaansen, K. M. Petersson, R. Oostenveld, D. G. Norris, and P. Hagoort, "Frontal theta EEG activity correlates negatively with the default mode network in resting state," *International Journal of Psychophysiology*, Vol. 67, pp. 242–251, Mar. 2008.

128. Bagshaw, A. P., and T. Warbrick, "Single trial variability of EEG and fMRI responses to visual stimuli," *NeuroImage*, Vol. 38, pp. 280–292, Nov. 2007.

129. Bénar, C.-G., D. Schön, S. Grimault, B. Nazarian, B. Burle, M. Roth, J.-M. Badier, P. Marquis, C. Liegeois-Chauvel, and J.-L. Anton, "Single-trial analysis of oddball event-related potentials in simultaneous EEG-fMRI.," *Human brain mapping*, Vol. 28, pp. 602–13, July 2007.

130. Debener, S., M. Ullsperger, M. Siegel, and A. K. Engel, "Towards single-trial analysis in cognitive brain research," *Trends in Cognitive Sciences*, Vol. 11, pp. 502–503, Dec. 2007.

131. Eichele, T., K. Specht, M. Moosmann, M. L. A. Jongsma, R. Q. Quiroga, H. Nordby, and K. Hugdahl, "Assessing the spatiotemporal evolution of neuronal activation with single-trial event-related potentials and functional MRI," *Proceedings of the National Academy of Sciences of the United States of America*, Vol. 102, pp. 17798–803, Dec. 2005.

132. Mulert, C., C. Seifert, G. Leicht, V. Kirsch, M. Ertl, S. Karch, M. Moosmann, J. Lutz, H.-J. Möller, U. Hegerl, O. Pogarell, and L. Jäger, "Single-trial coupling of EEG and fMRI reveals the involvement of early anterior cingulate cortex activation in effortful decision making," *NeuroImage*, Vol. 42, pp. 158–168, Aug. 2008.

133. Kilner, J., J. Mattout, R. Henson, and K. Friston, "Hemodynamic correlates of EEG: A heuristic," *NeuroImage*, Vol. 28, pp. 280–286, Oct. 2005.

134. Babajani, A., and H. Soltanian-Zadeh, "Integrated MEG/EEG and fMRI model based on neural masses," *Biomedical Engineering, IEEE Transactions on*, Vol. 53, no. 9, pp. 1794–1801, 2006.

135. Riera, J. J., X. Wan, J. C. Jimenez, and R. Kawashima, "Nonlinear local electrovascular coupling. i: A theoretical model," *Human Brain Mapping*, Vol. 27, no. 11, pp. 896–914, 2006.

136. Riera, J. J., J. C. Jimenez, X. Wan, R. Kawashima, and T. Ozaki, "Nonlinear local electrovascular coupling. ii: From data to neuronal masses," *Human Brain Mapping*, Vol. 28, no. 4, pp. 335–354, 2007.

137. Riera, J. J., A. Schousboe, H. S. Waagepetersen, C. Howarth, and F. Hyder, "The micro-architecture of the cerebral cortex: Functional neuroimaging models and metabolism," *NeuroImage*, Vol. 40, pp. 1436–1459, May 2008.

138. Ritter, P., and A. Villringer, "Simultaneous EEG-fMRI.," *Neuroscience and biobehavioral reviews*, Vol. 30, pp. 823–38, Jan. 2006.

139. Varela, F., J. P. Lachaux, E. Rodriguez, and J. Martinerie, "The brainweb: phase synchronization and large-scale integration.," *Nature reviews. Neuroscience*, Vol. 2, pp. 229–39, Apr. 2001.

140. Takahashi, T., "Activation methods," in *Electroencephalography, basic principles, clinical applications and related fields.* (E, N., and L. d. S. F, eds.), pp. 281–303, Philadelphia: Lippincott Williams & Wilkins, 5th ed., 2005.

141. Hillyard, S. A., H. Hinrichs, C. Tempelmann, S. T. Morgan, J. C. Hansen, H. Scheich, and H. J. Heinze, "Combining steady-state visual evoked potentials and fMRI to localize brain activity during selective attention.," *Human brain mapping*, Vol. 5, pp. 287–92, Jan. 1997.

142. Silberstein, R. B., P. Line, A. Pipingas, D. Copolov, and P. Harris, "Steady-state visually evoked potential topography during the continuous performance task in normal controls and schizophrenia.," *Clinical Neurophysiology*, Vol. 111, pp. 850–7, May 2000.

143. Silberstein, R. B., P. L. Nunez, A. Pipingas, P. Harris, and F. Danieli, "Steady state visually evoked potential (ssvep) topography in a graded working memory task.," *International Journal of Psychophysiology*, Vol. 42, pp. 219–32, Oct. 2001.

144. Silberstein, R. B., "Steady-state evoked potentials, brain resonances, and cognitive processes.," in *Neocortical Dynamics and Human EEG Rhythms* (Nunez, P. L., ed.), pp. 272–303, New York: Oxford University Press, 1995.

145. Smith, S. M., M. Jenkinson, M. W. Woolrich, C. F. Beckmann, T. E. J. Behrens, H. Johansen-Berg, P. R. Bannister, M. De Luca, I. Drobnjak, D. E. Flitney, R. K. Niazy, J. Saunders, J. Vickers, Y. Zhang, N. De Stefano, J. M. Brady, and P. M. Matthews, "Advances in functional and structural MR image analysis and implementation as FSL," *NeuroImage*, Vol. 23, no. Supplement 1, pp. S208—-S219, 2004.

146. Robinson, P. a., P.-c. Chen, and L. Yang, "Physiologically based calculation of steady-state evoked potentials and cortical wave velocities.," *Biological cybernetics*, Vol. 98, pp. 1–10, Jan. 2008.

147. Martínez-Montes, E., P. A. Valdes-Sosa, F. Miwakeichi, R. I. Goldman, and M. S. Cohen, "Concurrent EEG/fMRI analysis by multiway partial least squares.," *NeuroImage*, Vol. 22, pp. 1023–34, July 2004.

148. Traub, R. D., M. A. Whittington, I. M. Stanford, and J. G. Jefferys, "A mechanism for generation of long-range synchronous fast oscillations in the cortex.," *Nature*, Vol. 383, pp. 621–4, Oct. 1996.

149. Whittington, M. a., R. D. Traub, N. Kopell, B. Ermentrout, and E. H. Buhl, "Inhibition-based rhythms: experimental and mathematical observations on network dynamics.," *International journal of psychophysiology*, Vol. 38, pp. 315–36, Dec. 2000.

150. von Stein, a., and J. Sarnthein, "Different frequencies for different scales of cortical integration: from local gamma to long range alpha/theta synchronization.," *International journal of psychophysiology*, Vol. 38, pp. 301–13, Dec. 2000.

151. Uludağ, K., D. J. Dubowitz, E. J. Yoder, K. Restom, T. T. Liu, and R. B. Buxton, "Coupling of cerebral blood flow and oxygen consumption during physiological activation and deactivation measured with fMRI.," *NeuroImage*, Vol. 23, pp. 148–55, Sept. 2004.

152. Pastor, M. A., J. Artieda, J. Arbizu, M. Valencia, and J. C. Masdeu, "Human cerebral activation during steady-state visual-evoked responses.," *The Journal of Neuroscience*, Vol. 23, pp. 11621–7, Dec. 2003.